The Dissertation Committee for Ellison Milne Carter Certifies that this is the approved version of the following dissertation:

Removal of Formaldehyde from Indoor Air: Enhancing Surface-Mediated Reactions on Activated Carbon

Committee:

Lynn E. Katz, Supervisor

Gerald E. Speitel Jr., Co-Supervisor

Richard L. Corsi

Howard M. Liljestrand

Keith J. Stevenson

Removal of Formaldehyde from Indoor Air: Enhancing Surface-Mediated Reactions on Activated Carbon

by

Ellison Milne Carter, B. A., B. S. Biol., M. S. E.

Dissertation

Presented to the Faculty of the Graduate School of

The University of Texas at Austin

in Partial Fulfillment

of the Requirements

for the Degree of

Doctor of Philosophy

The University of Texas at Austin

August 2013

To my parents, who have loved me without condition.

To Rachel, for her words of _____.

To Chris, who put a ribbon in the sky.

And now to Rowan, who will never stop being a marvel to me.
Remember: “Be humble for you are made of earth. Be noble for you are made of stars.”

Acknowledgements

Upon entering graduate school at UT, my enthusiasm for research was perhaps matched only by my naiveté. That I am now completing my doctoral program with the same enthusiasm but a (hopefully) more sophisticated and critical approach to research is a testament to the great number of patient, kind, and bright individuals who have helped me along the way.

I am indebted to my two wonderful advisors, Dr. Lynn Katz and Dr. Gerald Speitel Jr. You both provided the mentorship and guidance I needed to develop my own research project, pursue research opportunities outside of UT and abroad, gain teaching experience, and begin my own career as a researcher and educator. Thank you for your consistent constructive criticism, unwavering support, and for knowing when I needed your encouragement most. Your confidence in me has been more important than you may know.

Special thanks to the members of my committee: Dr. Howard Liljestrand, I walked through your open door on many occasions, and I am thankful that I was always met with your patience, keen advice, and often a book or article to improve my scientific acumen. Dr. Keith Stevenson, your genuine concern for and interest in my research not only helped me to solve key, practical problems I faced, but also kept me going when my confidence in my hypothesis waned. Dr. Richard Corsi, you are a selfless role model for many students, and I am thankful for the opportunities you provided for me to experience the many facets of successful research that must take place away from the bench.

There are so many individuals within the Environmental and Water Resources Engineering program and across the UT campus who enriched my life as a graduate student. I wish I could devote more space to highlighting each unique contribution the following people made in my life: to Wil, Pat, and Virginia for being my first friends in Austin and for helping me to understand how engineers think; to Lauren for being an exceptional friend and professional role model; to Shannon for always making time for me when I know you had none; to Lisa, Leo, Tony, Cindy, and Eric for the outdoor lessons in free body diagrams at Enchanted Rock, the Greenbelt, and Yosemite; to Casey for our Peter Pan conversations; to Lee for his camaraderie and cheerfulness; to Anne, Celina, Yeonjeong, Fernando, JP, Bryant, Sarah, Taegyu, and Justin for unexpected and amazing friendships after I thought I was “done” being sociable; to Priscilla, Allison, Elizabeth, Mark, Michael, Brent, Elliott, and Matt for being excellent colleagues, offering valuable input regarding my experimental designs, and always being there to talk through

professional matters, as well as matters of the heart; to Corinne for the unparalleled sense of calm you could convey with only a few words and for making it at least seem like you believed in me; to Dr. Jay Banner for always setting the bar high; to Rosemary, Richard, Adam, Jeff, Daniel, and Wendy for making teaching an even greater joy than it already is and being there to commiserate about "kids these days"; to Tricia and Ana for giving me and so many other young women the opportunities to grow through leadership; to Linda, Elaine, Hortensia, Leslie, Chris, Kathy, Marcy, Sharon, and especially Dori and Rebecca for putting up with my many mundane, but all too often urgent, requests; to Hillary Hart for providing space in her office, as well as on the Pedernales River, to pretend to be an artist; to Jacquelyn, Jake, Kjell, Alex, and Tony for opening the door every time I knocked. Lastly, to Amanda, who was the first person to welcome me to UT as a recruit and who has been a perfect companion as we walked, or trudged as it were, this PhD path together. Thank you for being a friend that kept my mind sharp and sane.

I am grateful to several organizations for the laboratory work and fieldwork they facilitated that were vital to my doctoral research. Dr. Ramirez, it was such a gift that you let me work uninterrupted in your lab at Texas A&M Kingsville during a formative time in my research. Dr. Andy Persily, I deeply appreciate the countless doors you opened while I was a guest researcher at NIST, and the wisdom and mentorship you still provide so freely to this day. I am also eternally grateful for the loan of equipment without which I would never have completed my experiments. Finally, I wish to acknowledge Kathy Tyler and Michael Gatto who allowed me to do some of the fieldwork I was most passionate about through the Cottonwood Creek Environmental Justice Initiative.

I want to thank Katie Alfredo and Mo Oaxaca for being the best half of HillHome and making the time Chris and I spent in Austin "a win", hands-down. There is no question we are family after you have put up with my many irritating qualities for years and still choose to be my friend. You are both irreplaceable.

And my deepest thanks and love to Chris Carter. Thank you for upending your life and moving to Texas with me. Thank you for weathering my tears and despair. Thank you for our early morning tandem rides and for sleeping on Thermarests in my office, when that, too, was called for. Thank you for always asking the questions I have the hardest time answering. Thank you for wanting me to follow my heart.

Removal of Formaldehyde from Indoor Air: Enhancing Surface-Mediated Reactions on Activated Carbon

Ellison Milne Carter, Ph. D.

The University of Texas at Austin, 2013

Supervisors: Lynn E. Katz, Gerald E. Speitel, Jr.

Formaldehyde is a ubiquitous and hazardous indoor air pollutant and reducing concentrations in indoor environments is a public health priority. The goals of this doctoral work were to advance analytical methods for continuous monitoring of formaldehyde at very low concentrations (sub-20 ppb_v) and to improve fundamental, mechanistic understanding of how structural and chemical properties of activated carbon influence removal of formaldehyde from indoor environments. To achieve these goals, emerging sensor-based technology was evaluated for its ability to detect and quantify ppb_v-level formaldehyde concentrations on a continuous basis at relative humidity levels characteristic of residential indoor environments. Also, a combination of spectroscopic and selective titration techniques was employed to characterize molecular-level structural and chemical properties of traditional and chemically treated granular activated carbon (GAC). In addition to selecting two different commercially available GACs for study, design and preparation of a laboratory-prepared, chemically treated GAC was pursued to create nitrogen-doped GAC with desirable surface chemical properties. Performance of all GACs was evaluated with respect to formaldehyde removal through a series of packed bed column studies. With respect to continuous formaldehyde monitoring, a method detection limit for emerging sensor technology was determined to be approximately 2

ppb_v, and for relative humidity levels characteristic of indoor environments (> 40%), quantitative, continuous formaldehyde measurements less than 10 ppb_v were robust. The two commercially available GACs tested were both capable of removing formaldehyde; however, the GAC with greater density of basic surface functional groups and greater electron-donating potential (Centaur) removed twice as much formaldehyde (on a GAC mass basis) as the less basic GAC (BPL). A laboratory-prepared GAC (BPL-N) was successfully created to contain pyridinic and pyrrolic nitrogen, which was associated with increased surface density of basic functional groups, as well as with increased electron-donating potential. BPL-N exhibited better removal capacity for formaldehyde than BPL and Centaur. Furthermore, packed bed column studies of BPL-N and BPL formaldehyde removal performance yielded evidence to support the hypothesis that electron-donating potential, especially nitrogen functional groups at the BPL-N surface, promote catalytic removal of gas-phase formaldehyde via oxidation.

Table of Contents

List of Tables xii

List of Figures xiv

Chapter 1: Introduction/Motivation 1

1.1 Problem Statement 1

1.2 Motivation 2

1.3 Tasks 4

1.4 Dissertation Structure 6

Chapter 2: Literature Review 8

2.1 Overview 8

2.2 Formaldehyde 9

2.2.1 Chemical and physical properties 9

2.2.2 Sampling and detection 10

2.3. Indoor Air Treatment Strategies 12

2.3.1 Source emission removal and reduction 12

2.3.2 Ventilation 13

2.3.3 Pollutant control technology 15

2.4 Activated Carbon 19

2.4.1 Structural and chemical properties of activated carbon 19

2.4.2 Surface modification and nitrogen-doping of activated carbon 22

2.4.3 Techniques for structural and chemical characterization of activated carbon 24

2.4.4. Characteristics of removal processes at GAC surfaces 27

2.4.5 Impacts of relative humidity and water vapor adsorption on removal processes 31

Chapter 3: Continuous Measurement of Formaldehyde in Indoor Environments 34

3.1 Overview 34

3.2 Background Information 35

3.3 Methods and Instrumentation 42
3.3.1 Coupled Sensor Spectrophotometric Device 42
3.3.2 Calibration Setup 45
3.3.3 Field experimental setup 50
3.4 Results and Discussion 50
3.4.1 Calibration Results 50
3.4.2 Field Results 53
3.5 Conclusions 54

Chapter 4: Formaldehyde Removal by Commercially Available Granular Activated Carbon 57
4.1 Overview 57
4.2 Methods and Instrumentation 64
4.2.1 Granular activated carbons 64
4.2.2. Structural and chemical characterization of GAC 65
4.2.3. Experimental procedure for determination of water vapor adsorption isotherms on GAC 70
4.2.4. Experimental setup for measurement of formaldehyde removal through packed bed columns 71
4.3 Results and Discussion 77
4.3.1 Structural and chemical characterization of GAC 77
4.3.2 Water vapor adsorption isotherms on BPL and Centaur GACs .85
4.3.3. Formaldehyde removal through packed bed GAC columns 87
4.4 Conclusions 93

Chapter 5: The Influence of Surface Chemical Properties on Formaldehyde Removal by Chemically Treated GAC 96
5.1 Overview 96
5.2 Methods and Instrumentation 102
5.2.1 Surface modification and nitrogen-doping of granular activated carbon 102
5.2.2 Structural and chemical characterization of granular activated carbon 104

5.2.3 Experimental setup for packed bed columns 106
5.3 Results and Discussion 112
5.3.1 Structural characterization of GAC 112
5.3.2 Chemical characterization of GAC 118
5.3.3 The influence of surface chemical properties on formaldehyde removal through packed bed GAC columns 130
5.3.4 Evidence for catalysis of formaldehyde through packed bed GAC columns 137
5.4 Conclusions 150
Chapter 6: Conclusions 152
6.1 Overview 152
6.2 Results and Significance 152
6.3 Future Work 157
Appendices 159
A.1. Nitrogen Adsorption Isotherms 159
A.2. Boehm Titrations 159
References 161
Vita 175

List of Tables

Table 2.1. Chemical and physical properties of formaldehyde. 10

Table 2.2. Volatile organic compounds commonly detected in indoor environments. 16

Table 3.1: Recommended exposure limits and threshold limit values for formaldehyde with respect to non-cancer health effects.....36

Table 3.2. Summary of flow rates necessary to achieve desired target formaldehyde concentrations with respect to formaldehyde emission rates from standardized paraformaldehyde sources. 49

Table 4.1. Summary of experimental conditions for packed bed column tests of formaldehyde removal at 100 ppb_v by BPL GAC. 75

Table 4.2. Summary of experimental conditions for packed bed column tests of formaldehyde removal at 36 ppb_v by two commercially available GACs, BPL and Centaur.....76

Table 4.3. Summary of structural and chemical characteristics for two commercially available GACs, BPL and Centaur. 78

Table 4.4. Two-sided t-test for difference between the means for surface densities of acidic and basic functional groups and electron-donating potential for BPL and Centaur GACs.....80

Table 4.5. Two-sided t-test for difference between the mean O/C ratios for BPL and Centaur GACs.....81

Table 4.6. Average peak position of component peaks comprising the O 1s region for BPL and Centaur and associated peak ranges and assignments to specific types of oxygen complexes (Zhou et al., 2007; Sun et al., 2008).....82

Table 5.1. Summary of experimental conditions for packed bed column tests of formaldehyde removal at 100 ppb_v by BPL and BPL-N. 111
Table 5.2. Summary of experimental conditions for packed bed column tests of formaldehyde removal at 36 ppb_v by BPL and BPL-N. 112
Table 5.3. Summary of structural and chemical characteristics for BPL and BPL-N. 113
Table 5.4. Two-sided t-tests for difference between the means for surface densities of acidic and basic functional groups and electron-donating potential for BPL and BPL-N. 126
Table 5.5. Average peak position of component peaks comprising the O 1s region for BPL and BPL-N and associated peak ranges and assignments to specific types of oxygen complexes. 127
Table A-1. Triplicate measurements of NaOH uptake by BPL, Centaur, and BPL-N to determine surface density of acidic functional groups. 160
Table A-2. Triplicate measurements of HCl uptake by BPL, Centaur, and BPL-N to determine surface density of acidic functional groups. 160

List of Figures

Figure 2.1 Schematic of methylene glycol formation by hydration of formaldehyde in dilute aqueous systems.....9

Figure 2.2. Schematic representation of (a) overlapping aromatic carbon sheets and (b) a single graphene layer including oxygen-functional groups at edge-plane sites. Dots and dots with * represent unpaired sigma electrons and in-plain sigma pairs, respectively (Rodriguez-Reinoso and Molina-Sabio, 1998). 20

Figure 2.3. Representative oxygen-containing acidic and basic functional groups. Adapted from Rodriguez-Reinoso and Molina-Sabio, 1998. 22

Figure 2.4. Representative nitrogen-containing functional groups. Adapted from Lázló, 2005. 23

Figure 3.1. Schematic representation of PFBHA adsorption to SPME fiber prior to exposure to gas-phase formaldehyde. 38

Figure 3.2. Schematic of chemical reaction between PFBHA and formaldehyde to form oxime product.....38

Figure 3.3. Illustration of data analysis steps to determine formaldehyde concentrations from PFBHA-SPME-GC-ECD method: (a) quantitative determination of mass of oxime formed; (b) evaluation of reaction velocity for each of two formaldehyde concentration calibration standard levels; (c) determination of first-order reaction rate constant; and (d) equation for determination of formaldehyde concentration.....39

Figure 3.4. Schematic of sensor element illustrating side-by-side arrangement of uncoated reference glass sheet and chemically coated glass sheet for absorbance measurement within the CSSD (*reproduced with permission from Shinyei Technology Co., Ltd.)*. 43

Figure 3.5. Side view of sensor element illustrating light being shone on uncoated and chemically coated glass sheets during absorbance reading taken at 410 nm (*reproduced with permission from Shinyei Technology Co., Ltd.)*.44

Figure 3.6. Schematic of the experimental setup used to generate formaldehyde and test CSSDs. 46

Figure 3.7. Structure of one monomer of oxymethylene, where *n* indicates a sequence of monomers to form polyoxymethylene.....46

Figure 3.8. Emission rate of formaldehyde permeation tube, #32684.....47

Figure 3.9. Emission rate of formaldehyde permeation tube, #33896.....48

Figure 3.10. Correlation between reported formaldehyde concentrations from CSSDs and the DNPH-derivatization method.....52

Figure 3.11. Continuous formaldehyde sampling for five days in two manufactured homes in a colonia outside San Marcos, TX. Data points marked with 'X' are below the detection limit. 54

Figure 4.1. Illustrations of typical IUPAC isotherm shapes by classification (Carnody et al., 2007). 59

Figure 4.2. Evaluation of relationship between HCHO adsorption at 3 (□), 7 (△), and 11 (◇) ppm_v and the corresponding QL model parameter, ξ_0. Coefficients of determination are reported beside each trend line. ..61

Figure 4.3. Evaluation of relationship between HCHO adsorption at 3 (□), 7 (△), 11 (◇), and 15 (○) ppm_v and GAC surface density of basic functional groups. Coefficients of determination are reported beside each trend line. 63

Figure 4.4. Schematic of experimental setup for evaluation of formaldehyde removal through packed GAC columns.....71

Figure 4.5. Emission rate of formaldehyde permeation tube, #32684.....73

Figure 4.6. Emission rate of formaldehyde permeation tube, #33896.....74

Figure 4.7. Adsorption (closed symbols) and desorption (open symbols) branches of nitrogen sorption isotherms on BPL (△, ▲) and Centaur (□, ■). .77

Figure 4.8. Relative distribution of oxygen complexes, determined by peak position, for five replicates of BPL and three replicates of Centaur.....84

Figure 4.9. Adsorption (closed symbols) and desorption (open symbols) branches of water sorption isotherms on BPL (△, ▲) and Centaur (□, ■). 87

Figure 4.10. Effluent formaldehyde concentrations for BPL normalized by the influent formaldehyde concentration (100 ppb_v) and presented with respect to thousands of bed volumes fed. 88

Figure 4.11. Effluent formaldehyde concentrations for BPL (△) and Centaur (□) normalized by the influent formaldehyde concentration (36 ppb_v) and presented with respect to thousands of bed volumes fed.....90

Figure 4.12. Surface loading of formaldehyde for BPL (—) and Centaur (---) normalized by the mass of GAC in the column and presented with respect to thousands of bed volumes fed. 92

Figure 5.1. Schematic of experimental setup for evaluation of formaldehyde removal through packed GAC columns.....110

Figure 5.2. Comparison of BPL, BPL-N, and Centaur BET specific surface area and t-plot analysis of micropore surface area. 115
Figure 5.3. Comparison of BPL, BPL-N, and Centaur DFT total pore volume and DFT micropore volume.....115
Figure 5.4. Comparison of BPL (△), BPL-N (○), Centaur (□) differential surface area distribution with respect to pore width. 117
Figure 5.5. Comparison of BPL (△), BPL-N (○), and Centaur (□) differential volume distribution with respect to pore width. 117
Figure 5.6. Normalized intensity of representative high-resolution XP spectra across binding energy range associated with N 1s electrons for BPL (---) and BPL-N (—). 119
Figure 5.7. Normalized intensity of representative high-resolution XP spectra across binding energy range associated with N 1s electrons for BPL (---) and Centaur (—). 120
Figure 5.8. Normalized intensity of representative high-resolution XP spectra across binding energy range associated with N 1s electrons for Centaur (---) and BPL-N (—). 120
Figure 5.9. Relative distribution of nitrogen-containing functional groups, determined by peak position, for four replicates of BPL-N and three replicates of Centaur. 121
Figure 5.10. Relative distribution of sp^2-hybridized and sp^3-hybridized carbon, determined by peak position, for BPL, Centaur, and BPL-N. 123
Figure 5.11. Representative first-order Raman spectra of BPL (---) and BPL-N (—) normalized to the intensity of the band at 1588 cm^{-1}. 124

Figure 5.12. Relative distribution of oxygen complexes, determined by peak position, for five replicates of BPL, three replicates of Centaur, and four replicates of BPL-N.....129

Figure 5.13. Effluent formaldehyde concentrations for BPL (△) and BPL-N (○) normalized by the influent formaldehyde concentration (100 ppb_v) and presented with respect to thousands of bed volumes fed.....131

Figure 5.14. Effluent formaldehyde concentrations for BPL (△), Centaur (□), and two replicate columns of BPL-N (○; black and grey) normalized by the influent formaldehyde concentration (36 ppb_v) and presented with respect to thousands of bed volumes fed. 133

Figure 5.15. Surface loading of formaldehyde for BPL (—), Centaur (---), and BPL-N replicate 1 (•••) and replicate 2 (•••) normalized by the mass of GAC in the column and presented with respect to thousands of bed volumes fed. 134

Figure 5.16. Evaluation of relationship between apparent formaldehyde surface loading at 50% breakthrough at 36 ppb_v for BPL, Centaur, and BPL-N and surface density of basic functional groups, as determined by the Boehm titration technique. Coefficient of determination is reported beside the trend line. 135

Figure 5.17. Evaluation of relationship between apparent formaldehyde surface loading at 50% breakthrough at 36 ppb_v for BPL, Centaur, and BPL-N and electron-donating potential, as determined by the iodometric titration technique. Coefficient of determination is reported beside the trend line. 136

Figure 5.18. Evaluation of relationship electron-donating potential and surface density of basic functional groups for BPL, Centaur, and BPL-N and electron-donating potential with respect to GAC nitrogen content. Coefficients of determination are reported beside the trend line. ...137

Figure 5.19. Cycle 1. Effluent formaldehyde concentrations for BPL and BPL-N during formaldehyde exposure (△,○) and regeneration (▲,●) normalized by the influent formaldehyde concentration (38 ppb_v) and presented with respect to thousands of bed volumes fed. The influent formaldehyde concentration, as measured with DNPH, is also shown (◇). ...140

Figure 5.20. Cycle 2. Effluent formaldehyde concentrations for BPL and BPL-N during formaldehyde exposure (△,○) and regeneration (▲,●) normalized by the influent formaldehyde concentration (38 ppb_v) and presented with respect to thousands of bed volumes fed. BPL-N column effluent formaldehyde concentrations, as measured with DNPH, are also shown for the HCHO exposure phase (◇) and the regeneration (no HCHO) phase (◆). ...142

Figure 5.21. Cycle 3. Effluent formaldehyde concentrations for BPL and BPL-N during formaldehyde exposure (△,○) and regeneration (▲,●) normalized by the influent formaldehyde concentration (38 ppb_v) and presented with respect to thousands of bed volumes fed. BPL-N column effluent formaldehyde concentrations, as measured with DNPH, are also shown for the HCHO exposure phase (◇) and the regeneration (no HCHO) phase (◆). ...143

Figure 5.22. Effluent formaldehyde concentrations for BPL and BPL-N during formaldehyde exposure (△,○) and regeneration (▲,●) normalized by the influent formaldehyde concentration (38 ppb_v) and presented with respect to thousands of bed volumes fed. BPL-N column effluent formaldehyde concentrations, as measured with DNPH, are also shown for the HCHO exposure phase (◇) and the regeneration (no HCHO) phase (◆).....144

Figure 5.23. CSSD (+) and DNPH (◆) measurements of formaldehyde concentrations in experimental chambers when no columns are present and only ultra-zero, formaldehyde-free air passes through experimental system. Formaldehyde concentrations are normalized by hypothetical influent formaldehyde concentration, 38 ppb_v.....146

Figure 5.24. Effluent formaldehyde concentrations for BPL and BPL-N columns run with pure nitrogen carrier gas (△,○) and ultra-zero air (▲,●) normalized by the influent formaldehyde concentration (38 ppb_v) and presented with respect to thousands of bed volumes fed.....147

Figure 5.25. Effluent formaldehyde concentrations for BPL and BPL-N columns run at 50% RH (△,○) and 70% RH (▲,●) normalized by the influent formaldehyde concentration (38 ppb_v) and presented with respect to thousands of bed volumes fed.....149

Figure A-1. Adsorption (closed symbols) and desorption (open symbols) branches of nitrogen sorption isotherms on BPL (△, ▲), Centaur (□, ■), and BPL-N (○,●).....159

Chapter 1: Introduction/Motivation

1.1 Problem Statement

In our increasingly urbanized world, the potential for air pollution to adversely affect human health is significant. Indoor air pollution control has become a public health priority as human exposure to known carcinogens, mutagens, endocrine-disrupting compounds, and neurotoxins in indoor environments (such as the workplace, schools, hospitals, and in residential dwellings) is better understood. Among volatile organic compounds (VOCs) found indoors, formaldehyde is a low molecular weight carbonyl consistently measured in indoor environments at concentrations four to ten times higher than outdoors, where it is already listed as a hazardous air pollutant (HAP) regulated by the Clean Air Act of 1990 (US Environmental Protection Agency (EPA), 1991). Treatment of gas-phase air pollutants with activated carbon is a promising pollutant control technology, but its efficacy for low molecular weight aldehydes, has yet to be fully investigated. The goals of this work are four-fold: (1) advance formaldehyde measurement techniques and detection methods by evaluating emerging technology for continuous formaldehyde measurement at lower concentrations than have been tested previously; (2) assess the ability of commercially available activated carbon to control gas-phase formaldehyde concentrations under conditions relevant to indoor environments, (3) elucidate the influence of structural and chemical properties of activated carbon on gas-phase removal of formaldehyde; and (4) design, prepare, and characterize physicochemical properties and performance of activated carbon media that is modified to enhance gas-phase removal of formaldehyde. This work addresses a need to provide people with clean, indoor air by reducing their exposure to harmful aldehydes. The detailed investigation of sorption processes and catalytic activity of formaldehyde on activated carbon surfaces presented here takes into account often disregarded chemical

and physical properties of both the pollutant control technology and the pollutant in an attempt to relate them back to removal mechanisms. Applications of results from this research include development of selection criteria for activated carbon-based treatment technologies in indoor air treatment applications, as well a process design model to predict their performance and service life.

1.2 MOTIVATION

As a consequence of its ubiquitous occurrence in built environments and its established human health significance, reducing human exposure to formaldehyde is a leading public health goal. Formaldehyde concentrations in many different indoor environments regularly exceed known safe exposure limits and this fact provides the central motivation for this research. The primary pathway for human exposure to formaldehyde is inhalation in residential and occupational settings. Characteristic sources of formaldehyde include building materials, such as composite wood products, insulation, carpet, and laminate flooring and consumer products, such as cleaners, personal care products, clothing, textiles, and furniture (Salthammer et al., 2010). Formaldehyde is also generated indoors from combustion reactions associated with gas stoves, wood-burning fireplaces, and cooking activities (Zhang and Smith, 1999), as well as from ozone reactions with unsaturated volatile alkenes (Morrison and Nazaroff, 2002; Weschler, 2000).

Formaldehyde is the most abundant airborne carbonyl measured in indoor environments. In homes monitored across the United States, median formaldehyde concentrations are reported from 20 to 50 ppb_v (Liu et al., 2006) and range as high as several hundred ppb_v (Hodgson and Levin, 2003). These values are between 1.3 and 3.1 times greater than the chronic recommended exposure limit (REL) of 16 ppb_v for

formaldehyde set by the National Institute for Occupational Safety and Health and 2.9 to 7.1 times greater than the recommended exposure limit (REL) for formaldehyde set at 7 ppb_v by the Office of Environmental Health Hazard Assessment (OEHHA) in California (OEHHA, 2008). In manufactured (prefabricated) housing or temporary housing units, such as those provided by the United States Federal Emergency Management Agency (FEMA) to families who were displaced by hurricanes Katrina and Rita in 2005, baseline concentrations of formaldehyde determined from sampling by the Agency for Toxic Substances and Disease Registry (ATSDR) averaged 1,000 ppb_v and ranged from 100—3,066 ppb_v (ATSDR, 2007). In occupational environments over two million US workers are exposed to formaldehyde concentrations that can range from 100 ppb_v to above 10 ppm_v, depending on the industry (World Health Organization (WHO) International Agency on Research for Cancer (IARC) Monographs, 2006). Its ubiquity in these workplace and residential environments is of growing concern due to increased awareness regarding the health concerns associated with airborne exposure.

Formaldehyde is a sensory and respiratory irritant, and prolonged exposure to these pollutants has been associated with allergenic sensitization, reduced pulmonary function, and asthma (Thompson et al., 2008), especially in children (McGwin et al., 2010). In addition to non-cancer health effects, formaldehyde is classified by IARC as a known human carcinogen (WHO, 2006). Though formaldehyde exposure has long been linked to nasopharyngeal cancer and paranasal cancers, a causal association has been recently established, as well, between inhalation exposure to formaldehyde and all leukemias, myeloid leukemia, and lymphohematopoieitic cancers as a group (US EPA, 2010). Furthermore, with respect to exposure to known indoor air pollutants, formaldehyde makes the greatest contribution to the resulting cumulative cancer risk (Hun et al. 2009).

As a result of continued awareness of and concern about the health impacts of chronic exposure to formaldehyde, abundant information is available regarding indoor sources, concentrations of, and exposures to this pollutant. However, few studies have evaluated the use of air treatment technologies for its removal from indoor environments. Thus, another important motivation for this research is the need for data quantifying traditional and novel pollutant control technologies. Such studies would improve understanding of how to effectively reduce indoor formaldehyde concentrations and drive development of standards for gas phase indoor air pollutant control technology.

1.3 TASKS

The research presented in this dissertation advances knowledge and development of pollutant control technology to remove a hydrophilic, low molecular weight aldehyde, formaldehyde, which contributes to oxidative stress and poses serious health risks to those exposed to this pollutant through inhalation. To this end, this work combines detailed surface characterization of air treatment media with evaluation of pollutant removal performance to correlate properties of the air treatment media to treatment effectiveness. While such studies have been performed and proven effective for aqueous phase adsorption of moderately hydrophobic contaminants, the application of this approach to gas-phase adsorption has been limited. The outcome of this work provides guidance to further reduce human exposure to formaldehyde by investigating (1) the capacity of traditional and chemically treated granular activated carbon (GAC) media to remove formaldehyde, (2) physical and chemical surface properties that promote hypothesized removal mechanisms, (3) potential formaldehyde removal mechanisms, and (4) the impact of relative humidity on the performance of the GAC materials. The four

research goals presented above in Section 1.1 were achieved through the following specific tasks:

Task 1. *Advancing development of a novel formaldehyde detection method*. This work evaluates the performance of a portable, coupled formaldehyde sensor and spectrophotometric device for continuous measurement of formaldehyde in a laboratory setting. Measurement of gas-phase formaldehyde in indoor environments, especially those that are residential, with time resolution is a challenge within the field of indoor air. This task focuses on assessing the ability of emerging sensor technology to measure sub-20 ppb_v formaldehyde concentrations on a continuous basis under relative humidity conditions typical of indoor, residential environments.

Task 2. *Evaluating formaldehyde removal by commercially available GAC*. Although traditional activated carbon materials are considered inadequate for adsorption and removal of low molecular weight aldehydes (especially formaldehyde), very little research has investigated this assumption. Commercially available GACs are compared on the basis of structural and chemical characteristics, water vapor adsorption, and formaldehyde removal for concentrations of approximately 100 and 36 ppb_v, which are characteristic of typical indoor, residential and commercial environments.

Task 3. *Characterizing the influence of structural and chemical surface properties of GAC on formaldehyde removal*. Structural and chemical properties of the activated carbon surfaces, including specific surface area, pore size distribution, density of surface acidic groups, density of surface basic groups, and type and quantity of surface functional groups containing oxygen and nitrogen, are characterized using spectroscopic and selective titration-based surface analytical techniques. Relationships between GAC surface properties and formaldehyde removal performance are then investigated.

Task 4. *Modifying GAC and evaluating the influence of modification on formaldehyde removal*. Nitrogen-functionalized activated carbon materials show potential for increased formaldehyde removal. This task pursues the design, preparation, and physicochemical characterization of nitrogen-functionalized GAC. Then, formaldehyde removal by packed bed columns of commercially available traditional GAC, commercially available and chemically treated GAC, and laboratory-prepared, chemically treated GAC is evaluated for multiple experimental conditions. Relationships between structural and chemical properties of the GAC surface and formaldehyde removal performance are investigated, and results from packed bed column studies are compared across experimental conditions to elucidate removal mechanisms.

1.4 Dissertation Structure

This dissertation is organized into six chapters. The first chapter provides an introduction to and the motivation for the work presented throughout the dissertation. The second chapter gives a thorough review of the pertinent literature and identifies the key knowledge gaps, which this dissertation seeks to fill. Chapters 3, 4, and 5 focus on the research methods and techniques employed in and results garnered from this work. Chapter 3 presents evaluation of a portable formaldehyde sensor and coupled spectrophotometric device for continuous formaldehyde measurement in a controlled laboratory setting and in a residential field setting. Commercially available GACs are the subject of Chapter 4, and in addition to structural and chemical characterization, these GACs are evaluated for their performance with respect to water vapor adsorption and their ability to remove gas-phase formaldehyde when present at ppb_v concentrations typical of indoor residential and commercial environments. Chapter 5 details the design, preparation, and structural and chemical characterization of GAC that has been

chemically treated to incorporate nitrogen-containing functional groups. This chapter also analyzes the influence of GAC modification and nitrogen-doping on gas-phase formaldehyde removal at ppb_v concentrations and relative humidity levels typical of indoor residential and commercial environments. Special attention is given to determining whether the data collected support the hypothesis that nitrogen-doped GAC is capable of catalytic removal of formaldehyde. Chapter 6 presents a summary of the conclusions reached through this research and offers suggestions for application of this work and recommendations for future research.

Chapter 2: Literature Review

2.1 Overview

A review of appropriate literature was undertaken to identify key knowledge gaps in scholarly research that relates to development and application of pollutant control technology for removal of formaldehyde from indoor environments. This literature review is divided into three sections. The first section of this review focuses on fate, transport, sampling, and quantitative measurement of formaldehyde in indoor environments. Discussion in this section provides the basis for the experimental setup designed for this research. The second section of this review describes current indoor air treatment strategies and their impacts on indoor formaldehyde concentrations, leading to the focus in this work on gas-phase pollutant control technology. The third section of this literature review discusses structural and chemical properties, as well as surface modification through chemical treatment and nitrogen-doping in particular, of activated carbon to inform the selection and design of traditional (untreated chemically) and chemically treated granular activated carbons (GACs) studied in this research. Furthermore, this section of the review forms the foundation for investigation of the role of activated carbon surface chemistry and structure in formaldehyde removal by traditional and chemically treated GACs. Taking all three components together, this literature review provides the framework for the research undertaken to quantify formaldehyde removal by several different GACs under conditions relevant to indoor environments, assess the influence of structural and chemical surface properties of GAC on formaldehyde removal, and investigate potential removal mechanisms.

2.2 FORMALDEHYDE

2.2.1 Chemical and physical properties

Chemical and physical attributes of pollutants, such as polarity, hydrophobicity, electron-withdrawing and electron-donating capacity of functional groups, size, and structure strongly influence surface interactions and interfacial processes. Aldehydes are distinguished by the presence of a terminal carbonyl, or carbon-oxygen double bond. This carbonyl functional group is polar, and some aldehydes, such as formaldehyde, have dipole moments greater than that of water. Furthermore, the non-bonding electron pairs associated with the oxygen atom in the carbonyl imply that aldehydes are hydrogen bond acceptors. This increases their solubility in water. In fact, through reversible hydration, formaldehyde is converted almost exclusively to the hydrated geminal diol form, $CH_2(OH)_2$, by the aqueous reaction shown in Figure 2.1 (Bell, 1966):

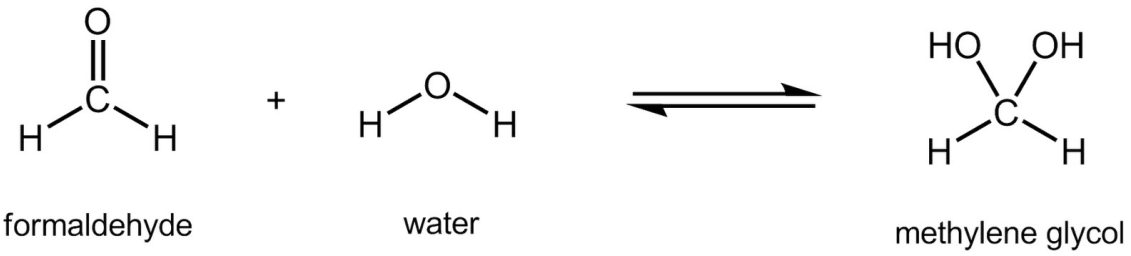

Figure 2.1 Schematic of methylene glycol formation by hydration of formaldehyde in dilute aqueous systems.

Table 2.1 lists the molecular weight, vapor pressure, and dipole moment of formaldehyde. Each of these parameters is a key measurable property that reflects important chemical or physical characteristics, specifically size, gas/liquid partitioning, and polarity, respectively. Among aldehydes, formaldehyde has been selected for the focus of this research on the basis of its ubiquity indoors (Liu et al., 2006) and potential for adverse human health effects (O'Brien et al., 2005) as outlined in Chapter 1.

Table 2.1. Chemical and physical properties of formaldehyde.

Compound	Structure	Property	Value	[Units]
Formaldehyde	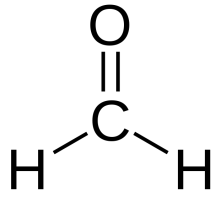	CAS number	50-00-0	
		Molecular weight	30.026	[g/mol]
		Dipole moment	2.33	[D]
		Vap. Press. @ 25°C	3890	[mmHg]
		Henry's constant	3.37E-7	[atm-m^3/mol]
		Solubility in water	4E5	[mg/L]
		Kinetic diameter	0.36	[nm]

2.2.2 Sampling and detection

Many different analytical techniques have been developed for the determination of formaldehyde. For outdoor applications, continuous quantitative determination of formaldehyde is often achieved through *in situ* spectroscopic techniques, including Fourier Transform infrared (FTIR) absorption, differential optical absorption spectroscopy (DOAS), laser-induced fluorescence spectroscopy (LIFS), and tunable diode laser spectroscopy (TDLS). In a thorough intercomparison of these techniques, Vairavamurthy et al. (1992) highlight the need for long path lengths to attain low detection limits as the greatest shortcoming of these spectroscopic techniques with respect to routine outdoor air applications. This requirement also makes these techniques unsuitable for indoor applications. More recently, techniques such as photoacoustic spectroscopy (PAS) (Wu et al., 2003; Ferus et al., 2008) and proton-transfer-reaction mass spectrometry (PTR-MS) (Lindinger and Jordan, 1998) have been investigated for carbonyl analyses in indoor environments. However, these techniques have met with minimal success with respect to indoor settings due to their susceptibility to interferences, low sensitivity to formaldehyde, and high detection limits (de Gouw et al., 2006; Wisthaler et al., 2008). Hak et al. (2005) offers a comprehensive review of multiple intercomparison studies of formaldehyde detection techniques. In this review, these authors also performed their own intercomparison of several techniques and reported

agreement between the FTIR, DOAS, and acetylacetone methods to within 11%, but the dinitrophenylhydrazine (DNPH)-derivatization method produced formaldehyde concentrations that were 25% lower than the results produced by the other three methods. This review by Hak et al. (2005), in addition to a more recent review by Wisthaler et al. (2008), are among the first to provide insightful comparisons between *in situ* and derivatization techniques. These reviews highlight the analytical advantage of low detection limits that results from long, batch-sampling methods employed when formaldehyde derivatization measurement techniques are selected.

Derivatization techniques, like the DNPH (Sandner et al., 2001) and acetylacetone (Nash, 1953; Salthammer and Mentese, 2008) methods mentioned above, involve the adsorption of formaldehyde to a solid surface or absorption into a liquid phase. Once removed from the gas-phase and trapped in a solid or liquid phase, formaldehyde undergoes a reaction with a derivatizing agent to form a derivative compound that is amenable to subsequent detection through gas or liquid chromatography or ultraviolet spectrophotometry. Derivatization techniques are well-suited for time-averaged sampling and detection of formaldehyde in indoor environments, and reviews by Barro et al. (2009) and Salthammer et al. (2010) describe, review, and compare many of these techniques. The chromotropic acid, acetylacetone, and DNPH methods have been the most widely applied methods for indoor air sampling in Europe, Asia, and North America, and the DNPH method, in particular, has been adopted as an international standard by the International Standardization Organization (ISO) (ISO, 2001) and is fully described by the US EPA TO11-A method (US EPA, 1999) and the ASTM D1597 method (ASTM, 2003).

However, an increased need for indoor formaldehyde sampling techniques that are fast, dynamic, and continuous has spurred recent research and development of sensor-

based technology. Salthammer et al. (2010) offers the most current and comprehensive review of research and applications of formaldehyde sensor technology. This review points out that most sensor-based technology still suffers from detection limits that are not competitive with derivatization techniques but that the research in this field is growing rapidly. The dissertation research presented subsequently in Chapter 3 investigates the performance of a newly developed formaldehyde sensor device that was not available at the time of the aforementioned review by Salthammer et al. (2010) and provides new insight into advances being made in this field.

2.3. INDOOR AIR TREATMENT STRATEGIES

Indoor air quality control strategies include source removal, emission reduction, ventilation, and pollutant control through treatment. This review of the literature will briefly cover source removal, emission reduction, and ventilation, while going into greater depth with respect to pollutant control technology that involves air treatment.

2.3.1 Source emission removal and reduction

Indoor sources of formaldehyde emissions in homes and non-residential indoor environments are not only abundant, but also frequently integrated directly into building infrastructure. Thus, to achieve acceptable indoor concentrations, it is often not feasible, cost-effective, or sufficient to remove the sources. Instead of removing sources, recent action to reduce indoor formaldehyde levels has focused on emissions reduction. Composite wood products, in particular, have been the target of recent state-level and federal legislation to reduce allowable formaldehyde emission rates from these materials. In 2007, the California Air Resources Board (CARB) approved an airborne toxics control measure to reduce formaldehyde emissions from hardwood plywood, particleboard, and medium density fiberboard, as well as home furnishings that incorporate these products

(CARB, 2007). Similar standards were adopted at the federal level when the *Formaldehyde Standards for Composite Wood Products Act* was signed into law in 2010 (US Congress, 2010). The United States Environmental Protection Agency has since been directed by Congress to publish and distribute the finalized standards starting in 2013. These two examples of current legislation are strong next steps in the continued effort to improve indoor air quality by reducing indoor formaldehyde concentrations. However, source emission removal or reduction does not address the significant contribution to formaldehyde concentrations made by primary emissions from numerous other building components and home furnishings that are not composite wood products (Weschler, 2009) and by chemical reactions in the gas-phase (*e. g.* reactions between ozone or free radicals and unsaturated organic compounds) (Destaillats et al., 2006; Weschler, 2006) and those that occur at surfaces (Morrison and Nazaroff, 2002; Wang and Morrison, 2006).

2.3.2 Ventilation

By definition, ventilation is the exchange of air in an enclosed space through recirculation or through replacement of air present in the space with outdoor air. Ventilation has long been recognized as a means to protect or improve indoor air quality (Tredgold, 1836; Billings, 1893; New York State Commission, 1931; Klauss et al., 1970). In recent decades, professional societies and agencies charged with setting standards for built environments have formulated standards for ventilation of indoor environments. For example, the American Society for Heating, Refrigerating, and Air-Conditioning Engineers (ASHRAE) developed Standard 62, which is a ventilation standard designed to achieve acceptable indoor air quality (ASHRAE, 2003). This standard has been revised several times since its initial publication and now includes Standard 62-2, which sets

specific standards for residential ventilation. One key assumption of this strategy is that freshly supplied air is less polluted than the air it replaces, reducing indoor pollutant concentrations. Another critical assumption is that the impact of an appropriate ventilation rate will dominate any other physical and chemical processes occurring in the indoor environment. However, the dependence of individual indoor pollutant levels on ventilation rates varies among pollutants (Sundell et al., 2011). In fact, using emission data from households across the United States, Sherman and Hodgson (2004) estimated an average whole-home emission rate of formaldehyde and found that this value remained steady over time independent of household ventilation rates. Physical and chemical characteristics of a given pollutant and processes that govern its fate and transport may make the pollutant more or less amenable to removal via ventilation. Seasonal and diurnal variation in temperature and relative humidity may also have a substantial impact on the capacity of ventilation to reduce indoor concentrations of certain pollutants, such as formaldehyde (Matthews et al., 1986; Silberstein et al., 1988). With respect to the impact of ventilation on indoor formaldehyde concentrations, studies that have investigated the direct impact of ventilation on formaldehyde concentrations have not demonstrated an association between increasing ventilation rates and decreasing long-term formaldehyde concentrations (Hodgson et al., 2000; Hun et al., 2009; Malkin-Weber et al., 2009). Only in new homes, where initial concentrations are generally highest, have increasing ventilation rates been weakly correlated to decreasing formaldehyde concentrations (Hun et al., 2009; Gilbert et al., 2008). In many buildings, ventilation rates exceed standard requirements, yet formaldehyde concentrations are still above guideline values. Even when increased ventilation correlates to a measurable decrease in formaldehyde concentrations, additional treatment strategies may be needed (Hodgson et al., 2003).

In the majority of residential housing and commercial buildings, proper ventilation is achieved with the aid of mechanical processes that consume energy. However, as demand for energy efficient buildings and residences increases, strategies to reduce building or home energy consumption frequently reduce air exchange rates. For example, home weatherization assistance programs received a substantial increase in federal funding in 2009 through the American Recovery and Reinvestment Act to increase energy efficiency in the affordable housing sector. The funding was provided to support weatherization of homes by adding insulation, sealing leaks, and modernizing heating and air conditioning equipment. Under these conditions, air exchange rates decrease and the potential for indoor air quality to be negatively impacted increases. Thus, alternatives to ventilation are greatly needed to simultaneously achieve desired energy efficiency and healthy indoor air quality.

2.3.3 Pollutant control technology

To date, the indoor air treatment industry has focused almost exclusively on particle filtration, but when gas phase pollutant control systems are employed, the most widely used method for pollutant removal is adsorption (VanOsdell et al., 1996). Physical adsorption is defined as the preferential partitioning and accumulation of one or more chemical species at an interfacial layer. Intermolecular interactions of this type are due to van der Waals forces, comprising Keesom, Debye, and London dispersion forces, all of which are weaker than traditional chemical bonds. Typical enthalpies of physical adsorption range in the tens of kJ per mole compared to chemical bond enthalpies in the hundreds of kJ per mole. The most common adsorbent material used is activated carbon with granular activated carbon (GAC) representing the most common form of activated

carbon in use (Henschel, 1998). More recently, applications using carbon fibers are increasing as the technology matures.

Activated carbon is widely used as a part of gas-phase pollutant control systems in both individual, single-family households, as well as commercial and industrial environments. In such applications, activated carbon is typically employed to remove well-known hydrophobic organic compounds, such as benzene and toluene. The volatile organic compounds (VOCs) listed in Table 2.2 represent commonly monitored compounds in indoor environments. Due to the frequency with which these compounds are detected, the concentrations at which they are measured, and the potential health risks posed by either acute or chronic exposure at measured indoor concentrations, activated carbon adsorption of nearly all of these compounds has been studied.

Table 2.2. Volatile organic compounds commonly detected in indoor environments.

Compound family	Compound	GM concentration [$\mu g/m^3$]	Reference
aromatics	Benzene Toluene m-Xylene p-Xylene o-Xylene Styrene	3, 3.6 15.1, 31.4 3.8, 7.4 4.2 3.2 0.9, 1.3	Wallace, 1991; Brown et al., 1994; Wallace, 2001; Singh et al., 2002; Daisey and Angell, 2003; Hodgson, 2003
chlorinated	Chloroform 1,1,1-Trichloroethane Trichloroethylene Tetrachloroethylene p-Dichlorobenzene	2.1, 4.1 1.4, 2.7 2.1 1.9 2.9, 96.4-301.2	Wallace, 1991; Brown et al., 1994; Singh et al., 2002
phenolic	d-Limonene α-Pinene	1.1, 30.5 3.7, 125.4	Wallace, 1991; Brown et al., 1994; Hodgson, 2003; Rappaport and Kupper, 2004
aldehydes	Formaldehyde Acetaldehyde	20.4, 122.7–404.9 29.0	Wieslander et al., 1997; Hodgson, 2003

As a recent example, Yao et al. (2009) focused on predicting the adsorption behavior of 18 select VOCs on activated carbon fibers over a concentration range of 20-

300 ppb_v using Dubinin-Radushkevich (D-R) and Freundlich models. Although Yao et al. initially considered formaldehyde among their 18 primary VOCs for evaluation, ultimately no assessment of its adsorption behavior was made because the D-R model was not considered appropriate for polar compounds with dipole moments greater than 2 Debye (μ_{HCHO} = 2.33 Debye).

Only a limited number of investigations have been conducted to evaluate gas-phase formaldehyde adsorption on activated carbon. Most of these studies have considered single formaldehyde concentrations ranging from 2.3 ppm_v-74,000 ppm_v, which are much higher than what is observed in indoor environments (Rong et al., 2001; Boonammuayvitaya et al., 2005; Song et al., 2007). Only one study has evaluated activated carbon performance at a concentration of formaldehyde (30 ppb_v) relevant to typical residential environments (Sidheswaran et al., 2010). No studies generated sufficient data to develop a complete isotherm or evaluate appropriate adsorption isotherm models. Moreover, no studies have measured or modeled the impact of water vapor on formaldehyde adsorption onto activated carbon. Adsorption of acetaldehyde (which differs from formaldehyde by the replacement of a hydrogen with a methyl group) has been studied more extensively than formaldehyde adsorption with respect to indoor air treatment, and pertinent studies were reviewed for the insight they might provide, by extension, regarding formaldehyde treatment. Acetaldehyde adsorption to activated carbon has been the subject of several studies, including one study that applied the Dubinin-Radushkevich equation to model an acetaldehyde adsorption isotherm (Cal et al., 1997). Still, no literature data for acetaldehyde adsorption at typical indoor concentrations has been reported, and no efforts have yet been made to quantify, model, or predict the impacts of water vapor on acetaldehyde adsorption. Furthermore, of the small number of studies examining the impact of the physical and chemical properties of

activated carbon on formaldehyde (Song et al., 2007) or acetaldehyde adsorption (Dimotakis et al., 1995; El-Sayed and Bandosz, 2002), none have used these relationships to propose removal processes on a mechanistic level. Previous research indicates that activated carbon surface properties can be used to develop a systematic method of predicting sorption behavior (Cal et al., 1997; Karanfil and Kilduff, 1999; Franz et al., 2000). Only a handful of researchers have looked at gas-phase adsorption in systems with two or more components. This work has been limited to traditional, hydrophobic organic compounds, such as toluene and benzene, but suggests that competitive adsorption is also important to consider for formaldehyde.

Because very few studies have quantified formaldehyde removal by activated carbon, understanding of formaldehyde removal mechanisms facilitated by activated carbon is also limited. If formaldehyde were removed by GAC via adsorption, as a polar, hydrophilic pollutant rather than a hydrophobic one, it would be more likely to be removed by GAC via specific interactions controlled by chemical surface functional groups or electron-donating regions at the GAC surface. Catalysis of volatile organic compounds on supported noble metals, single/mixed metal oxides, noble metal/metal oxide combinations, and photocatalysts such as titanium dioxide have been studied in depth. However, much less is understood about the role that activated carbons play as heterogeneous catalysts. No known studies have suggested or investigated catalytic oxidation of formaldehyde by GAC, but recently, several researchers investigating acetaldehyde removal using GAC (El-Sayed and Bandosz, 2002), and hydrogen sulfide removal using GAC (Adib et al., 2000; Bashkova et al., 2007) independently proposed that, in addition to adsorption, catalytic activity takes place at the activated carbon surface. Unfortunately, the use of the term catalytic activity lacked clarity, and no definition or evidence of catalytic behavior was presented in the

work published on this topic. The work presented in this dissertation sought to elucidate the role of surface chemistry in sorptive and potentially catalytic mechanisms that govern gas-phase treatment of formaldehyde using activated carbon.

2.4 ACTIVATED CARBON

2.4.1 Structural and chemical properties of activated carbon

The general structure of activated carbon has been well studied, and understanding of this material as an adsorbent has evolved through its application to water treatment, industrial air treatment, and vapor recovery. This knowledge may be adaptable to indoor applications. Activated carbon is a favored adsorbent because of its high specific surface area situated within a network of pores classified by size into three categories: micropores (width less than 2 nm), mesopores (width from 2-50 nm), and macropores (width greater than 50 nm) (Gregg and Sing, 1982). Of these three, micropores not only contribute most to the specific surface area, but their narrow dimensions and consequently higher adsorption potentials (relative to wider pores or flat, graphitic surfaces) promote adsorption of small molecules, such as gases, which otherwise would not be captured by the adsorbent. Furthermore, the shape of the micropores may result in hysteresis, a potentially desirable phenomenon with respect to air treatment in which molecules, once adsorbed, will only desorb at relative pressures lower than those at which they adsorbed.

While microporosity is necessary for a given activated carbon adsorbent to exhibit high adsorption capacity, the chemical properties play an equally important role in adsorption processes. However, in research and in practice the surface chemical characteristics of activated carbon are often underappreciated. Activated carbon consists of overlapping aromatic sheets of carbon (Figure 2.2 (a)), and the less ordered the

arrangement of the graphitic carbon sheets, the more likely there is to be variation in the distribution of the electron clouds associated with the carbon skeleton. A disordered arrangement creates unpaired electrons and incompletely saturated valences (Figure 2.2 (b)), which influence adsorption processes, especially for polar or polarizable compounds.

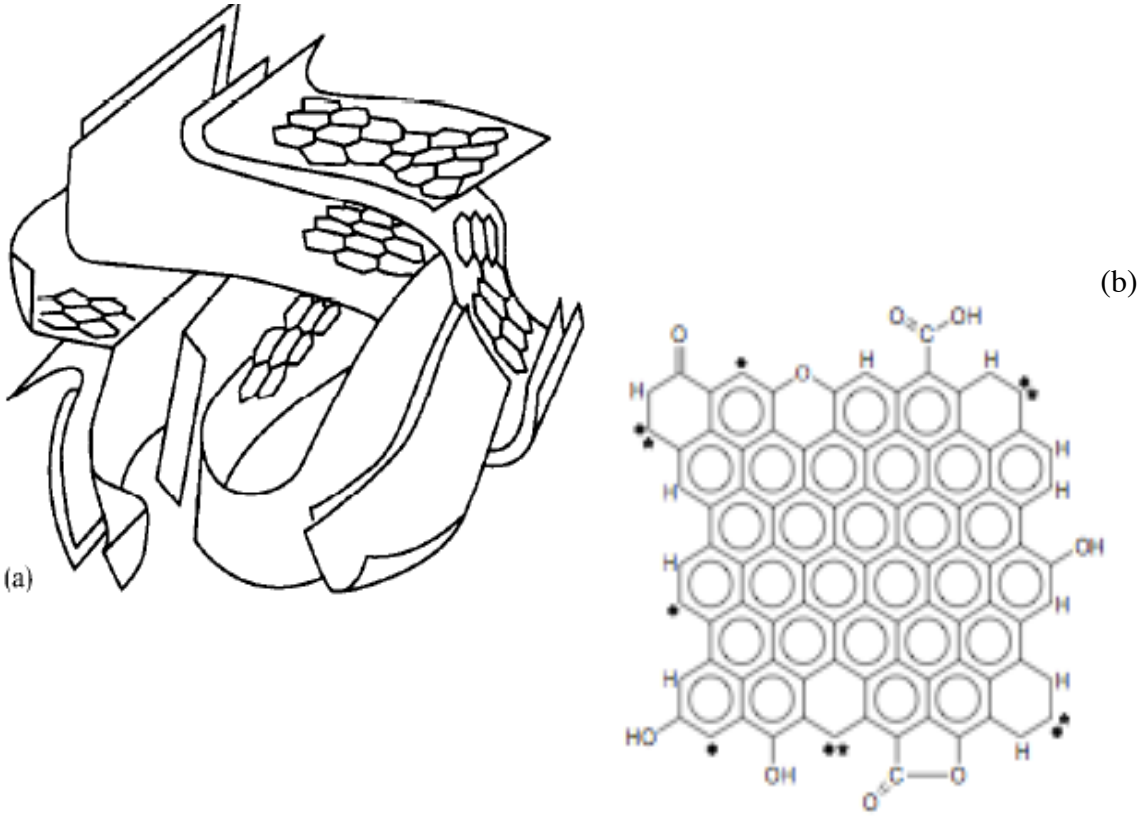

Figure 2.2. Schematic representation of (a) overlapping aromatic carbon sheets and (b) a single graphene layer including oxygen-functional groups at edge-plane sites. Dots and dots with * represent unpaired sigma electrons and in-plain sigma pairs, respectively (Rodriguez-Reinoso and Molina-Sabio, 1998).

The edges of the overlapping sp^2- hybridized carbon sheets are also interspersed with functional groups containing heteroatoms—mostly oxygen and hydrogen, and sometimes nitrogen. Surface functional groups (SFGs) frequently have either electron-

withdrawing or electron-donating character and, thus, affect neighboring electron density distribution. Although often accounting for no more than 10-15% of the activated carbon chemical composition, the presence and chemical character of surface functional groups control a variety of the activated carbon surface properties, including polarity, acidity, basicity, and reactivity. SFGs also clearly influence the mechanisms associated with adsorbate-surface interactions and the extent and specificity of adsorption (Dimotakis et al., 1995; Karanfil and Kilduff, 1999; Li et al., 2002), as well as heterogeneous catalysis (Rodriguez-Reinoso, 1998). Identification and quantification of SFGs is critical to the elucidation of mechanisms governing adsorption and heterogeneous catalysis and could lead to useful performance metrics for activated carbon and even other adsorbent media.

Oxygen atoms bound to the surface of activated carbon via chemisorption yield a variety of functional groups that account for the majority of activated carbon's surface acidic or basic character and play a decisive role in adsorption behavior. Carboxyl, hydroxyl, and lactonic groups, as illustrated in Figure 2.3, impart acidic and hydrophilic properties to the activated carbon surface, and the abundance of such sites is increased through treatment without great difficulty (Cal et al., 1997; Barton et al., 1997) and readily quantifiable (Boehm, 2002). Adsorbates capable of sorptive interactions with electron-accepting SFGs may associate more with specific acidic surface sites and be less susceptible to desorption.

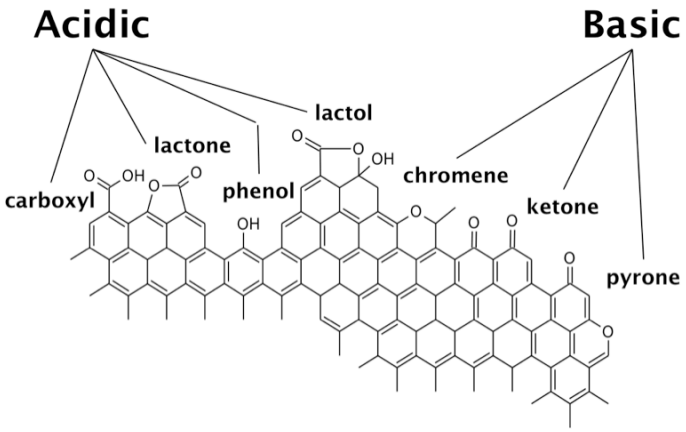

Figure 2.3. Representative oxygen-containing acidic and basic functional groups. Adapted from Rodriguez-Reinoso and Molina-Sabio, 1998.

Additional surface oxides anticipated to exist or be generated through treatment at the edges of activated carbon basal planes include chromenes, pyrones, and quinones, (Figure 2.3), which contribute to activated carbon basicity (Menendez, 1996). Suárez et al. (1999) showed that a wide range of base strength may be predicted for pyrone-like structures. However, numerous investigations suggest that the majority, or at least a significant portion, of the basic character of activated carbon is instead attributable to aromaticity, or delocalized π electrons. Thus, it is more challenging to differentiate and precisely quantify basic surface sites using the same methods that are typically employed for surface acidity quantification because basicity can result from either specific SFGs or dispersed Lewis basicity (electron-donating character) arising from the carbon structure (Barton et al., 1997).

2.4.2 Surface modification and nitrogen-doping of activated carbon

Nitrogen is another important heteroatom that alters the physicochemical properties of activated carbon materials. Whether incorporated into the carbon ring structure or as functional groups at the edge plane sites, nitrogen has the potential to

appreciably enhance basic properties of carbon surfaces (Montes-Moran, 2004). Intentional nitrogen-doping of activated carbon has been shown to increase surface basicity (Menendez et al., 1996; Biniak et al., 1997; Abe et al., 2000; Lázló, 2001; Nowicki et al., 2008) and impart apparent catalytic properties (Stoehr et al., 1991; Bagreev et al., 2004) to the carbon. Depending on the nitrogen-doping process used, a variety of nitrogen-containing surface functional groups and moieties may result, many of which are illustrated in Figure 2.4.

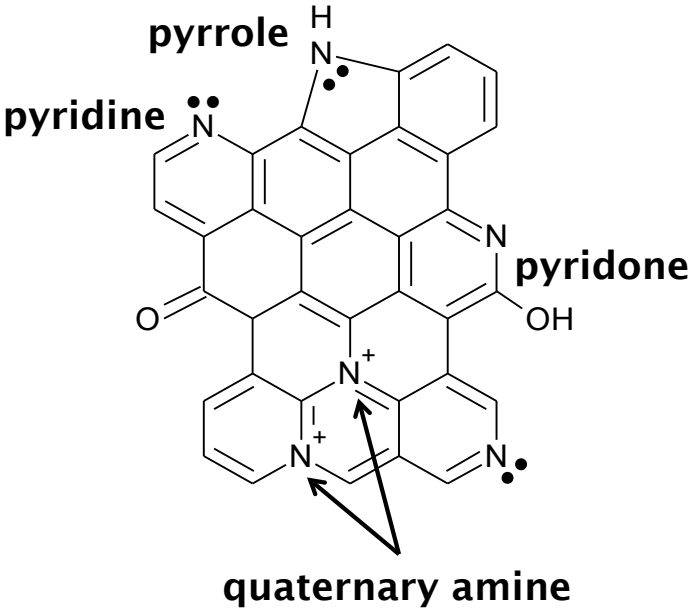

Figure 2.4. Representative nitrogen-containing functional groups. Adapted from Lázló, 2005.

The more desirable nitrogen-containing surface functional groups, with respect to carbon catalysts, include the pyridinic and pyrrolic species, because of their contribution of p orbital π-electrons to the graphitic π-system. Delocalized over the sp^2-hybridized graphene layers, these extra electrons could significantly alter catalytic properties of the activated carbon toward reactions involving electron transfer. For example, removal of hydrogen sulfide gas (Bagreev et al., 2004; Mihkalovsky and Zaitsev, 1997) and removal

of sulfur dioxide gas (Strelko et al., 2000; Bimer et al., 1998; Mochida et al., 1992) have been enhanced by employing nitrogen-doped granular activated carbons or activated carbon fibers.

2.4.3 Techniques for structural and chemical characterization of activated carbon

A distinctive and vital component of this work will be the series of molecular-level analyses each activated carbon sample will undergo to elucidate structural and chemical surface properties of the GACs investigated in this research. With respect to physical and structural properties, GACs are microporous materials that exhibit high specific surface areas and heterogeneous pore size distributions. Inert gas adsorption to this varying pore structure results from two mechanisms: 1) primary pore-filling through capillary condensation in pore widths of one to two adsorbate (*e.g.*, nitrogen, N_2) molecular dimensions and 2) secondary pore-filling due to adsorbate-adsorbate (e.g.N_2-N_2) interactions (not capillary condensation) in pore widths between 2-5 adsorbate molecular dimensions (Rodriguez-Reinoso and Molina-Sabio, 1998). Analysis of surface area, pore volume, and pore size distribution is often made using nitrogen adsorption isotherms at 77 K. The Brunauer, Emmett, and Teller (BET) model is widely used and suitable for determining and comparing specific surface area among a set of the selected GACs (Stoehr et al., 1991). Models based on molecular-based, statistical, thermodynamic Density Functional Theory (DFT), which work well with microporous materials, are effective for determining pore dimensions, pore size distributions, and pore volumes (Olivier et al., 1995).

To address chemical characterization, a combination of spectroscopic and selective titration techniques can be used to investigate the carbon surface chemical properties, including X-ray photoelectron spectroscopy (XPS), Raman spectroscopy, and

Boehm and iodometric titrations. XPS analysis of GAC samples allows for quantitative determination of the surface elemental composition and the oxidation states of the elements detected (Jansen and Bekkum, 1995). In this way, it is possible to confirm the presence or absence of important non-carbon surface functional groups. XPS analysis is also critical for evaluation of the oxidation state of nitrogen added to a GAC matrix and verification that desirable nitrogen-containing moieties are produced.

To further improve understanding of the interfacial processes that govern formaldehyde removal at the activated carbon surface, additional characterization of surface chemistry is often necessary. In addition to the techniques mentioned above, Raman spectroscopy is particularly well suited for structural characterization of carbon materials (Dresselhaus et al., 1988; 2005), offering key information about non-carbon, edge-plane defects and sp^2 cluster size relative to sp^3 bonding structure content (Shimodara and Masui, 2002), or put another way, the graphitic and disordered nature of a given material. Activated carbon, inherently an amorphous carbon allotrope, exhibits both sp^2- and sp^3-hybridized regions of carbon bonding, and nitrogen-doping is likely to alter the proportion of those two regions relative to one another. Graphitic, or sp^2-hybridized carbon, is associated with the Raman G (for graphitic) band, while disordered, sp^3-hybridized carbon is associated with the Raman D (for disordered) band. The ratio of the intensity of the D band, I_d, to that of the G band, I_g, can be determined through analysis of first-order Raman spectra and used to quantify the extent of disorder in a carbon material. Second-order Raman spectra analysis can provide additional, interesting evidence of extent of disorder in a given carbon matrix (Maldonado and Stevenson, 2005). In the case of activated carbon, it has been shown that plotting the Raman peak shift and the full width at half maximum for the G and D bands yields additional

information about the size and extent of sp^2 graphitic domains and sp^3 disordered bond domains (Shimodara and Masui, 2002).

Boehm and iodometric titration techniques support identification and quantification of acidic and basic surface sites. Boehm pioneered efforts to characterize oxygen-containing surface functional groups by titrating the activated carbon surface with several bases of varying strengths (Boehm, 1994). This approach is a successful method for quantifying oxygen-containing surface functional groups that act as Brønsted acids. Similarly, the Boehm method is also capable of quantifying surface sites that act as Brønsted bases. However, this method does not elucidate Lewis basicity. Oxygen-containing groups that have potential to act as Lewis bases, including ethers and carbonyls, may not be accounted for at all. To make up for this shortcoming, iodometric titrations can be employed as an additional chemical titration technique. Iodometric titrations have been instrumental in various studies that seek to determine the electron-donating character of carbons, and the method employed by Oliviera et al. (2004) has become routine in the activated carbon field. Normalized on a per-mass basis, results from iodometric titrations are expected to exceed those of the Boehm titrations, and the difference should represent carbon basicity arising from delocalized π electrons in the carbon matrix.

Research geared toward the evaluation or selection of activated carbons for specific contaminants require this wide array of surface analytical techniques to clearly identify and quantify all unique contributions to acidity and basicity at the activated carbon surface. In so doing, it is possible to identify sources of electron-donating and electron-withdrawing behavior and then evaluate their relative contribution to overall removal and potential degradation of contaminants such as gas-phase formaldehyde. Detailed surface chemical characterization of activated carbons, taken in conjunction

with studies that confirm the positive impact of carbon basicity on gas phase adsorption of aldehydes (El-Sayed and Bandosz, 2002; Song et al., 2007), motivates a shift away from traditional trial and error approaches to adsorbent media selection toward one in which fundamental surface analysis precedes the design of surfaces for removal and selection of a desired pollutant control technology. In this light, activated carbon is a particularly attractive adsorbent material because of its proven potential to acquire desired surface functionality through treatment (Franz et al., 2000; Abe et al., 2000; Lillo-Rodenas et al., 2002). The combination of analytical techniques to evaluate surface chemical characteristics provides an unprecedented level of specific knowledge about the surfaces of traditional and chemically treated commercially available GACs, as well as chemically treated, laboratory-prepared GAC with respect to their applications in environmental engineering. This knowledge is central to evaluating the potential for adsorption, desorption, and catalytic activity over the service life of a given GAC.

2.4.4. Characteristics of removal processes at GAC surfaces

Adsorption and catalysis are the two removal processes by which GAC is capable of pollutant control. Adsorption on GAC is studied to a much greater extent and more widely applied than catalytic processes. Adsorption and desorption processes are strongly influenced by a variety of sorptive mechanisms controlling the interactions between the pollutant adsorbates and the GAC media. Irreversible adsorption, also known as chemisorption, develops from a chemical reaction that forms a bond between an adsorbate and a specific site on the adsorbent surface with a bond energy on the order of several hundred kilojoules per mole (kJ/mol), which is typical of covalent chemical bonding. While irreversible adsorption minimizes desorption potential, it also limits the potential for adsorbent regeneration. In contrast, physisorption is weaker than

chemisorption and reversible, being governed by short-range, attractive, intermolecular forces including permanent dipole-dipole, induced dipole-dipole, and London dispersion forces. Physisorption may arise from non-specific or specific surface interactions. Traditionally, non-specific surface interactions have proven advantageous for conventional adsorption of hydrophobic hydrocarbons. To increase the adsorption capacity of activated carbon for polar molecules, such as formaldehyde, it is necessary to modify the surface chemistry of the activated carbon to become more polar (Rodriguez-Reinoso et al., 1998).

Specific, yet weaker, hydrogen bonding between adsorbates and surface sites may also promote removal of a gas-phase species to the activated carbon surface. Compounds with electron-donating character and hydrogen bond formation potential, like aldehydes, could experience enhanced removal through these specific interactions. Furthermore, the presence of water vapor at the activated carbon surface may also provide additional opportunity for hydrogen bonding to take place (Dimitrova, 1993) and thus further mediate removal of formaldehyde or acetaldehyde to the activated carbon surface.

To understand the long-term capacity of activated carbon to reliably control pollutant concentrations, it is important to understand the desorption potential of the given pollutant. If the activated carbon is intended for disposal after use, as is frequently the case with filters designed for residential heating, ventilating, and air-conditioning (HVAC) systems, irreversible adsorption would be desirable. In contrast, if the activated carbon will be regenerated during its lifetime, adsorption must be reversible, at least under certain conditions. Even if the activated carbon will be regenerated numerous times during its service life, slow desorption kinetics, or desorption hysteresis, is desirable in the context of this work such that, once adsorbed, the pollutant will not readily desorb once the contamination event has passed.

Slow pollutant desorption is influenced by the extent to which specific surface interactions develop between the pollutant and surface sites and the strength of these interactions (Yonge et al., 1985). Furthermore, specific interactions that increase the likelihood of irreversible removal are more likely to predominate at low surface coverage—the condition on which this work will focus. Irreversible adsorption can also result from chemical reactions catalyzed by the carbon surface, yet strong evidence verifying catalytic activity at activated carbon surfaces in environmental engineering applications is lacking from current literature.

The application of carbon-based materials as catalysts is becoming more widespread, and numerous compounds are already known to be readily oxidized at the activated carbon surface as a result of surface oxide ions that form when aromatic π electrons transfer to irreversibly adsorbed oxygen (Zawadzki, 1989). Edge-plane sites, where electron transfer rates are reported to be 105 times higher than in the basal planes (Rice and McCreery, 1990), play a particularly important role in the catalytic potential of activated carbon. It is understood that oxygen gas diffuses to the activated carbon surface, where it is subsequently reduced to $O_2^{-}\bullet$, yielding an adsorbed superoxide radical. However, the active sites that facilitate this reaction and possibly provide a site for the adsorbed superoxide radical are still not well understood. To evaluate the catalytic potential of activated carbon, it is critical that a better understanding of catalytically active sites be developed.

Catalytic transformation of formaldehyde and acetaldehyde at the activated carbon surface most likely results from oxidation of these species. Oxygen-containing surface functional groups represent one potential group of surface sites that could promote catalysis. For instance, the Mars-van Krevelen (MvK) catalytic mechanism proposed that oxygen-containing surface functional groups initiate the reaction sequence

with the insertion of a single oxygen atom into the adsorbate. To accommodate this reaction, neighboring atoms in the treatment media matrix must be capable of changing their oxidation state to facilitate the redox cycle and electron transfer (Doornkamp and Ponec, 2000). It is expected that the surface oxygen sites are subsequently replenished by atmospheric O_2 (Doornkamp and Ponec, 2000). This mechanism has been proposed for formaldehyde oxidation by metal oxide catalysts (Sidheswaran et al., 2010). If oxygen-containing functional groups are present at the activated carbon surface, this same mechanism could potentially take place such that activated carbon catalytically oxidizes formaldehyde.

Nitrogen-containing surface functional groups also play a critical role in promoting catalysis, and the impact of nitrogen content on catalytic activity of activated carbons involving electron transfer reactions has been well documented (Rideal and Wright, 1926; Stoehr et al., 1991; Strelko, 2000). Yet, the specific contribution of nitrogen to catalytic activity at the activated carbon surface is one that needs further investigation (Strelko, 2000). Several research groups postulate that nitrogen-containing functional groups contribute π electrons to the basal planes and at edge sites and thus enhance catalytic activity of activated carbon by facilitating the formation of superoxide species (Rodriguez-Reinoso, 1998; Figueiredo and Pereira, 2010). Alternatively, a phenomenological approach taken by Strelko et al. (2000) interprets observed correlations between nitrogen content and activated carbon activity in light of semiconductor properties. This approach proposes that incorporation of nitrogen atoms into the graphitic carbon matrix lowers the band gap, which increases electron mobility and lowers the electron work function at the activated carbon/gas phase interface relative to unaltered carbons. As a result, electron transfer reactions proceed more readily, enabling superoxide radical production and subsequent pollutant oxidation.

As mentioned above, formaldehyde or acetaldehyde removal capacity of activated carbon materials has been shown to increase with increasing incorporation of nitrogen at edge-plane sites (El-Sayed and Bandosz, 2002; Song et al., 2007). Only recently have similar studies drawn the conclusion that enhanced removal of a low molecular weight aldehyde (in this case, acetaldehyde) was attributable to catalytic activity (Bagreev and Bandosz, 2004). This is a hypothesis that could reasonably be extended to formaldehyde as well.

2.4.5 Impacts of relative humidity and water vapor adsorption on removal processes

Previous work has also shown that the adsorption of organic vapors onto surfaces depends on temperature and relative humidity (Pennell et al, 1992). Indoor environments are unsaturated with respect to water vapor, with relative humidity levels typically ranging from 30-70%. Hence, competition with water vapor for the activated carbon surface should be fully understood throughout this range. As mentioned previously, adsorption of hydrophobic gas phase organic compounds to activated carbon typically decreases as relative humidity increases above 30-40% (Cal et al., 1997; Qi and LeVan, 2005). Water vapor can out-compete hydrophobic organic compounds for adsorption sites by clustering at and blocking pore entrances or by filling pores (capillary condensation). However, if the gas-phase organic compounds are polar and highly soluble in water, such as is the case for low molecular weight aldehydes, cooperative adsorption may occur via dissolution of aldehydes into an adsorbed water vapor film or condensed phase. This would be beneficial for low molecular weight aldehyde removal from indoor environments where relative humidity is generally high enough to observe non-negligible water vapor adsorption onto activated carbon.

Typically, the competition for adsorption at the activated carbon surface between hydrophobic organic compounds and water vapor introduced via relative humidity tends to drive down organic vapor adsorption and is seen as disadvantageous (Rudisill et al., 1992; Chou and Chiou, 1997; Qi and LeVan, 2005). Competition between water vapor and low molecular weight polar organic compounds has not been studied. Extensions of the work by Pennell et al. (1992) reveal that relationships describing the dependence of organic vapor adsorption and desorption on temperature and relative humidity are governed by parameters that correlate to physical and chemical properties of the adsorbates, such as liquid vapor pressure and capacity for hydrogen-bond formation (Goss, 1997). Similarly, adsorbent chemical and physical properties have a measureable impact on the mechanism and extent of adsorbate-adsorbent interactions (Dimotakis et al., 1995; Karanfil and Kilduff, 1999; Franz et al., 2000). Findings such as these stress the importance of seeking a fundamental, physical/chemical basis for parameters used to model sorption behavior and the need to study multi-solute adsorption that includes water vapor among the solutes of interest.

Interfacial processes greatly influence the mobility and distribution of many indoor contaminants (Lee et al., 2005), but these processes are not yet well characterized for indoor environments (Tichenor et al., 1991; Colombo et al., 1993; Morrison, 2008) and not characterized at all for formaldehyde. Furthermore, mechanisms additional to physical adsorption, such as chemisorption or catalytic oxidation, have yet to be studied in depth for formaldehyde on activated carbon, although there is evidence to suggest that such additional mechanisms may make a non-negligible contribution to formaldehyde removal. Surface analytical techniques can be used in conjunction with carefully designed experimental studies of contaminant removal to elucidate removal mechanisms and to eventually develop models to predict treatment efficiency. Surface analytical tools

can also be used to identify and quantify structural and chemical properties of activated carbon, which, in turn, need to be linked to type and extent of contaminant removal mechanisms, a connection that has often been lacking in the indoor environmental literature.

In response to the need for sustainable and healthy indoor environments, there is steady interest in tailoring the surfaces of building materials to remove gas phase pollutants. This literature review has demonstrated the value of considering chemical and physical properties of both pollutants of interest and pollutant control technology when a mechanistic understanding of pollutant removal is sought. Unfortunately, it also highlights the lack of data available for studies under indoor environmental conditions that carefully consider pollutant physical/chemical properties or analyses of surface characteristics of pollutant control technology (Ataka et al., 2004). As a result, removal mechanisms in indoor environments remain largely unspecified.

Chapter 3: Continuous Measurement of Formaldehyde in Indoor Environments

3.1 Overview

Despite long-standing awareness of adverse health effects associated with chronic human exposure to formaldehyde, this hazardous air pollutant remains a challenge to measure in indoor environments. Traditional analytical techniques evaluate formaldehyde concentrations over several hours to several days in a single location in a residence, making it difficult to characterize daily temporal and spatial variation in human exposure to formaldehyde. There is a need for portable, easy-to-use devices that are specific and sensitive to gas-phase formaldehyde over short sampling periods so that dynamic processes governing formaldehye fate, transport, and potential remediation in indoor environments may be studied more effectively. A recently developed device couples a chemical sensor element with spectrophotometric analysis for detection and quantification of part per billion (ppb_v) gas-phase formaldehyde concentrations. This study established, for the first time, in a laboratory setting, the ability of the coupled sensor-spectrophotometric device (CSSD) to report formaldehyde concentrations accurately and continuously on a thirty-minute sampling cycle at low ppb_v concentrations previously untested for this device in a laboratory setting. Determination of the method detection limit (MDL), based on forty samples each at test concentrations of 5 and 10 ppb_v, yielded MDL values of 1.9 and 2.0 ppb_v, respectively. Performance of the CSSD was compared to the dinitrophenylhydrazine (DNPH)-derivatization method for formaldehyde concentrations ranging from 5-50 ppb_v, and a linear relationship with a coefficient of determination, R^2, of 0.983 was found between these two analytical techniques. The CSSD was also used to continuously monitor indoor formaldehyde concentrations in two manufactured mobile homes over the course of five days. During

this time formaldehyde concentrations varied from below detection limit to 65 ppb_v and were above the US National Institute for Occupational Safety and Health (NIOSH) recommended exposure limit (REL) of 16 ppb_v, which is also the exposure limit value required by the U.S. Federal Emergency Management Agency (FEMA) to procure manufactured housing, 80% and 100% of the time, respectively.

3.2 BACKGROUND INFORMATION

Increased understanding of the health risks associated with human exposure to formaldehyde at concentrations observed in indoor environments, which may range from ~4-110 ppb_v (Offermann, 2009), and a growing trend to lower chronic recommended exposure limits have accelerated the need for analytical techniques capable of measuring ppb_v formaldehyde concentrations dynamically.

Numerous international organizations and national- or state-level governmental agencies have developed a range of recommended exposure limits for formaldehyde. For instance, following reports from the Agency for Toxic Substances and Disease Registry and the US Centers for Disease Control of high formaldehyde concentrations in manufactured (prefabricated) housing provided by the United States Federal Emergency Management Agency (FEMA) to families who were displaced by hurricanes Katrina and Rita in 2005, FEMA implemented procurement guidelines for manufacturers of mobile and manufactured housing. The guidelines require formaldehyde in all manufactured housing units to be less than the recommended exposure limit (REL) set by the National Institute for Occupational Safety and Health (NIOSH) of 16 ppb_v over an eight hour period (NIOSH, 2009). On the global scale, the World Health Organization has set a 30-minute and chronic recommended exposure limit (REL) for formaldehyde of 81 ppb_v (WHO, 2010), which has been under consideration for twenty-five years (WHO, 1987).

A summary of recommended exposure limits for non-cancer effects from various agencies in the US and around the world is presented in Table 3.1.

Table 3.1: Recommended exposure limits and threshold limit values for formaldehyde with respect to non-cancer health effects

Agency	Recommended Exposure Limits for Non-Cancer Health Effects [ppb_v]	Exposure Time Period
CA EPA OEHHA[1]	7.3	8-hr and chronic
France AFSSET[2]	8.1	Threshold limit
US EPA[3]	Under review	NA
US NIOSH[4]	16	10-hr in 40-hr work week
HK IAQ MG[5]	<24	8-hr
CA EPA ARB[6]	26	8-hr
Health Canada[7]	40	8-hr
WHO[8]	81	30 min

[1] California Environmental Protection Agency, Office of Environmental Health Hazard Assessment (CA OEHHA, 2008)

[2] French Agency for Environmental and Occupational Health Safety, AFSSET (Mandin et al., 2009)

[3] US Environmental Protection Agency

[4] (NIOSH, 2009)

[5] Hong Kong Indoor Air Quality Management Group (HK IAQ MG, 2003)

[6] California Environmental Protection Agency, Air Resources Board (CARB, 2004)

[7] (Health Canada, 2006)

[8] World Health Organization (WHO, 2010)

A different recommended exposure limit has been developed for formaldehyde to take into consideration cancer effects associated with formaldehyde exposure. Only in exceptional cases would the guideline value of 1.63 ppb_v for 1 in 100,000 lifetime cancer risk set by the CA OEHHA (CA OEHHA, 2009), which is less than typical outdoor levels (Offermann, 2009), be attainable in residences. Current analytical techniques must

continue to advance to monitor indoor formaldehyde concentrations down to this low level.

Traditional sampling methods for formaldehyde in indoor environments rely on pre-concentration and derivatization phases during sampling, after which the sample must undergo further preparation to be analyzed by the appropriate chromatographic or spectroscopic technique. Numerous reviews thoroughly describe *in situ* and derivatization-based sampling methods and analytical techniques or directly compare in detail two or more existing techniques (Hak et al., 2005; Wisthaler et al., 2008; Salthammer and Mentese, 2008; Barro et al., 2009; Salthammer et al., 2010). Of the many techniques outlined in these studies, the DNPH method has become the accepted international standard procedure for analysis of formaldehyde in indoor air by the International Organization for Standardization and is described within the EPA method TO-11A and the ASTM D5197 for the determination of aldehydes in air. This and other derivatization methods suffer from long sampling times, typically several hours to several days, thus precluding the study of dynamic processes. In response to a need for shorter sampling times, Martos and Pawliszyn (1998) developed a method that employs derivatization of formaldehyde with o-(2,3,4,5,6-pentafluorobenzyl) hydroxylamine hydrochloride (PFBHA) on solid phase microextraction (SPME) fibers followed by thermal desorption onto a gas chromatograph and detection by flame ionization (FID) or electron capture (ECD).

Initial efforts to achieve near-continuous, dynamic sampling and quantitative determination of low ppb_v, gas-phase formaldehyde concentrations were made in this work using the on-fiber derivatization PFBHA-SPME-GC-ECD method. This method starts with PFBHA adsorption to the polydimethylsiloxane/divinylbenzene (PDMS/DVB) coating on an extruded SPME fiber (Figure 3.1).

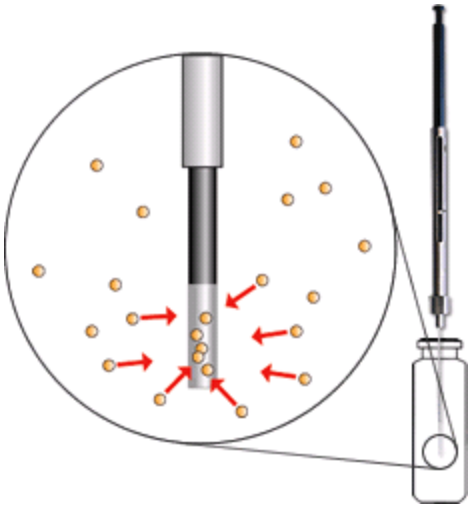

Figure 3.1. Schematic representation of PFBHA adsorption to SPME fiber prior to exposure to gas-phase formaldehyde.

Then, the PFBHA-loaded SPME fiber is exposed to the experimental environment, and gas-phase formaldehyde adsorbs to the fiber surface, where a reaction between formaldehyde and PFBHA will produce an oxime (Figure 3.2) that remains adsorbed to the surface.

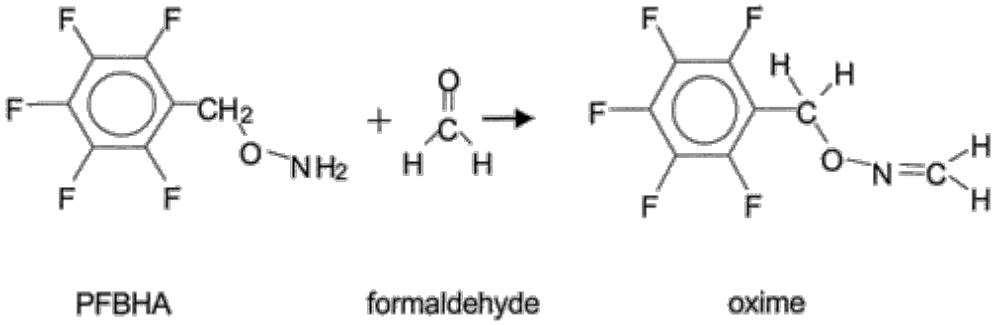

Figure 3.2. Schematic of chemical reaction between PFBHA and formaldehyde to form oxime product.

Subsequent analysis using GC-ECD allows for the quantitative determination of the mass of the oxime formed (Figure 3.3 (a)). To relate the mass of oxime formed to the gas-phase formaldehyde concentration, the inverse of the mass of oxime formed is plotted

against the inverse of the fiber exposure time for each calibration standard selected over the range of formaldehyde concentrations of interest (Figure 3.3 (b)). The slope of the line for each calibration standard corresponds to a reaction velocity specific to the given formaldehyde concentration. The reaction velocities are then plotted against the inverse of the formaldehyde concentration (Figure 3.3 (c)). The slope of the line in Figure 3.3 (c) yields the first-order reaction rate constant for PFBHA with formaldehyde, which can then be used to calculate unknown formaldehyde concentrations (Figure 3.3 (d)).

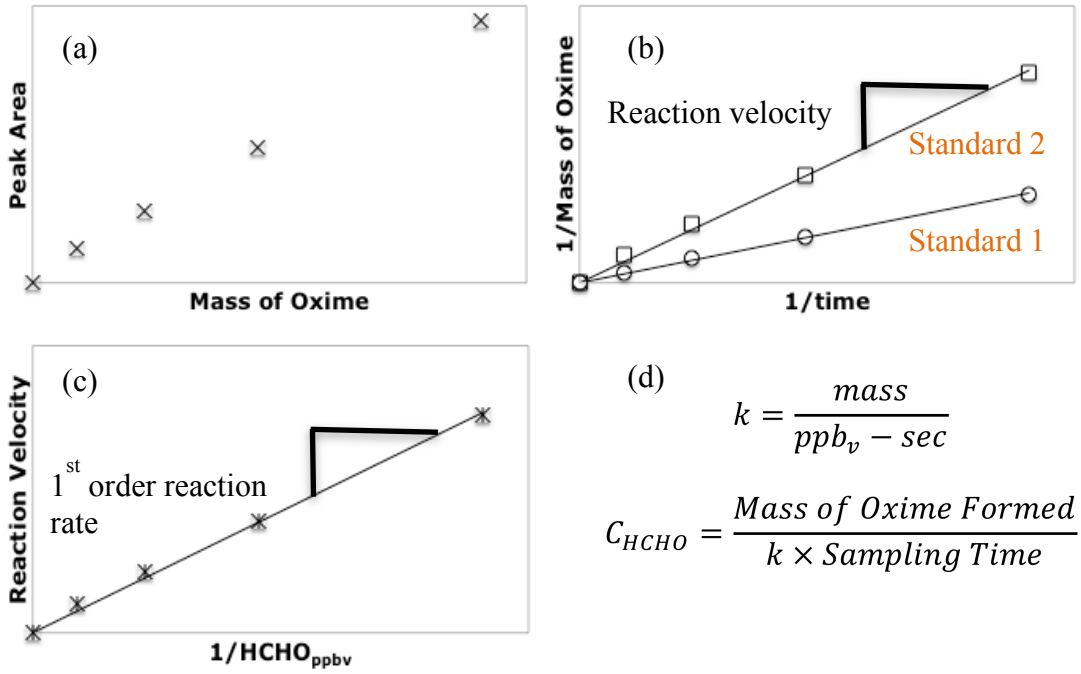

Figure 3.3. Illustration of data analysis steps to determine formaldehyde concentrations from PFBHA-SPME-GC-ECD method: (a) quantitative determination of mass of oxime formed; (b) evaluation of reaction velocity for each of two formaldehyde concentration calibration standard levels; (c) determination of first-order reaction rate constant; and (d) equation for determination of formaldehyde concentration.

Ultimately, this method was not pursued further in this work for several reasons. While direct sampling times are reduced to the range of one to ten minutes, preparation of the SPME fiber prior to sampling (*e. g.* exposure time to coat fiber with PFBHA) and subsequent GC-FID or ECD analysis extends the overall sampling time. Furthermore, this method is entirely manual, making continuous, dynamic sampling labor- and time-intensive. Accordingly, SPME-based formaldehyde monitoring has not achieved widespread use, and the need persists for sensor technology that can perform real-time measurement of formaldehyde and that is easy to transport to and use in the field.

Development of sensor-based sampling methods and analytical techniques is growing rapidly with increasing demand for such technology. Traditional real-time sensor technology employing the Hantzsch method, which relies on the quantitative transfer of formaldehyde from the gas phase to the liquid phase (Junkermann and Burger, 2006), is labor- and resource-intensive (Salthammer et al., 2010). Several commercially available real-time formaldehyde sensors that use either electrochemical or photoelectric photometry technologies were recently tested by the National Research Council of Canada under conditions similar to those used in this study and demonstrated good linearity, stability, and repeatability (Won et al., 2011; Xiao et al., 2011). However, method detection limits were not evaluated for any of these devices nor was performance evaluated at concentrations less than 20 ppb_v. Until recently, major shortcomings of real-time formaldehyde sensor technology have been high detection limits (Salthammer et al. 2010), sensitivity to relative humidity and temperature, and cost. A new chemical sensor element (Maruo et al., 2008) has demonstrated the ability to reliably report formaldehyde concentrations as low as 20 ppb_v over thirty-minute time scales in residential environments (Maruo et al., 2010). Sensor technology of this kind can be readily incorporated into a small, portable device. This study investigated performance, in the

laboratory, of one such coupled sensor-spectrophotometric device (CSSD) at ppb_v concentrations below 20 ppb_v relative to the standard DNPH-derivatization method and evaluated the method detection limit at two test concentrations for four unique devices of the same design. The particular CSSD was also selected because the cross-sensitivity of device measurements to numerous, common, indoor air pollutants has been previously addressed in the literature (Tokumitsu et al., 2008; Maruo et al., 2010). These authors found that interference with formaldehyde measurement is negligible at concentrations of tested indoor air pollutants below 1 ppm_v, which is well below typical concentrations anticipated for these pollutants in residential settings.

The development of new formaldehyde sampling methods and analytical techniques well suited for dynamic indoor environments is of critical importance. Field evaluation of formaldehyde detectors must address both the low detection levels required and the potential spatial and temporal variability in formaldehyde concentrations in indoor settings. Currently, when residential formaldehyde concentrations are reported, they represent an average value weighted over a time span of several hours to several days. For example, in two of the most recent and broadest human exposure assessments to include formaldehyde—the US EPA National Human Exposure Assessment Survey (NHEXAS) (Gordon et al., 1999) conducted in 189 homes in Arizona and the Relationships of Indoor, Outdoor, and Personal Air (RIOPA) study conducted in 311 homes in three urban centers in the US (Weisel et al., 2005)—the formaldehyde concentrations were reported as time-weighted averages taken over a 6-7 day period and a 48-hour sampling period, respectively. The median formaldehyde concentration in the NHEXAS study and the mean formaldehyde concentration in the RIOPA study were 17 ppb_v and 21.6 ppb_v, respectively. However, it is important to consider upper limit concentrations as well as central limit tendencies, especially in light of evidence that

suggests peak exposure dose metrics are stronger than cumulative exposure dose metrics when evaluating causal associations between formaldehyde exposure and risk for certain lymphohematopoietic cancers (National Research Council, 2011). Monitoring formaldehyde concentrations over shorter time scales would be valuable for developing a better understanding of temporal concentration variations. Small, portable, rugged devices also make it possible to monitor formaldehyde in several different locations in a home. This information would not only allow for better characterization of daily human exposure to formaldehyde, but it could also inform the timely application and installation of potential treatment strategies.

Manufactured homes are expected to exhibit higher levels of formaldehyde relative to site-built residences because of the building materials used in their manufacture (Hodgson et al., 2000). Housing developments in the state of Texas known as "colonias" are dominated by single-family manufactured homes. These communities frequently lack safe and healthy housing (Ward and Peters, 2007), and knowledge of indoor environmental quality in these homes is completely absent. Therefore, manufactured homes in the *colonias* represent an ideal location to assess the potential for continuous, dynamic capabilities of the CSSD and sensor technology. This study undertook to investigate the performance of the recently developed CSSD in the field by measuring formaldehyde concentrations in several manufactured homes in a *colonia* outside of San Marcos, Texas.

3.3 Methods and Instrumentation

3.3.1 Coupled Sensor Spectrophotometric Device

The sensor element used in this study was designed for spectrophotometric analysis and consists of one chemically coated porous glass sheet adjacent to one non-

coated glass sheet. The chemically coated glass sheet reacts with formaldehyde, producing a change in color on the glass, as indicated by the shaded (yellow) color in the chemically coated glass sheet shown in Figure 3.4. When the absorbance at 410 nm is measured through both the coated and the un-coated glass sheet, as illustrated in Figure 3.5, the difference in absorbance is proportional to the formaldehyde concentration.

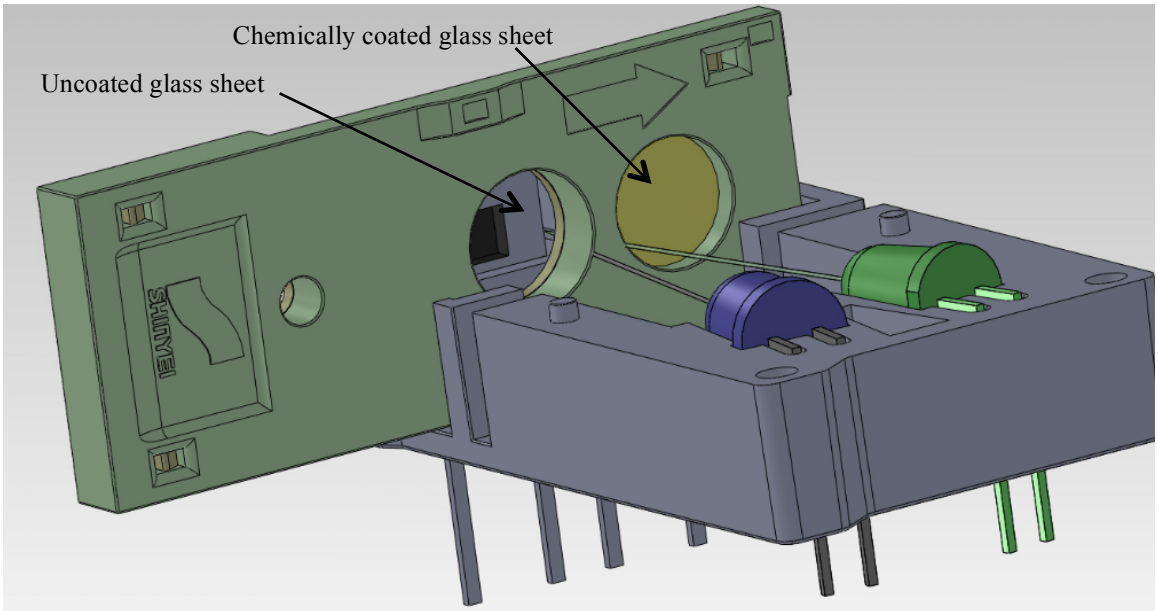

Figure 3.4. Schematic of sensor element illustrating side-by-side arrangement of uncoated reference glass sheet and chemically coated glass sheet for absorbance measurement within the CSSD (*reproduced with permission from Shinyei Technology Co., Ltd.)*.

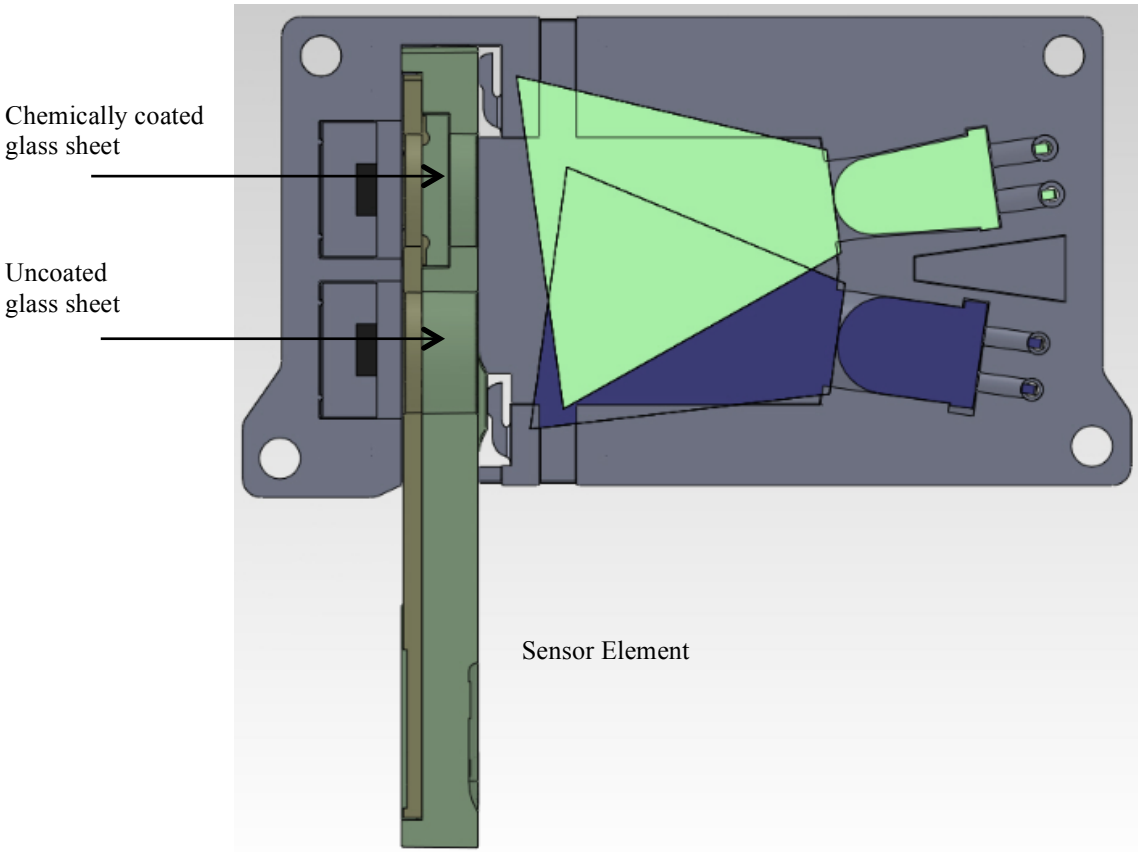

Figure 3.5. Side view of sensor element illustrating light being shone on uncoated and chemically coated glass sheets during absorbance reading taken at 410 nm (*reproduced with permission from Shinyei Technology Co., Ltd.)*.

Development of this sensor technology has been fully described elsewhere (Maruo et al., 2008). The CSSD (Shinyei Technology Co., Ltd; Kobe, Japan; Formaldehyde Multi-Mode Monitor) is a battery-operated unit, housing both the chemical sensor element and the spectrophotometric equipment necessary to evaluate the sensor absorbance on a semi-continuous basis. In addition to formaldehyde measurements, temperature and relative humidity are also monitored on a thirty-minute cycle. The data is stored in the CSSD until it can be downloaded to an available computer.

3.3.2 Calibration Setup

The experimental setup used to calibrate the CSSDs is illustrated in Figure 3.6. Four CSSDs, each equipped with an individual chemical sensor element, were placed in a single, 10 L, stainless steel sampling chamber (Eagle Stainless, CTH-24, Warminster, PA, USA) into which was fed a single stream of nitrogen gas with a known formaldehyde concentration. The formaldehyde concentrations tested were 5, 10, 13, 25, and 50 ppb_v. A zero concentration case was also tested, during which time only zero grade (99.998%) nitrogen gas was fed to the sampling chamber. Each concentration was tested for 4-6 hours, corresponding to 8-12 sensor absorbance readings per monitor. The temperature in the sampling chamber during sampling was 20 ± 1°C, and the relative humidity was maintained at 50 ± 2% to reflect a level of relative humidity that would be encountered in a typical residential setting, where CSSDs will potentially receive wide application.

Formaldehyde gas was generated using a Kin-Tek standard gas generator (Kin-Tek, model 491MB, LaMarque, TX, USA), which is equipped with a temperature-controlled oven to incubate a NIST-certified formaldehyde permeation tube at a specified temperature to maintain the certified emission rate. The effluent formaldehyde concentration from the standard gas generator can then be adjusted using the internal mass flow-controller to change the flow of nitrogen gas passed over the permeation source. As the flow of nitrogen increases, the concentration of the formaldehyde-laden gas stream is diluted. Two permeation sources (Kin-Tek, 33896 and 32684, LaMarque, TX, USA) with different certified emission rates were used separately to achieve the full range of concentrations tested. The permeation source with the lower emission rate, #33896, was used to achieve formaldehyde concentrations below 25 ppb_v, while the permeation source with the higher emission rate, #32684, was used to achieve formaldehyde concentrations of 25 ppb_v and above. The gas permeation sources are pure,

solid phase polyoxymethylene (Figure 3.7), which generate a constant emission of formaldehyde at a constant temperature.

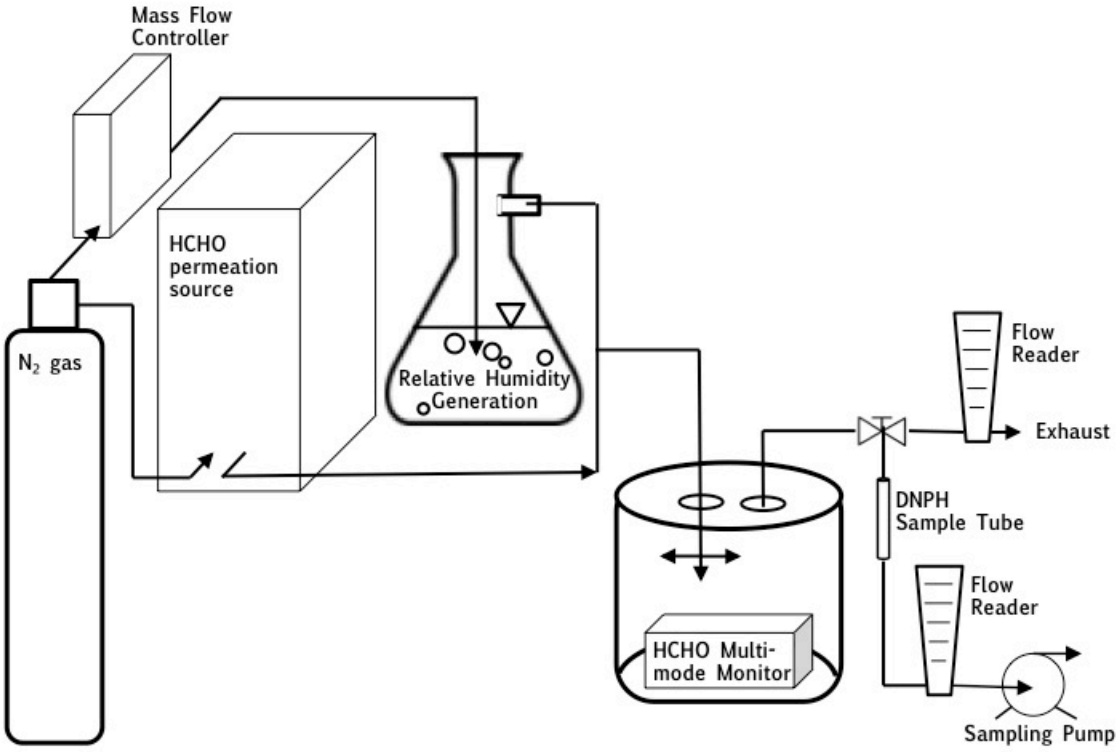

Figure 3.6. Schematic of the experimental setup used to generate formaldehyde and test CSSDs.

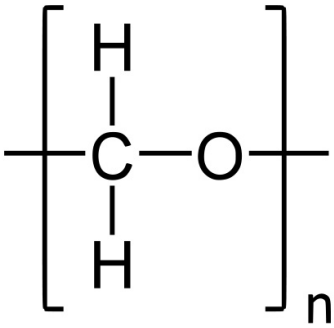

Figure 3.7. Structure of one monomer of oxymethylene, where *n* indicates a sequence of monomers to form polyoxymethylene.

While permeation tubes are standardized for given emission rates at specified, constant temperatures, to verify emission rates, the permeation tube mass can be monitored over time. The change in mass with time is equal to the emission rate. Figure 3.8 shows the mass of permeation tube #32684 measured over the course of a year. The slope of the equation of the best-fit line is the permeation source emission rate. By convention, this rate is reported on a ng/min basis. Thus, the emission rate of #32684 determined from this data is 36.4 ng/min.

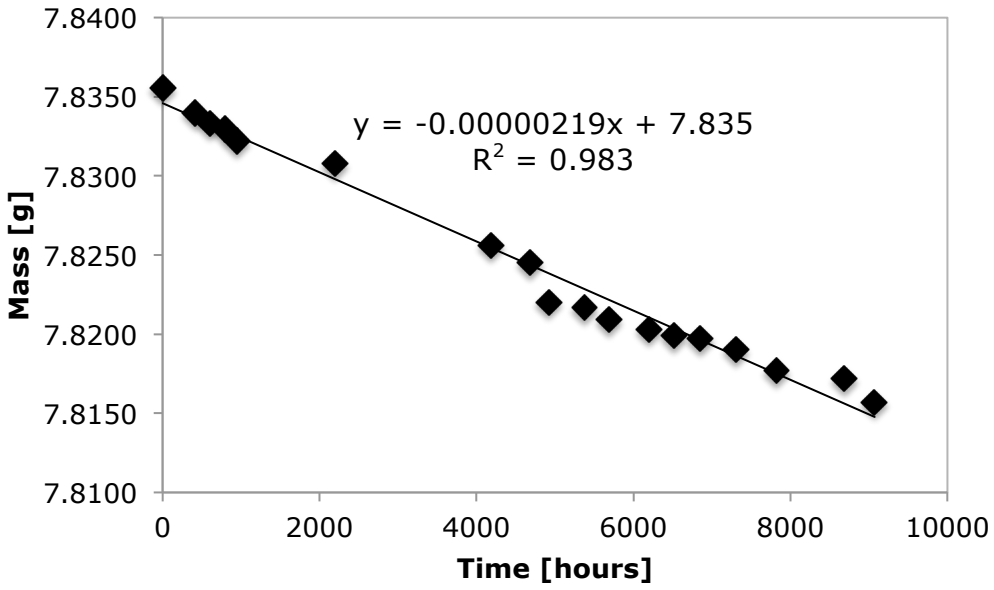

Figure 3.8. Emission rate of formaldehyde permeation tube, #32684.

In similar fashion, Figure 3.9 shows the mass of permeation tube #33896 measured with respect to time. The emission rate for this permeation source during its time of use was determined to be 10.2 ng/min.

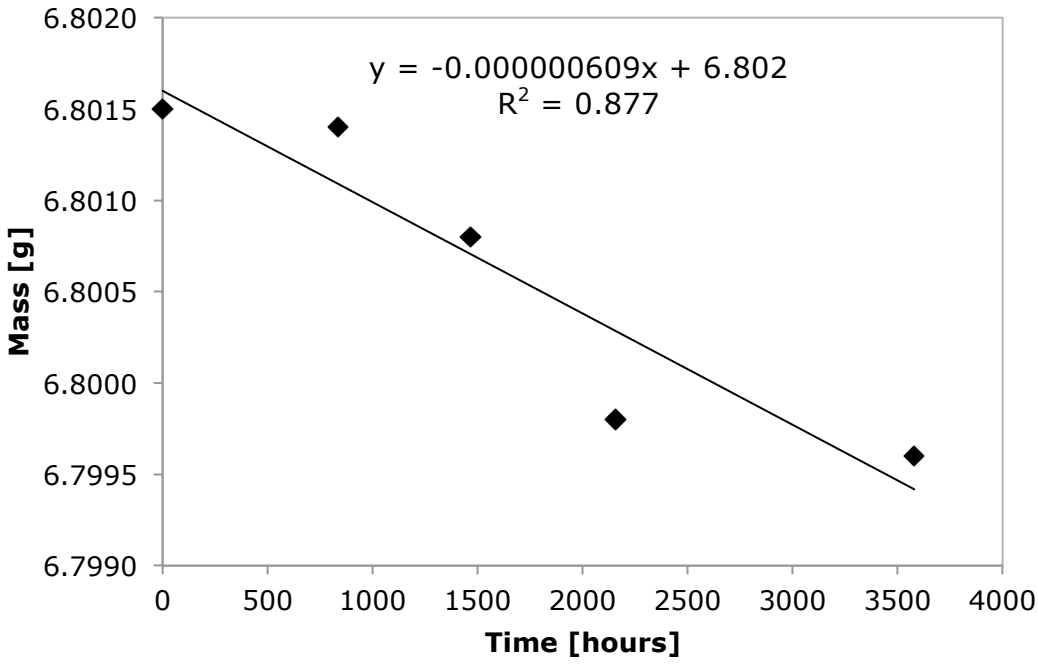

Figure 3.9. Emission rate of formaldehyde permeation tube, #33896.

With the known emission rate, target concentrations are achieved by varying flow rates through the standard gas generator. The following equation shows how to solve for a target total flow rate, Q_{Total}, for a selected target formaldehyde concentration, C_{HCHO}, and an emission rate, E_{HCHO}, determined from a standard paraformaldehyde source.

$$Q_{Total,\ target} = [E_{HCHO}/(MW_{HCHO}/V_{m,\ air})]/C_{HCHO},$$

where

MW_{HCHO} = 30.026 g/mol, and

$V_{m,\ air}$ = 24.061 L/mol (at 20°C and 1 atm).

Table 3.2 summarizes the flow rates through the Kin-Tek (Q_K) and through the relative humidity generation component of the experimental setup (Q_{RH}) to achieve the target concentrations. Because the target relative humidity level was 50%, Q_K and Q_{RH} were determined by dividing Q_{Total} by two.

Table 3.2. Summary of flow rates necessary to achieve desired target formaldehyde concentrations with respect to formaldehyde emission rates from standardized paraformaldehyde sources.

Emission rate of source	Target concentration	Q_K [a]	Q_{RH} [b]	Q_{Total} [c]
[ng/min]	[ppb_v]	[L/min]	[L/min]	[L/min]
10.2	5	0.80	0.80	1.60
10.2	10	0.40	0.40	0.80
36.4	13	1.08	1.08	2.16
36.4	25	0.56	0.56	1.12
36.4	50	0.28	0.28	0.56

[a] Q_K is the flow rate of nitrogen gas passing through the Kin-Tek standard gas generator.

[b] Q_{RH} is the flow rate of nitrogen gas passing through the water-filled flask to humidify the gas stream to the desired relative humidity.

[c] Q_{Total} is the sum of Q_K and Q_{RH}.

To test the performance of the formaldehyde monitors under conditions similar to actual environments, the formaldehyde gas stream was humidified to achieve a constant relative humidity of 50%, as mentioned above. To accomplish this, nitrogen gas was regulated by a mass flow controller (Omega Engineering Inc., FMA5514ST, Stamford, CT) before being bubbled through an Erlenmeyer flask containing de-ionized water to humidify the gas stream and subsequently combined with the formaldehyde-enriched effluent from the Kin-Tek to achieve a total flow rate that corresponded to a given target formaldehyde concentration.

While continuous CSSD measurements were taken, formaldehyde samples were simultaneously collected for analysis using the DNPH-derivatization method. In accordance with the EPA TO-11A and ASTM D5197 standard procedures, DNPH-coated sorbent tubes (Eighty Four, PA, USA; SKC; 226-119), connected to an air sampling pump, actively sampled the effluent leaving the stainless steel chamber at a flow rate of

493 mL/min over the same period of time (4-6 hours) that the CSSDs were exposed to the same concentrations. Following sample collection, the sample cartridge was eluted with acetonitrile and analyzed directly with high performance liquid chromatography (Milford, MA, USA; Waters; Model 486) using a modified EPA TO-11A procedure. The eluent used was a 65/35 percent by volume acetonitrile/water solution, which was pumped (Brea, CA, USA; Beckman Instruments Inc.; 1106) at a constant flow rate of 1.5 mL/min through two 5 μm Reverse Phase C18 columns connected in series. The first column was 250 mm in length (Santa Clara, CA, USA; Agilent Technologies; Zorbaz ODS) and the second column was 150 mm in length (St. Louis, MO, USA; Supelco Analytical; LC18).

3.3.3 Field experimental setup

One CSSD was placed in each of two manufactured homes and were undisturbed for five days while they continuously measured formaldehyde concentrations in these homes. The homes were similar in size (approximately 500 m^3 in total volume), layout, (3-bedroom homes of approximately 140 m^2 each) and age (each over ten years old), and they were occupied during the entire field measurement period. New sensor elements were installed in the CSSDs at the start of field sampling in the homes, and the CSSDs were placed in a common room (not a bedroom or the kitchen) at a height of approximately 1.5 m above floor level. The CSSDs were placed to avoid any direct contact with known sources of formaldehyde emissions (*e. g.* on top of cabinetry made from medium density fiberboard). After five days, the CSSDs were retrieved.

3.4 Results and Discussion

3.4.1 Calibration Results

Four CSSDs were used to measure six different formaldehyde concentrations continuously for four to six hours, taking an absorbance reading every thirty minutes.

Performance by the four CSSDs was evaluated for equivalence using a two one-sided test (TOST) procedure. For this analysis, a $(1 - 2\alpha)$ 100 percent confidence interval was constructed (Huh, 1994; Barker et al., 2001), where $\alpha = 0.05$ (just as with null hypothesis difference analysis) and $z_{1-\alpha} = 1.645$. The null hypothesis for this analysis was that the CSSDs differ by at least $\Delta = \pm 10$ percent. Thus, any two CSSDs were considered equivalent if the 90 percent confidence interval calculated for the difference between two CSSDs was contained within the interval ± 10 percent.

According to the TOST analysis, all four CSSDs were found to behave equivalently demonstrating the precision of the devices. The data from all CSSDs were then pooled to determine an average concentration over the given sampling period. Formaldehyde concentrations determined using the CSSDs were plotted versus formaldehyde concentrations determined using the DNPH-derivatization method and presented in Figure 3.10. The statistical analysis showed very strong agreement between the two analytical techniques with a coefficient of determination of 0.983. This result is important because it demonstrates the ability of the CSSD to closely match the performance of the DNPH standard procedure for formaldehyde monitoring, which is currently considered the most accurate formaldehyde detection method. Based on the slope of the linear curve fit (Figure 3.10), CSSD measurements tend to be slightly higher than DNPH measurements. Of particular note, manufacturers of the CSSDs evaluated in this study have been yet unable to test performance at concentrations below 10 ppb_v and currently report a detection limit of 20 ppb_v, so this study has provided new and valuable insight into the performance of a coupled sensor and spectrophotometric device.

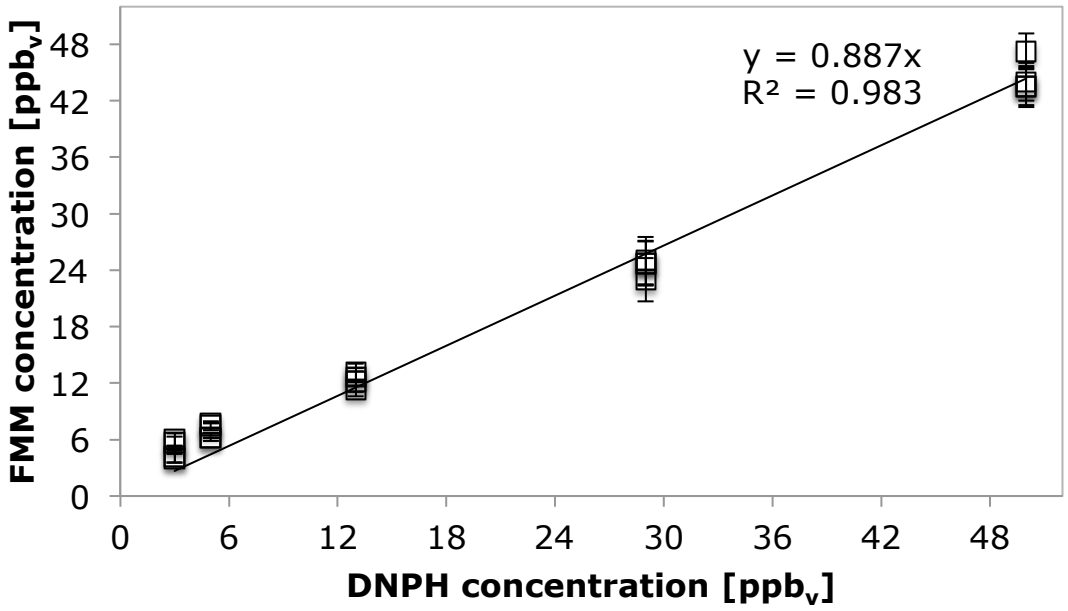

Figure 3.10. Correlation between reported formaldehyde concentrations from CSSDs and the DNPH-derivatization method.

Devices such as these, which base detection on measurement of optical absorbance, may be subject to solvatochromic effects. In the laboratory setting for this study, obtaining stable formaldehyde measurements at relative humidity levels below 30% was found to be challenging. However, for the relative humidity level selected for this study (50% RH), the CSSDs were found to be robust with respect to formaldehyde detection and quantification based on the agreement observed between simultaneous CSSD and DNPH measurements. Robust performance by the formaldehyde sensor element at 50% RH was also observed by Tokumitsu et al. (2008) and Maruo et al. (2010).

The method detection limit (MDL) associated with 40 measurements taken at a 5 ppb_v level by the four CSSDs was estimated as the product of the standard deviation of the 40 replicate samples at a 5 ppb_v level ($sd_{5ppb} = 0.947$) and the one-tailed t-statistic for

n = 39 degrees of freedom at the 95% confidence level ($t_{(n=39,\alpha=0.95)}$ = 2.042). The estimated MDL was 1.9 ppb_v.

To test the robustness of the MDL estimate, the same procedure was applied at the 10 ppb_v level. With sd_{10ppb} = 0.982 and $t_{(n=39,\alpha=0.95)}$ = 2.042, the estimated MDL was 2.0 ppb_v, suggesting that this evaluation is robust and not dependent on the initial test concentration.

3.4.2 Field Results

The formaldehyde concentration data presented in Figure 3.11 were obtained from continuous monitoring of two manufactured homes over the course of five days, with measurements recorded every thirty minutes. Concentrations in both homes are typically, in the case of home 2, and exclusively, in the case of home 1, above the NIOSH REL. In fact, formaldehyde concentrations in Manufactured Home 1 are above the NIOSH REL for the entire sampling period. In Manufactured Home 2, formaldehyde concentrations are above the NIOSH REL 80% of the time. Even so, it is significant to consider that over the course of five days of monitoring, the formaldehyde concentrations show considerable variability. The time-weighted average formaldehyde concentrations evaluated over five days in Manufactured Homes 1 and 2 are 34.2 and 22.4 ppb_v with standard deviations of ± 6.5 and ± 10.7 ppb_v, respectively. Formaldehyde concentrations in Manufactured Home 1 ranged from 17-53 ppb_v, while those in Manufactured Home 2 ranged from below the detection limit to 65 ppb_v. It was observed that Manufactured Home 1 contained more home furnishings, wood-paneled walls, and composite wood products than did Manufactured Home 2, which might provide some explanation for the higher average formaldehyde concentration. At the same time, occupants in Manufactured Home 2 cooked meals more frequently and for longer duration than

occupants of Manufactured Home 1, and whether cooking events influence variability of indoor formaldehyde concentrations would be worth further study, especially in light of evidence that cooking practices can contribute to formaldehyde emissions in indoor environments (Schauer et al., 2002; Ho et al., 2006).

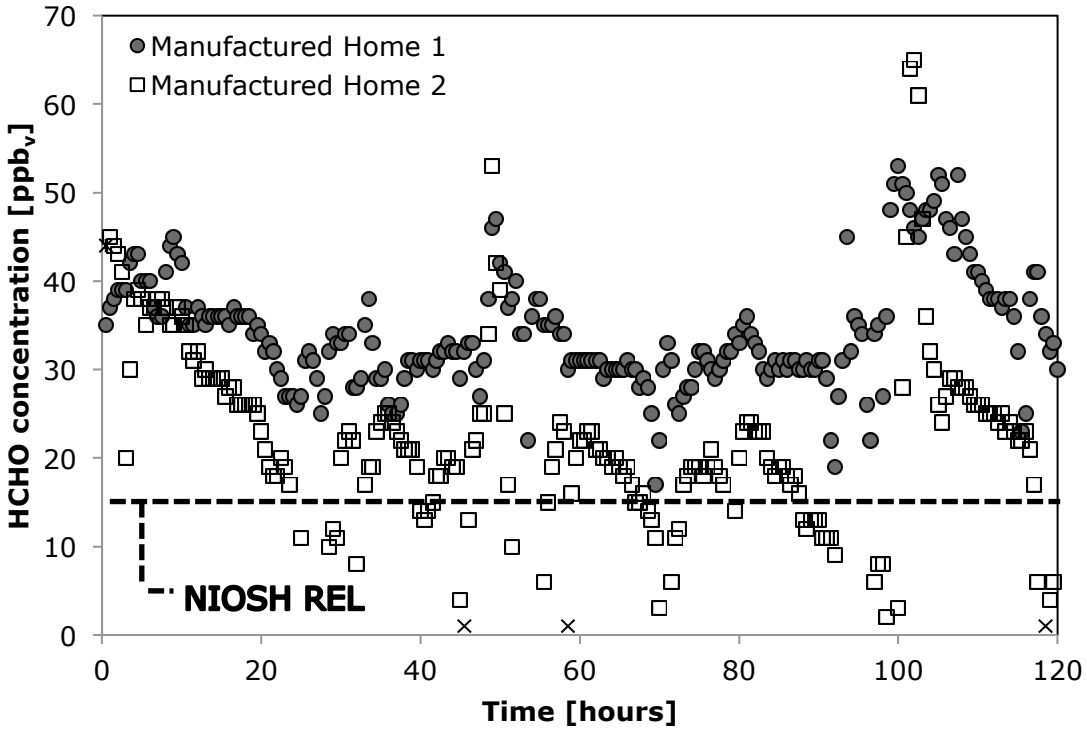

Figure 3.11. Continuous formaldehyde sampling for five days in two manufactured homes in a colonia outside San Marcos, TX. Data points marked with 'X' are below the detection limit.

3.5 CONCLUSIONS

These results could have important implications for the ability to conduct dynamic formaldehyde monitoring in actual residential, commercial, and occupational environments, where previously only single, time-averaged data points could be collected. Continuous characterization of indoor formaldehyde concentrations, as has been presented here, makes it possible to identify internal or external environmental

parameters, including relative humidity and temperature indoors and outdoors, or specific activity patterns that may influence or exacerbate human exposure to formaldehyde indoors. Devices such as the one evaluated in this study enable researchers to quickly develop rich datasets of temporal and spatial variation in formaldehyde concentrations in a large number of homes. Taken together with housing characteristics and occupant time-activity patterns, strategies to reduce human exposure to formaldehyde, such as modifying a certain behavior or removing a specific source, can be targeted and effective.

This analytical technique also makes it possible to evaluate treatment strategies for their performance on a dynamic basis. During development of treatment materials or strategies to reduce formaldehyde exposure in indoor environments, knowledge of real-time formaldehyde concentrations upstream and downstream of a particular treatment strategy can shed light on the removal mechanisms at work, as well as the ability of a given treatment strategy to maintain formaldehyde levels below acute and chronic recommended exposure limits. Knowledge of spatial variability in indoor formaldehyde concentrations would also make it possible to target specific placement of a treatment material. Similarly, it would be possible to identify specific timing or frequency of a treatment material's use, once greater understanding of temporal variability in indoor formaldehyde concentrations is available.

This study improved understanding of a newly developed coupled sensor-spectrophotometric device (CSSD) capable of continuous measurement of gas-phase formaldehyde concentrations at relative humidity levels typical of residential indoor environments. The method detection limit, in a laboratory setting, for the new instrument determined in this study was shown to be competitive with the widely accepted standard method of DNPH-derivatization. Furthermore, the CSSD requires only two hours or less to report an initial 30-minute average formaldehyde concentration without additional

sophisticated analysis in the laboratory on the part of the researcher. This combined sampling method and analytical technique impacts the ability of homeowners, regulators, public health investigators, and researchers to assess temporal and spatial variability of formaldehyde concentrations within a home and across a wide range of indoor environments. This capability is especially important when investigating the relative impacts of formaldehyde treatment strategies. The application of the CSSD is not intended to replace the internationally accepted DNPH-derivatization method, or other such well-established methods. However, the CSSD offers regulators, scientists, and engineers the ability to complement data from traditional analytical methods by revealing more finely resolved spatial and temporal trends in formaldehyde concentrations that inform both policy-level decisions, as well as design of appropriate pollutant control technology.

While this study shows great promise in measuring sub-20 ppb levels of formaldehyde in the laboratory, a limitation of this study was that DNPH samples were not obtained during field sampling. Additional study is needed to obtain field correlations between the CSSD device and the DNPH-derivatization method. Furthermore, consistency of results in the field between CSSD units and individual sensors, particularly between sensor batches, and consistency of CSSD measurements at relative humidity levels that are below 30% RH await further study.

Chapter 4: Formaldehyde Removal by Commercially Available Granular Activated Carbon

4.1 Overview

Although human exposure to formaldehyde has been a leading public health concern for several decades, development of pollutant control technologies that effectively remove formaldehyde from indoor environments has been slow. In the 1980s, great efforts were made to ban or limit the production and use of certain classes of building materials that incorporate urea-formaldehyde, such as urea-formaldehyde foam insulation. These efforts made a significant impact on formaldehyde concentrations in indoor environments, and similar efforts continue presently, exemplified by the recent congressional act passed in 2009 and signed into law in 2010 limiting the formaldehyde emissions that may come from composite wood products. Still, formaldehyde levels in nearly all types of indoor environments, from homes and schools to office buildings and hospitals, remain above chronic recommended exposure levels. Even in the absence of high-emitting building materials, primary formaldehyde emissions from non-wood-based products contribute greatly to overall formaldehyde concentrations indoors. Furthermore, reactions of many other common indoor air pollutants with highly reactive compounds, such as hydroxyl and nitrate radicals, at surfaces or in the gas-phase produce formaldehyde as a reaction by-product.

As was discussed in greater detail in section 2.3.1, direct, physical removal of formaldehyde sources from indoor environments is currently impractical. Apart from source removal and emission reduction, ventilation has been the predominant approach taken to reduce indoor formaldehyde concentrations. However, not only has ventilation proven to be an ineffective or inadequate formaldehyde control strategy, but the prevailing emphasis in research and in practice on building energy efficiency necessitates

a shift away from reliance on energy-intensive ventilation to achieve healthy indoor environmental quality.

Thus, to achieve healthy indoor environmental quality, greater knowledge of air-cleaning strategies and pollutant control processes is needed to develop technologies that will deliver clean indoor air without significantly increasing building energy consumption. The majority of existing pollutant control technologies address removal of particles through filtration. To remove gas-phase pollutants, air-cleaning media that remove pollutants via adsorption are most common. Both of these strategies rely on the preferential transport of particles or gas-phase pollutants to treatment surfaces. To be effective, the air in need of cleaning must flow past the treatment surface, and this is typically achieved through active means that require energy. For passive pollutant control alternatives that would consume less energy to be developed successfully, the potential for surface characteristics to enhance pollutant control must be better understood. The characteristics of treatment surfaces are critical to the effectiveness of a given pollutant control technology but have typically been undervalued. Understanding the role of molecular-level structural and chemical characteristics of pollutant control media is especially important for the removal of recalcitrant pollutants, such as formaldehyde.

Previous research by Carter et al. (2011) took a fundamental approach to investigating the role of structural and chemical surface characteristics of activated carbon with respect to formaldehyde removal. Prior to this work, formaldehyde adsorption isotherms had not been previously investigated; therefore, no model had yet been proposed to fit and describe its adsorption to activated carbon. Moderately hydrophobic organic compounds tend to exhibit adsorption behavior on activated carbon classified as Type I behavior according to the International Union of Pure and Applied Chemistry (IUPAC) isotherm classification system, characterized by an adsorption curve

concave to the abscissa, rising steeply at low partial pressures and approaching a limiting value as saturation pressure is reached (Gregg and Sing, 1982). Adsorption behavior of this type is shown in Figure 4.1 and is often described by the Langmuir and Freundlich models.

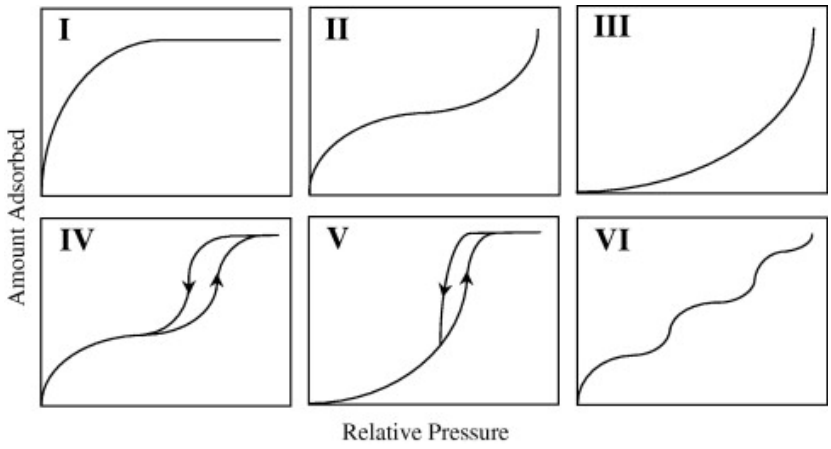

Figure 4.1. Illustrations of typical IUPAC isotherm shapes by classification (Carnody et al., 2007).

However, formaldehyde adsorption isotherms produced by Carter et al. (2011) exhibited a sigmoidal adsorption curve characteristic of Type V isotherms. Type V isotherms develop for adsorbates whose adsorbate-adsorbent interactions are weak relative to adsorbate-adsorbate interactions such that adsorption is low at low partial pressures but increases at higher partial pressures once capillary condensation takes place (Gregg and Sing, 1982). Adsorption at low partial pressures may be enhanced on porous adsorbents and/or in the presence of surface functional groups that interact favorably with the adsorbate.

Though Type V isotherms are uncommon, many mathematical models have been proposed to describe the most well-known adsorbate, water vapor, to exemplify this adsorption behavior. Two recent reviews (Sullivan et al., 2007; Furmaniak et al., 2008)

detailed a large set of semi-empirical and theoretical models, including the Dubinin-Radushkevich (D-R), Dubinin-Serpinsky (D-S), and Do-Do (D-D) families of models, in addition to several others, including the Qi-LeVan (Q-L), Qi-Hay-Rood (QHR), Mahle (M), and Talu-Meunier (T-M) models that have been more recently proposed. The D-R type models are not appropriate for this work because, as stated previously, they cannot be reliably applied to adsorbates with dipole moments greater than 2 Debye. The D-S type models are also inadequate because they do not provide a good fit of the adsorption isotherm over the full range of partial pressures investigated. The Mahle model is derived from the adsorbate pore size distribution, which must conform to a normal distribution. Since activated carbon pore size are not necessarily normally distributed, this model was not selected either. The D-D and T-M models were not used in this analysis because the assumption that the adsorbate forms surface clusters could not be verified for formaldehyde.

Ultimately, the QL model (Qi and LeVan, 2005) was selected to model the observed formaldehyde adsorption behavior because it met two important criteria: (1) reduction to a finite, nonzero limit at low partial pressures and (2) description of the adsorption isotherm over the entire range of adsorption considered. The model parameters are unique to an adsorbent-adsorbate pair and reflect the influence of reaction equilibrium interactions between the adsorbate and surface adsorption sites, oxygen complexation, and pore structure. In particular, the first model parameter, ξ_0, represents the adsorbate-adsorbent partition coefficient at low enough relative pressures to be within the Henry's Law (linear) region. According to Qi and LeVan (2005), the first parameter of their model, ξ_0, should reflect the affinity of the adsorbent surface for the adsorbate. Thus, increasing adsorption capacity for formaldehyde on activated carbon should be associated with increasing values of the ξ_0 parameter. This expectation was substantiated

through analysis of the relationship between formaldehyde adsorption capacity and the corresponding ξ_0 parameter (Carter et al, 2011). Figure 4.2 illustrates this relationship. Furthermore, the relationship between adsorption capacity and ξ_0 is concentration-dependent. High values of ξ_0 were associated with high adsorption capacity at low formaldehyde (HCHO) concentrations ([HCHO] < 15 ppm_v) but not at high HCHO concentrations ([HCHO] > 15 ppm_v).

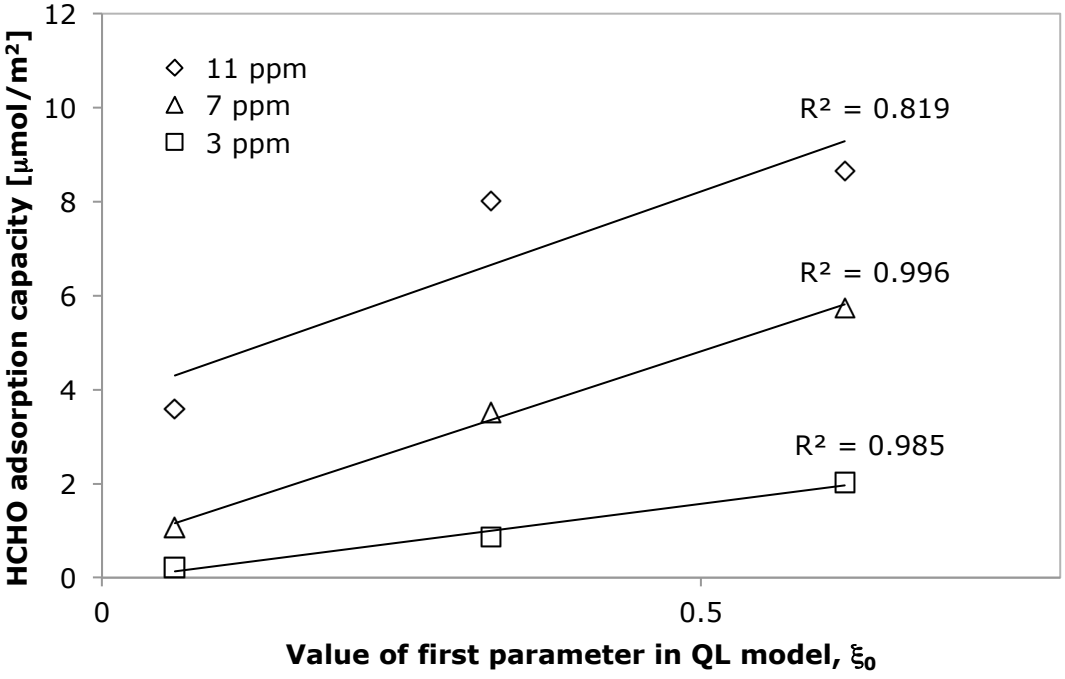

Figure 4.2. Evaluation of relationship between HCHO adsorption at 3 (□), 7 (△), and 11 (◇) ppm_v and the corresponding QL model parameter, ξ_0. Coefficients of determination are reported beside each trend line.

Among the few studies of formaldehyde adsorption on activated carbon, two have suggested that increased nitrogen content is associated with increased HCHO adsorption (Song et al., 2007; Matsuo et al., 2008). Although no mechanism was proposed to explain this observation, Matsuo et al. (2008) suggested that amino groups behave as Schiff bases

during the adsorption process. Thus, for the GACs investigated previously by this author (Carter et al., 2011), it was hypothesized that formaldehyde uptake should increase with increasing surface density of basic functional groups. Plotting formaldehyde adsorption capacity for three different GACs at four concentrations at or below 15 ppm_v with respect to surface density of basic functional groups (Figure 4.3) shows that the strength of this correlation was good for low concentrations (3, 7, 11 ppm_v). However, at higher formaldehyde concentrations this relationship was not evident. As formaldehyde concentrations approach 15 ppm_v, multilayer adsorption is expected to commence, at which point intermolecular interactions between the activated carbon surface and formaldehyde would no longer be the driving force behind subsequent formaldehyde adsorption. These observations lead to two important conclusions: 1) adsorbate surfaces with more basic character have increased potential for formaldehyde removal than surfaces with less basic character, and 2) this potential may be greatest at low formaldehyde concentrations.

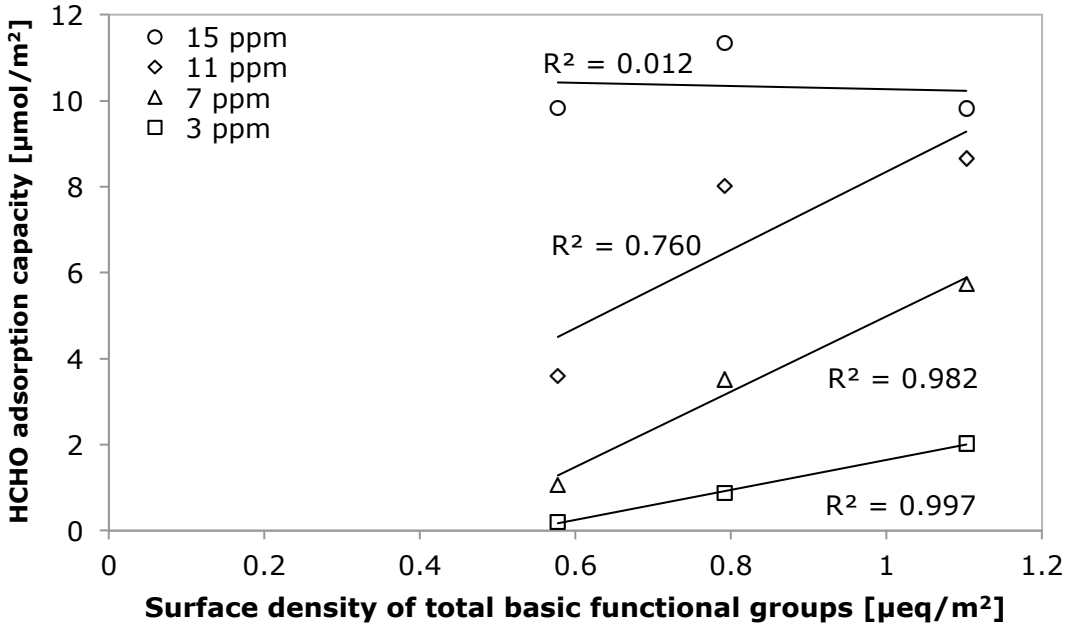

Figure 4.3. Evaluation of relationship between HCHO adsorption at 3 (□), 7 (△), 11 (◇), and 15 (○) ppm_v and GAC surface density of basic functional groups. Coefficients of determination are reported beside each trend line.

Based on these conclusions, the research presented in this chapter sought to strengthen understanding of formaldehyde removal by GAC by extending the aforementioned work in three key ways. First, the influence of GAC chemical characteristics on formaldehyde removal was examined more closely. To isolate the impact of chemical characteristics on formaldehyde removal, the two commercially available GACs selected were expected to share similar structural properties but differ with respect to their surface chemical composition. Second, the research in this chapter focused on removal of formaldehyde by GAC at lower concentrations than has been previously studied. The formaldehyde concentrations selected for study were within the range that characterizes typical residential and workplace environments. Third, to closely approximate typical indoor environments, formaldehyde removal was evaluated in the presence of relative humidity levels characteristic of indoor environments. It is important to understand the adsorption behavior of water vapor as a single component on the GAC materials before investigating the removal behavior of formaldehyde and water vapor

together in a multi-component system. For this reason, water vapor adsorption isotherms were developed for the two GACs tested prior to evaluating formaldehyde removal. By focusing on the role of physicochemical surface properties of GAC on formaldehyde removal under conditions characteristic of residential and commercial indoor environments, the research presented below addresses a longstanding knowledge gap in the field of indoor air pollution control.

4.2 METHODS AND INSTRUMENTATION

A distinguishing component of this work is the molecular-level surface analytical techniques with which each GAC sample is characterized. In addition to discussing selection of GAC materials and providing the details of each of the surface characterization techniques applied, this section outlines the measurement of water vapor isotherms for each of the GACs studied, as well as the experimental setup designed to test GAC performance with respect to formaldehyde removal at concentrations characteristic of indoor environments.

4.2.1 Granular activated carbons

Two commercially available GACs were selected for pollution control performance evaluation. BPL 4x10 (BPL) is a virgin, bituminous coal-based, steam-activated GAC produced by Calgon Carbon Corporation (Pittsburgh, PA) for use in gas-phase applications. BPL was selected because it is widely used for industrial and commercial abatement of volatile organic compounds and because it represents a GAC that has not undergone any chemical treatment. In contrast, Centaur 4x6 (Centaur) is a virgin, bituminous coal-based, steam-activated GAC manufactured according to a patented process involving nitrogen addition to the activated carbon matrix to impart catalytic functionality to the carbon, according to the manufacturer (Calgon Carbon

Corporation; Pittsburgh, PA). Centaur is representative of an emerging class of commercially available GACs designed for treatment of hydrogen sulfide gas (Bashkova et al., 2007) and was selected for this research to investigate whether the surface chemical functionality (nitrogen content and surface basicity) of Centaur, which is similar to surface functionality of other commercially available GACs, would enhance formaldehyde as was anticipated. Both BPL and Centaur were ground and sieved to 24x30 mesh, rinsed with distilled-deionized water to remove fines, dried in a 105°C oven to constant mass, and stored in sealed amber glass bottles at room temperature in a desiccator until use.

4.2.2. Structural and chemical characterization of GAC

Structural characterization. For surface area and pore analysis, nitrogen adsorption isotherms were evaluated at 77 K (ASAP 2020, Micromeritics, Atlanta GA). GAC samples were de-gassed on the instrument at 300°C for 24 hours and then weighed to obtain their dry mass before nitrogen adsorption began. Surface area was calculated applying the Brunauer, Emmett, and Teller (BET) model, which is described through the following equation:

$$\frac{1}{q\left[\left(p_0/p\right)-1\right]} = \frac{(c-1)}{q_m}\left(\frac{p}{p_0}\right) + \frac{1}{q_m c} \quad , \qquad (1)$$

where p and p_0 are the equilibrium and saturation pressure of the adsorbate (nitrogen gas) at the temperature of adsorption, q is the volume of adsorbed gas, q_m is the monolayer adsorption capacity of the adsorbent for the given adsorbate, and c is a thermodynamic parameter that describes the difference between the heat of adsorption for the first monolayer and the heats of adsorption for the subsequent layers. The value for c can vary across orders of magnitude. For microporous adsorbents, such as activated carbon, the

value of c should fall approximately between 50 and 800 (Gregg and Singh, 1982). Equation 1 given above represents the adsorption isotherm. To apply the BET model, $1/\{q_m[(p_0/p)-1]\}$ is plotted with respect to the relative pressure, p/p_0. Over the linear portion of this plot, which is referred to as the BET plot, the slope of the line and the y-intercept are then used to calculate the monolayer adsorption capacity, q_m, and the parameter c, according to the following two equations:

$$q_m = \frac{1}{slope+intercept}, \qquad (2)$$

$$c = 1 + \frac{slope}{intercept}, \qquad (3)$$

Although the traditional application of the BET model is over the range of relative pressures from 0.05 to 0.35, for microporous adsorbents, and especially in the case of activated carbon, it is not appropriate to use this entire range of data because the BET plot does not remain linear through this entire range. Instead, the range of relative pressures over which nitrogen adsorption isotherms tend to be linear on activated carbon is from 0.001 to 0.1. Thus, it is important to determine the precise set of data within this relative pressure range that should be used for analysis with the BET model.

Micropore volume and micropore surface area were evaluated using t-plot analysis. This technique compares the isotherm of a microporous material to a standard non-porous Type II isotherm, plotting the experimental data (*i. e.* the volume of gas adsorbed) as a function of the standard multilayer thickness, t, of the same volume of gas adsorbed on the non-porous, reference material. Differences between the shape of the two isotherms result in a non-linear t-plot from which information is obtained about the micropore volume and micropore surface area of the adsorbent. The shape of the nitrogen adsorption isotherm for activated carbon materials is classified as a Type I isotherm. Type I and Type II isotherms are shown previously in Figure 4.1.

Density Functional Theory, a molecular-based statistical thermodynamic theory, facilitates determination of the pore size distribution, total pore volume, and micropore volume. The Microactive (Micromeritics, Atlanta, GA) software program was used to apply Density Functional Theory to the data collected, and the pore size distribution with respect to surface area and volume were determined assuming a slit-shaped pore geometry and evaluating the data with N_2 as the selected adsorbent.

*Chemical characterization***.** A combination of X-ray photoelectron spectroscopy (XPS) and Boehm and iodometric titrations was used to investigate the carbon surface chemical properties.

Surface elemental composition was determined by X-ray photoelectron spectroscopy (XPS). XPS spectra were taken prior to formaldehyde removal experiments using an AXIS Ultra DLD (AXIS Ultra DLD Kratos Analytical, Spring Valley, NY) dual anode (Mg and Al K α source) with 180° hemispherical analyser. After survey spectra were recorded from 0 to 1200 eV for each activated carbon at a pass energy of 20 eV in 1 eV steps, high-resolution spectra of C 1s, O 1s, and N 1s lines were recorded in 0.1 eV steps at a pass energy of 20 eV. Curve-fitting of elemental regions was performed assuming Gaussian peak shapes after the using the Shirley algorithm to subtract background for all elemental spectra. Subsequent analysis of the components of each region was accomplished with the CasaXPS software program to deconvolve the region into a minimum number of peaks, which represent different oxidation states of the element.

The Boehm titration technique was used complementary with XPS to detect and quantify acidic and basic functional groups. A known mass (approximately 0.1 g, but measured precisely to the thousandth of a gram for each sample replicate) of activated carbon was added individually to 20mL solutions of 0.05 N sodium hydroxide (NaOH;

BDH pellets, 97%; Houston, TX) and hydrochloric acid (HCl; Sigma-Aldrich 37 wt. % in H_2O, 99.999% trace metals basis; Houston, TX). Samples were prepared in triplicate with CO_2-free water in an anaerobic chamber (Labconco, Kansas City, MO) with an atmosphere of high purity nitrogen. In addition to NaOH and HCl solutions prepared with activated carbon, NaOH and HCl blanks of the same volume and same concentration were prepared containing no activated carbon. Sample vials and blanks were sealed and tumbled for five days. After equilibration, all vials were returned to the anaerobic chamber, and 10 mL aliquots of supernatant were titrated with either nominally 0.05 N HCl (for sample prepared in NaOH) or nominally 0.05 N NaOH (for samples prepared in HCl) using a 1000-μL electronic digital pipette (Rainin, EDP2 Electronic Digital Pipette, Oakland, CA). Acid (trace metal grade HCl standardized with Na_2CO_3 (BDH pellets, 99.7%; Houston, TX), 0.048 N) or base (NaOH standardized with HCl, 0.051 N) was added in increments as low as 0.01 mL, while pH was monitored simultaneously (ThermoScientific, Orion 8103BN ROSS electrode, Waltham, MA). For each sample, the difference between the amount of acid or base needed to reach pH 7 in the supernatant of the sample and the blank was evaluated. This difference corresponded to the uptake of either acid or base by the surface of the GAC and was converted to microequivalents per square meter of surface area of GAC by first dividing the acid or base uptake of the sample supernatant by the mass of activated carbon that had been in the vial and then dividing by the specific surface area of the particular GAC, as determined using the BET model discussed earlier. Total HCl uptake by GAC samples corresponded to total basic surface sites. Total NaOH uptake by GAC samples corresponded to total acidic surface sites comprising carboxylic, lactonic, and phenolic groups.

Finally, iodometric titrations were also performed with the selected GACs to evaluate total surface basicity, including the electron-donating capacity of Lewis bases,

which is not captured using the Boehm titration technique. The iodometric titration technique involves several steps, including preparation of a nominally 0.1 N iodine (I_2; ACS 99.5%; Houston, TX) solution for mixing with GAC, preparation of a nominally 0.1 N sodium thiosulfate (NaS_2O_3; Alfa Aesar, anhydrous, 99%, Houston, TX) solution for titrating the iodine solution, and a nominally 0.1 N potassium iodate (KIO_3) solution for standardizing the NaS_2O_3. First, the I_2 solution was prepared in a fume hood by mixing 12.705 g of I_2 (s) with 19.103 g of potassium iodide (KI, BDH 99%, Houston, TX) in 50 mL of de-ionized water to achieve a KI:I_2 ratio of 1.5:1. This solution was left to stand for three hours, after which time additional de-ionized water was added for a total volume of 1 L. This solution was stirred and stored in an amber glass container away from light sources until use. The NaS_2O_3 solution was prepared by dissolving 24.821 g NaS_2O_3 with 0.1 g of sodium bicarbonate (Na_2CO_3; to minimize the chance for bacterial decomposition of the solution) in 1 L of de-ionized water that had been boiled for three hours. This solution was also stored away from light sources in amber glass containers until use. A minimum of four days storage time for the NaS_2O_3 solution was recommended before standardizing this titrant solution (Oliveira et al, 2004). The KIO_3 solution was prepared by dissolving 3.566 g of primary standard grade KIO_3, which was dried overnight in a 105°C oven, into approximately 100 mL of de-ionized water before transferring to a 1 L volumetric flask and filling the flask to 1 L with additional de-ionized water.

GAC iodometric titration samples were prepared in triplicate by weighing out approximately 20 mg of GAC (GAC mass was precisely recorded to the thousandth of a gram for each sample), which was combined with 10 mL of the I_2 solution (0.097 N) in 20 mL amber glass vials. Samples were sealed, wrapped with parafilm, covered with aluminium foil, and shaken for seven days. Once the samples were ready for titration analysis, the normality of the NaS_2O_3 solution was standardized with the KIO_3 solution

(0.100 N) and determined to be a 0.1543 N. Then, this solution was used to titrate 10 mL sample volumes of iodine solution that had been equilibrated with individual GAC samples and determine the new concentration of I_2in each GAC sample vial on an equivalence basis. The difference between the normality of the original I_2 solution and the new I_2 concentration, as determined through titration, quantifies the electron-donating capacity of the GAC surface on an equivalence basis. This quantity was normalized by the mass of GAC in each sample vial and by the surface area of the given GAC.

4.2.3. Experimental procedure for determination of water vapor adsorption isotherms on GAC

Measurement of water vapor adsorption isotherms was performed gravimetrically (Quantachrome, Aquadyne Dynamic Vapor Gravimetric Water Sorption Analyzer, Boynton Beach, FL). The mass of the GAC sample was monitored continuously with an electronic microbalance (weighing resolution of 0.1 μg) while relative humidity was increased automatically using mass flow controllers to blend dry carrier gas (N_2) with a saturated gas (N_2) stream in the proper proportion to achieve relative humidity levels from 0-90% at approximately 10% intervals. The adsorption branch of the isotherm was determined from the mass change in the GAC as the relative humidity increased. To determine the desorption branch of the isotherm, the GAC mass was continuously monitored while the relative humidity was decreased in intervals to approximately the same relative humidity levels as were attained during the adsorption phase. Throughout an entire experimental run, temperature was held constant at 25°C. Dry GAC samples were approximately 20 mg.

4.2.4. Experimental setup for measurement of formaldehyde removal through packed bed columns

A schematic of the entire experimental set up is provided in Figure 4.4. To evaluate formaldehyde removal by the selected GACs, packed bed columns were prepared. Glass columns (length: 11cm; inner diameter: 1.5 cm) with PTFE fittings were packed in the following order: glass wool, glass beads, GAC of a depth specific to achieve a consistent empty bed contact time across all experiments, glass beads, and glass wool. The arrangement of these column layers is schematically represented in Figure 4.3. To achieve a column diameter to particle diameter ratio of 20:1, 4x10 mesh GAC (commercially available mesh size for selected GACs) was ground and sieved to achieve a 24x30 mesh size. With the exception of the PTFE column fittings, all gas lines were stainless steel with Swagelok™ stainless steel fittings.

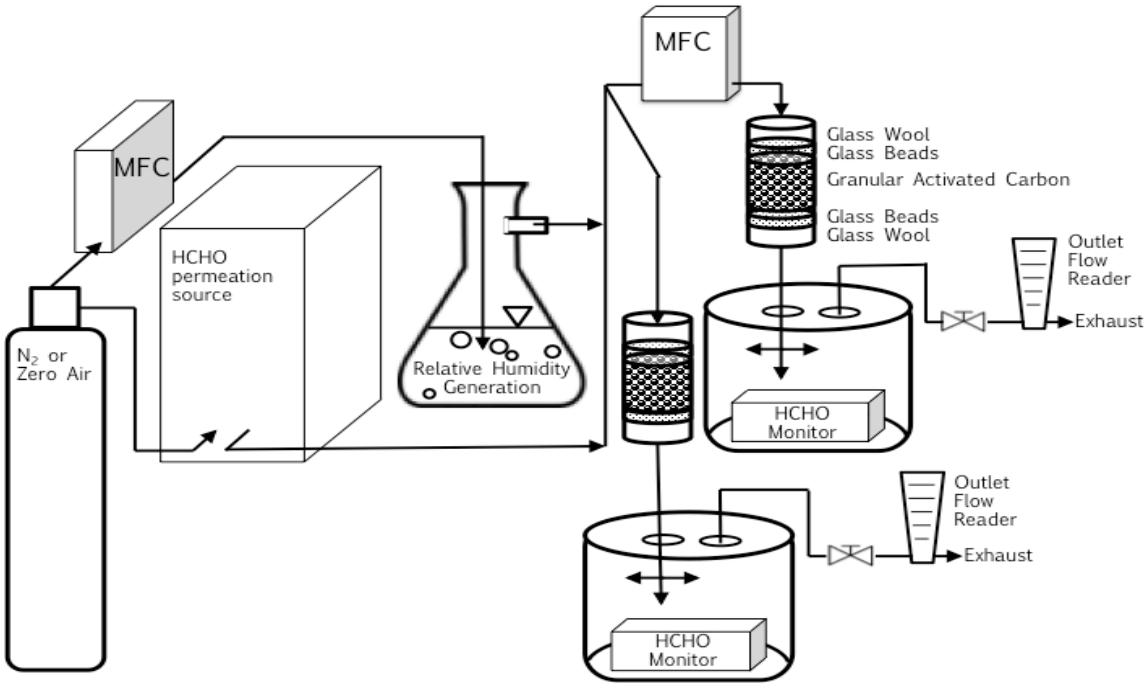

Figure 4.4. Schematic of experimental setup for evaluation of formaldehyde removal through packed GAC columns.

Formaldehyde gas was generated from a solid permeation source heated to 60°C in a Kin-Tek standard gas generator (Kin-Tek, LaMarque, TX, USA; model 491MB) as described in section 3.3.2. Two permeation sources (33896 and 32684, Kin-Tek, LaMarque, TX, USA) with different certified emission rates were used separately to achieve the two concentrations tested. The permeation source with the lower emission rate, #33896, was used to achieve a formaldehyde concentration of 36 ppb_v, while the permeation source with the higher emission rate, #32684, was used to achieve a formaldehyde concentration of 100 ppb_v. The emission rate for #32684 was continuously monitored and determined to be 34.6 ng/min using the data presented in Figure 4.5. The emission rate for #33896 was also continuously monitored throughout column testing. The mass loss from the permeation source is plotted in Figure 4.6 with respect to time, and from the slope of this line, the emission rate was found to be 13.6 ng/min.

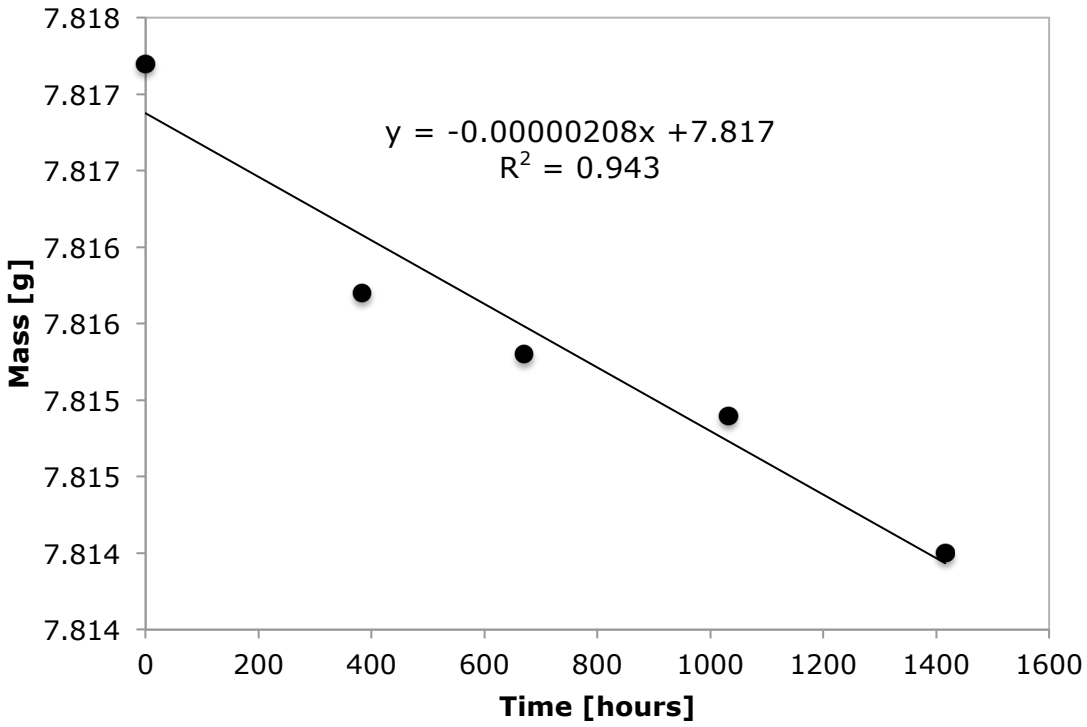

Figure 4.5. Emission rate of formaldehyde permeation tube, #32684.

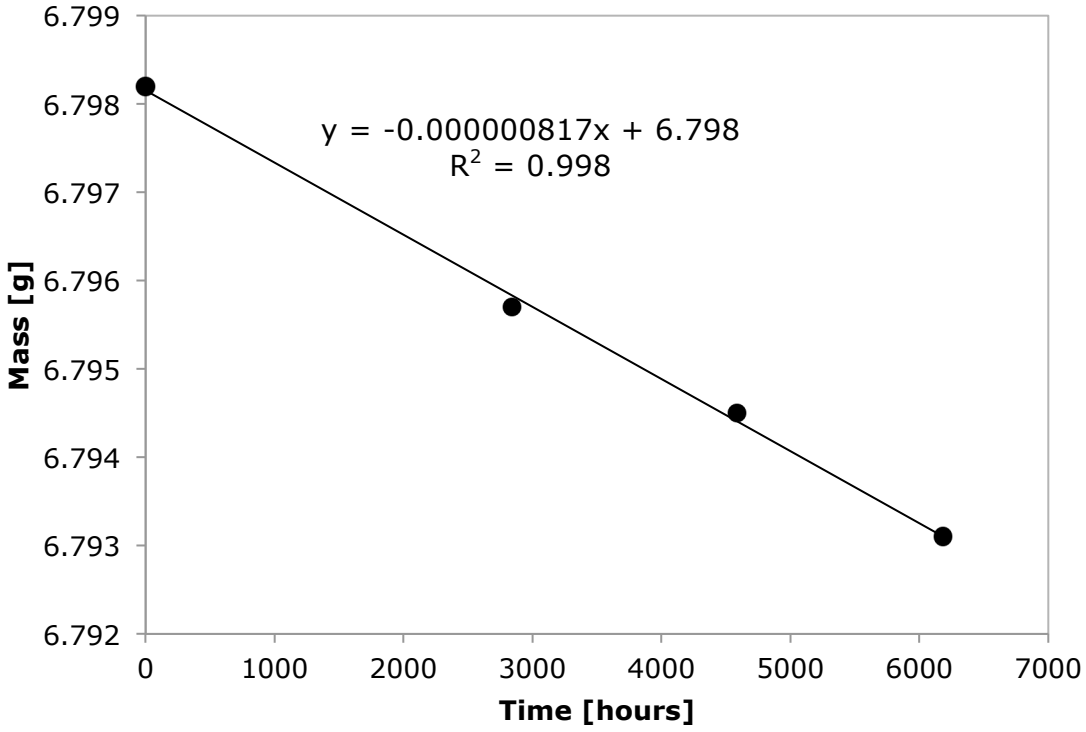

Figure 4.6. Emission rate of formaldehyde permeation tube, #33896.

To humidify the influent gas stream to the test column, the gas line coming from the nitrogen tank that also supplied the Kin-Tek standard gas generator was split, controlled by a mass flow controller (Omega Engineering Inc., FMA5514ST, Stamford, CT), and bubbled through an Erlenmeyer flask filled with de-ionized water to saturate the gas stream. This humidified gas stream was then rejoined with the formaldehyde-enriched effluent gas stream from the standard gas generator. The flow rates through the standard gas generator, Q_K, and the relative humidity generator, Q_{RH}, were equivalent, such that the target formaldehyde concentration and the desired influent total flow rate, Q_{Total}, were achieved while maintaining a relative humidity level of approximately 50% throughout testing. In order to run two packed bed columns simultaneously, Q_{Total} was subsequently split evenly between the two columns. A second mass flow controller

(Omega Engineering Inc., FMA5514ST, Stamford, CT) was used to control the flow to one column, thereby controlling the flow to the second column. Column effluent flow rates were monitored to ensure that the expected, individual column flow rates were achieved. Experimental conditions are summarized in Table 4.1 and Table 4.2.

Table 4.1. Summary of experimental conditions for packed bed column tests of formaldehyde removal at 100 ppb_v by BPL GAC.

Parameter	Units	BPL
Q_K [a]	L/min	0.14
Q_{RH} [b]	L/min	0.138
Q_C [c]	L/min	0.138
Q_{Total} [d]	L/min	0.275
Emission source, rate	--, ng/min	#32684, 34.6
HCHO concentration	ppb_v	106
Column bed depth	cm	5.5
Empty bed contact time	s	2.1
Column face velocity	cm/s	2.6
GAC mass	g	4.343

[a] Q_K is the flow rate of nitrogen gas passing through the Kin-Tek standard gas generator.

[b] Q_{RH} is the flow rate of nitrogen gas passing through the water-filled flask to humidify the gas stream to the desired relative humidity.

[c] Q_C is the flow rate through the column.

[d] Q_{Total} is the sum of Q_K and Q_{RH}.

Table 4.2. Summary of experimental conditions for packed bed column tests of formaldehyde removal at 36 ppb_v by two commercially available GACs, BPL and Centaur.

Parameter	Units	BPL	Centaur
Q_K [a]	L/min	0.15	
Q_{RH} [b]	L/min	0.15	
Q_C [c]	L/min	0.15	
Q_{Total} [d]	L/min	0.3	
Emission source, rate	--, ng/min	#33896, 13.6	
HCHO concentration	ppb_v	36.3	
Column bed depth	cm	2.7	
Empty bed contact time	s	1.9	
Column face velocity	cm/s	1.41	
GAC mass	g	2.633	2.675

[a] Q_K is the flow rate of nitrogen gas passing through the Kin-Tek standard gas generator.

[b] Q_{RH} is the flow rate of nitrogen gas passing through the water-filled flask to humidify the gas stream to the desired relative humidity.

[c] Q_C is the flow rate through the column.

[d] Q_{Total} is the sum of Q_K and Q_{RH}.

Effluent lines from the packed bed columns ran through separate, 10 L, stainless steel sampling chambers (Eagle Stainless, CTH-24, Warminster, PA, USA). Within these sealed chambers, effluent formaldehyde concentrations were measured automatically every thirty minutes using the coupled sensor-spectrophotometric devices (CSSD) described in detail in section 3.3.1. Sampling chambers were opened only to change CSSD batteries periodically (approximately every four weeks) and/or to download and save the data and subsequently clear the data so that the data storage (4000 data points) was not exceeded.

4.3 RESULTS AND DISCUSSION

4.3.1 Structural and chemical characterization of GAC

Structural characterization. All replicate samples of BPL and Centaur exhibited Type I isotherms as expected. A representative nitrogen isotherm with adsorption and desorption branches is shown for each carbon in Figure 4.7. The determination of the appropriate range of relative pressures for which the BET plot was constructed considered the coefficient of determination (> 0.999) and the value of the *c* parameter ($100 < c < 800$). Given these constraints, the relative pressure range considered for BET evaluation was consistently found to be 0.02 to 0.1 for all samples. The BET specific surface area for BPL and Centaur are reported in Table 4.3. These mean values were determined from two replicate samples each and were not found to be statistically different based on a two-sided t-test (df: 2, $\alpha = 0.05$, $t_{critical} = 4.303$).

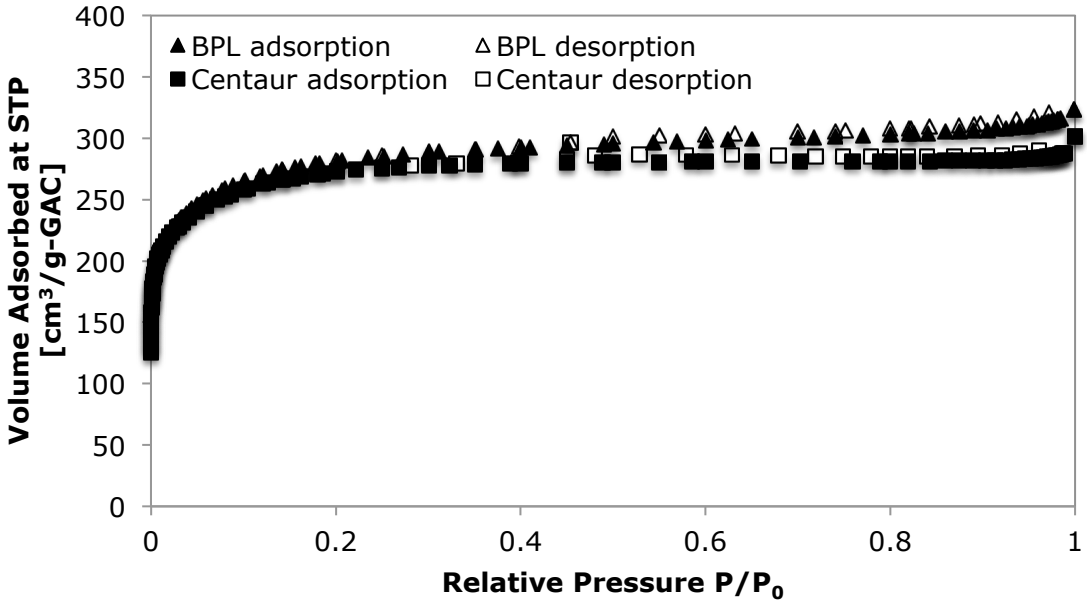

Figure 4.7. Adsorption (closed symbols) and desorption (open symbols) branches of nitrogen sorption isotherms on BPL (△, ▲) and Centaur (□, ■).

With respect to structural properties of the GACs selected, Table 4.3 also includes the t-plot micropore surface area and micropore volume, and DFT total pore volume and micropore volume. Both the t-plot analysis and DFT analysis yield results for micropore volume that are consistent with respect to how the two GACs compare to one another, although the t-plot analysis yields results that are lower than the DFT results.

Table 4.3. Summary of structural and chemical characteristics for two commercially available GACs, BPL and Centaur.

Parameter	**Units**	**BPL**		**Centaur**	
Structural Characteristics		Mean	**SD**[a]	Mean	**SD**
BET Specific Surface Area	m^2/g-GAC	1089	31	1056	27
t-plot Micropore Surface Area	m^2/g-GAC	792	121	770	78
DFT Total Pore Volume	cm^3/g-GAC	0.42	0	0.41	0.02
DFT Micropore Volume	cm^3/g-GAC	0.36	0.03	0.35	0.01
t-plot Micropore Volume	cm^3/g-GAC	0.32	0.05	0.30	0.02
Chemical Characteristics					
Total Atomic % C		92.1	4.57	87.4	4.14
Total Atomic % O		7.8	4.57	12.0	4.24
Total Atomic % N		nd[b]		0.36	0.33
Surface Density of Acidic Functional Groups	µeq/m^2-GAC	0.317	0.03	0.238	0.05
Surface Density of Basic Functional Groups (Boehm)	µeq/m^2-GAC	0.470	0.05	0.626	0.03
Surface Density of Electron-Donating Potential (iodometric)	µeq/m^2-GAC	6.5	0.35	7.5	0.43

[a] standard deviation

[b] not detected

Based on the pore volume analysis using DFT, micropores account for 86% and 85% of the total pore volume for BPL and Centaur, respectively. Similarly, the micropore surface area accounts for 73% of the total BET specific surface area for both BPL and Centaur. Micropores are pores with diameters less than 2 nm. The minimum pore

diameter measured in this work for BPL and Centaur was 0.80 and 0.86 nm, respectively. Given that formaldehyde has a kinetic diameter of 0.36 nm, size exclusion of formaldehyde should not have a significant negative impact on removal, since the dominant GAC micropores have widths equivalent to between two and five pollutant diameters and the remaining GAC mesopores are even larger. Furthermore, the BET specific surface area and the available pore volume are similar between the two GACs, suggesting that structural characteristics are not likely to explain observed differences between the two GACs with respect to formaldehyde removal.

Chemical characterization. A summary of the quantitative chemical characteristics, as determined by XPS analysis, Boehm titrations, and iodometric titrations, are included in Table 4.3. Looking first at the titration results, BPL has higher surface density of acidic functional groups, while Centaur has higher surface density of basic functional groups as well as a higher surface density of electron-donating potential. These differences were evaluated for their statistical significance using a two-sided t-test (df: 4, $\alpha = 0.05$, $t_{critical} = 2.776$). Based on the results of this evaluation, shown in Table 4.4, the differences between the mean surface densities of acidic functional groups and the mean surface densities of basic functional groups for the two GACs, as determined using the Boehm titration technique, are statistically significant. Similarly, the difference between the mean surface densities of electron-donating potential for the two GACs, as determined using the iodometric titration technique, is also statistically significant. Both the Boehm and iodometric titration techniques provide valuable, quantitative information about the bulk surface density of acidic and basic functional groups, but further interpretation of these results is facilitated by additional analysis of the types of surface functional groups present.

Table 4.4. Two-sided t-test for difference between the means for surface densities of acidic and basic functional groups and electron-donating potential for BPL and Centaur GACs.

	Units	BPL	Centaur
		Surface Density of Acidic Functional Groups (Boehm)	
mean	μeq/m^2-GAC	0.317	0.233
standard deviation	μeq/m^2-GAC	0.025	0.046
n		3	3
calculated t-value		2.801	
		Surface Density of Basic Functional Groups (Boehm)	
mean	μeq/m^2-GAC	0.470	0.626
standard deviation	μeq/m^2-GAC	0.053	0.034
n		3	3
calculated t-value		4.270	
		Surface Density of Electron-Donating Potential (iodometric)	
mean	μeq/m^2-GAC	6.490	7.476
standard deviation	μeq/m^2-GAC	0.347	0.425
n		3	3
calculated t-value		3.114	

Looking next at the results from XPS analysis, the two GACs consist almost exclusively of carbon and oxygen with the exception that Centaur contains a trace amount of nitrogen. According to the manufacturers of the commercially modified GAC, this elemental addition constitutes the only modification made to the GAC, which is subsequently marketed as a catalytic adsorptive GAC. BPL has a slightly higher carbon content than Centaur; thus, Centaur has higher oxygen content. One way to analyse this difference is to consider the oxygen to carbon ratio (O/C). Table 4.5 shows the mean O/C ratio for each GAC. In addition, the number of replicates, the standard deviation, and the calculated t-value for a two-sided t-test (df: 6, $\alpha = 0.05$, $t_{critical} = 2.447$) are reported in

Table 4.5. Because the calculated t-value is less than the critical t-value, there is no statistical difference between the two means.

Table 4.5. Two-sided t-test for difference between the mean O/C ratios for BPL and Centaur GACs.

	BPL	Centaur
	O/C Ratio	
mean	0.087	0.139
standard deviation	0.057	0.056
n	5	3
calculated t-value	1.265	

Analysis of XP spectra for BPL and Centaur reveal that the surface functional groups that contribute to either the surface acidity or surface basicity, as determined using selective titration techniques discussed above, must be exclusively (BPL) or predominantly (Centaur) oxygen-based complexes. To reconcile the conclusion that the O/C ratio for these two GACs is not different with the conclusion from the Boehm titrations that surface acidity and surface basicity are different between the two GACs, it is necessary to compare the types of oxygen-containing surface functional groups that are present. BPL should have more acidic oxygen-containing surface functional groups than Centaur. Similarly, Centaur should have more basic oxygen-containing surface functional groups than BPL. To explore this hypothesis, deconvolution of the oxygen O 1s peak was completed and resulted in either four or five distinct curves for each replicate sample. Assignment of individual component peaks of the O 1s region can be especially difficult with activated carbon because of the myriad chemical environments in which an individual non-carbon element, such as oxygen, might exist (Figure 2.2 (b)). With this in mind, the binding energies of the fitted curves were categorized in the following manner: 530-530.9, 531-531.9, 532-532.9, 533-533.9, and 534-535.9eV. These ranges were

selected based on consistency with several studies in the literature that have evaluated the application of XPS analysis for determination of oxygen complexes present in carbon-based materials (Zhou et al., 2007; Sun et al., 2008). They were also selected based on the observed average peak positions for each GAC reported in Table 4.6. The type of oxygen complex associated with each position range (and its abbreviation) is included in Table 4.6.

Table 4.6. Average peak position of component peaks comprising the O 1s region for BPL and Centaur with associated peak ranges and assignments to specific types of oxygen complexes (Zhou et al., 2007; Sun et al., 2008).

BPL		Centaur			
O 1s component peak position				Peak Range [eV]	Peak Assignment (abbreviation)
Mean	SD[a]	Mean	SD		
530.46	0.18	530.50	0.06	530-530.9	carbonyl oxygen (carbonyl)
531.61	0.23	531.54	0.24	531-531.9	carbonyl oxygen in quinones (carbonyl-q)
532.64	0.24	532.49	0.14	532-532.9	carbonyl oxygen in esters, anhydrides, and oxygen atoms in hydroxyl groups (carbonyl-est, anhy, hyd)
533.63	0.16	533.67	0.08	533-533.9	non-carbonyl oxygen in esters and anhydrides (non-carbonyl-est, anhy)
534.88	0.40			534-535.9	oxygen atoms in carboxyl groups (carboxyl)

[a] standard deviation

Using these O 1s peak range classifications, the relative distribution of oxygen complexes for each GAC can be evaluated. Because the relative distribution among these oxygen complexes varied across replicates, the results for each replicate are presented in Figure 4.8. Across three replicates, the O 1s region measured for Centaur was consistently fit with the same four peaks corresponding to the following oxygen complexes: carbonyl oxygen, carbonyl oxygen in quinones, carbonyl oxygen in esters, anhydrides, and oxygen atoms in hydroxyl groups. The relative distribution between these peaks was also consistent, as shown in Figure 4.8. On the other hand, the O 1s region measured for five replicates of BPL was broken down into either four or five component peaks corresponding to the following oxygen complexes: carbonyl oxygen, carbonyl oxygen in quinones, carbonyl oxygen in esters, anhydrides, oxygen atoms in hydroxyl groups, and oxygen atoms in carboxyl groups. Based on the variability observed across replicates, BPL appeared to be somewhat more heterogeneous than Centaur. BPL also contained carboxylic acid groups, which were not observed for Centaur. Thus, this additional analysis of the XP spectra supports the conclusion drawn from the Boehm titration results, which indicated that BPL has higher surface density of acidic functional groups than Centaur.

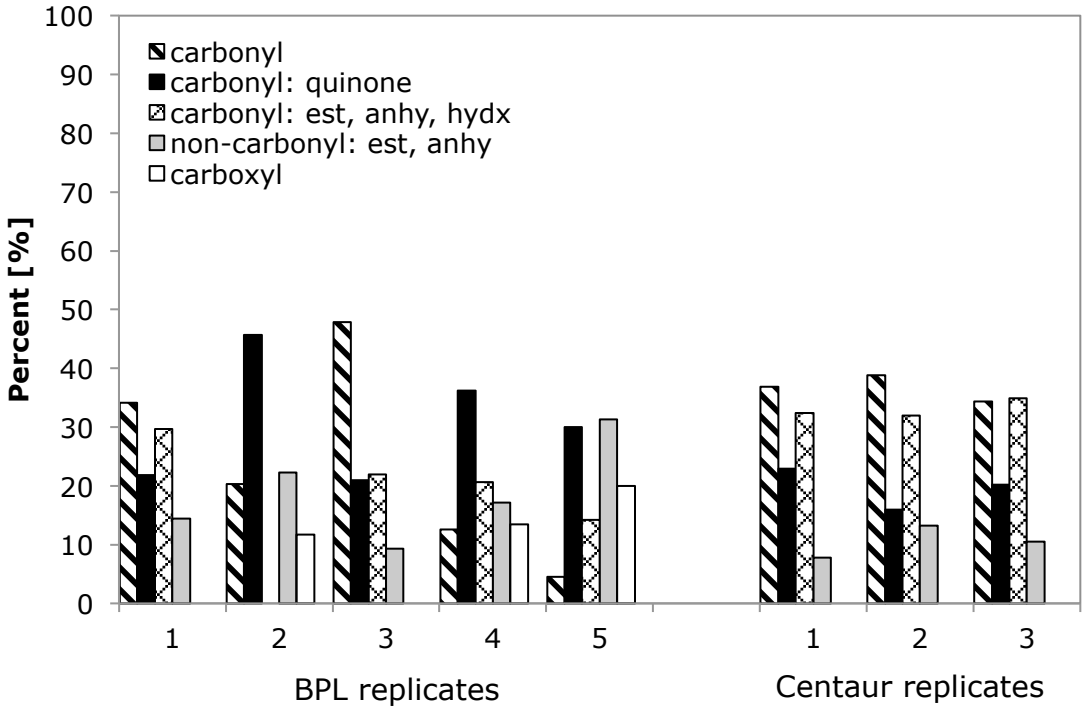

Figure 4.8. Relative distribution of oxygen complexes, determined by peak position, for five replicates of BPL and three replicates of Centaur.

By both Boehm and iodometric titration techniques, Centaur exhibited higher surface density of basic sites. Unlike activated carbon acidity, sources of basicity are less dependent on specific oxygen-containing functional groups. Instead, activated carbon basic properties are more closely associated with electron-donating capacity of the conjugated π electrons that characterize activated carbon basal planes. Oxygen-containing surface functional groups tend to disrupt the conjugated π electrons that characterize activated carbon basal planes, so carbons with less oxygen content have exhibited increased basicity. Thus, two activated carbons may have comparable total oxygen content but have different basic properties, as was the case with the two GACs considered. This result can be understood in light of the XPS results shown in Figure 4.8,

which revealed the lack of acidic surface functional groups (*i.e.* carboxylic acid functional groups) present in Centaur relative to BPL GAC.

4.3.2 Water vapor adsorption isotherms on BPL and Centaur GACs

Adsorption and desorption branches of water sorption isotherms on BPL and Centaur GAC are presented in Figure 4.9. The shape of the adsorption branch for both isotherms follows that of a Type V isotherm as classified according to the IUPAC system (Figure 4.1). Water vapor adsorption on activated carbon follows this sigmoidal shape because water vapor-GAC surface interactions are weak relative to water vapor-water vapor interactions. Thus, at low partial pressures water vapor adsorption is minimal but increases rapidly once capillary condensation takes place. Typically, capillary condensation in the micropores of GACs is initiated within the range of 40 to 70% relative humidity (RH). As anticipated, both of the GACs considered here adsorb the majority of their total water vapor adsorption capacity over this same range of 40 to 70% RH. Between 43% and 73% RH, BPL and Centaur gain 57% and 69% of their maximum water vapor adsorption capacity, respectively. Water vapor adsorption isotherms are not available in the literature for Centaur, but such isotherms have been previously evaluated for BPL. Based on the water vapor adsorption isotherm for BPL reported by Sullivan et al. (2007), BPL gained 63% of its maximum water vapor adsorption capacity between 40 and 70% RH. These same authors also report a maximum water vapor adsorption capacity of approximately 380 mg/g-GAC at 90% RH, which is similar to the results reported in this work (350 mg/g-GAC at 95% RH).

BPL and Centaur also exhibit desorption behavior characteristic of water vapor desorbing from microporous activated carbon (Gregg and Sing, 1982), which typically includes a hysteresis loop. The extent of hysteresis observed for both GACs is influenced

by the complexity of heterogeneous, interconnected pore structures and surface chemical characteristics (Sullivan et al., 2007). Focusing on the impact of chemical characteristics, Sullivan et al. (2007) observed that increasing hydrophobicity in a series of activated carbon cloths lead to a hysteresis loop with a wider base. A similar result is observed in Figure 4.9, where the RH level at which the hysteresis loop closes for BPL and Centaur differs by approximately 10%. With more acidic surface functional groups, BPL is less hydrophobic than Centaur, which could explain both the slight difference observed at the low-RH end of the hysteresis loop, as well as the more minimal degree of hysteresis observed for Centaur above 60% RH relative to BPL.

In anticipation of running formaldehyde removal experiments at approximately 50% RH, it is also important to focus on the water vapor adsorption capacity of BPL and Centaur between 40 and 50% RH. At both 40 and 50% RH, water vapor adsorption capacity was similar for BPL (48 and 101 mg/g-GAC) and Centaur (59 and 113 mg/g-GAC). Taking the kinetic diameter of water vapor to be 0.26 nm (Shah et al., 2000), it is possible to roughly estimate the percent of the total pore volume available that would be occupied by water vapor at a given RH level. It is important to remember, however, that adsorption of water vapor through the lower range of the adsorption isotherm (RH < 50%) is more likely to be driven by affinity of the water vapor for primary adsorption sites rather than by a pore-filling mechanism (Sullivan et al., 2007; Carter et al., 2011). Thus, surface chemical composition of the GAC and the affinity of water vapor for specific surface sites relative to the affinity of a volatile organic compound, such as formaldehyde, strongly influences the removal of competing gas-phase species. Even if water vapor and formaldehyde do not compete for the same specific adsorption sites, competition for access to adsorption sites is likely. The presence of water vapor adsorbed

to specific adsorption sites for which it has a strong affinity may still block access of formaldehyde to neighboring sites.

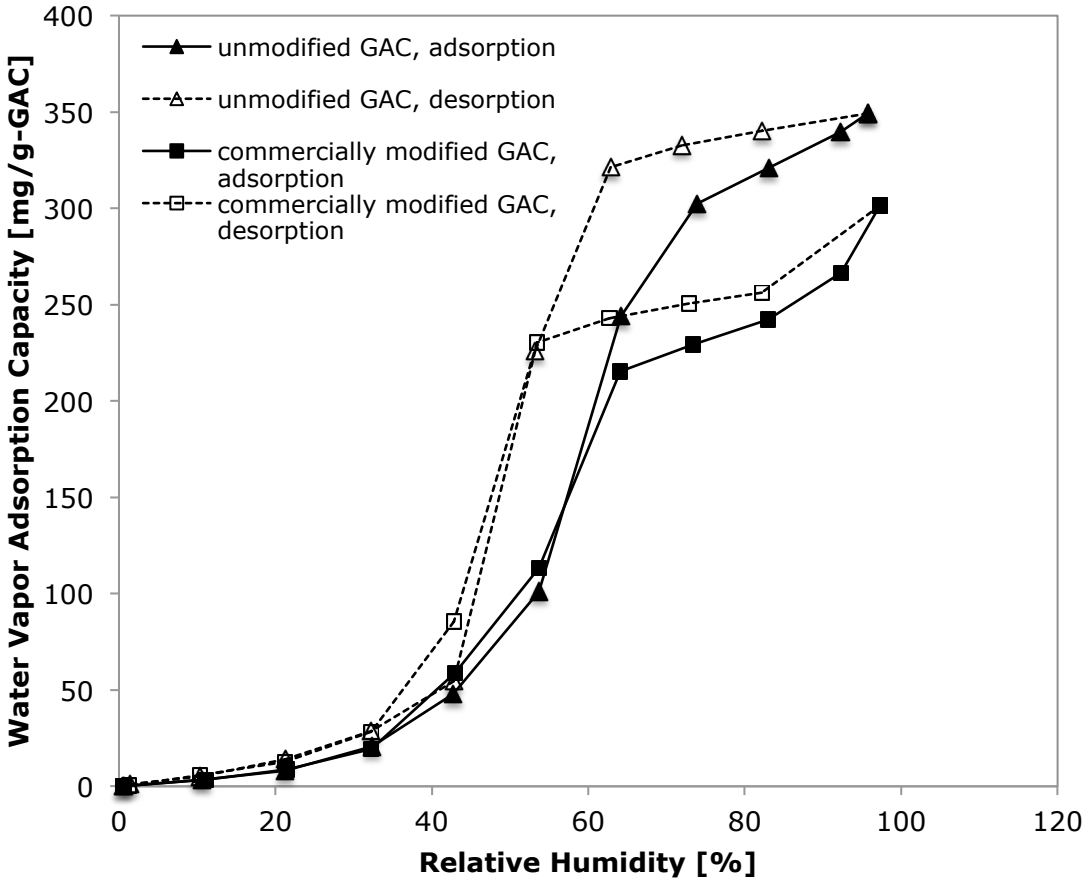

Figure 4.9. Adsorption (closed symbols) and desorption (open symbols) branches of water sorption isotherms on BPL (△, ▲) and Centaur (□, ■).

4.3.3. Formaldehyde removal through packed bed GAC columns

Formaldehyde removal through a packed bed column of BPL GAC was first tested at a concentration of 100 ppb_v, which would be considered high but not atypical for indoor environments. Six-hour, time-weighted averaged results are shown for three replicate columns of BPL GAC in Figure 4.10. To demonstrate the reproducibility of the

reported results, all three replicate sets of normalized effluent formaldehyde concentrations are shown in this figure.

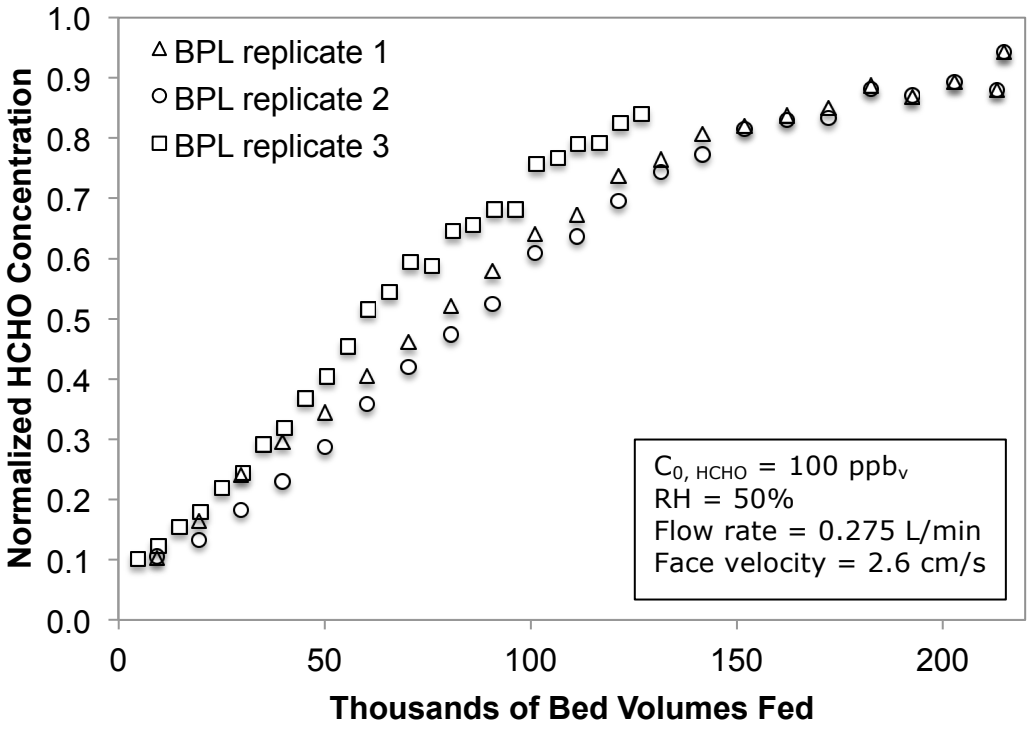

Figure 4.10. Effluent formaldehyde concentrations for BPL normalized by the influent formaldehyde concentration (100 ppb_v) and presented with respect to thousands of bed volumes fed.

Although 100% breakthrough was not achieved, one purpose of these experiments was to obtain a rough estimate of the equilibrium capacity of BPL for formaldehyde at ppb_v-level equilibrium concentrations. For this reason, the formaldehyde removal capacity calculated for 95% breakthrough with respect to an inlet formaldehyde concentration of 100 ppb_v was determined to be 23 μg/g-GAC. Although there are no reported experimental results at similar concentrations to which this result may be compared, it is possible to use the reduced form of the aforementioned QL adsorption

model (section 4.1) at low partial pressures to try to predict the expected surface loading at an influent concentration of 100 ppb_v. At low partial pressures, or low gas-phase concentrations, the QL adsorption model reduces to:

$$p = n/\xi_0, \qquad (4)$$

where p is the partial pressure of the gas-phase species, n is the surface loading, and ξ_0 is the parameter that serves as the partitioning coefficient representing the affinity between the gas-phase species and the surface. From previous application of this model to formaldehyde removal under dry conditions (RH = 0%) by the same BPL (Carter et al., 2011), ξ_0 was determined to be 0.0756 mol_{HCHO}/kg_{GAC}-ppm_v Using this value for ξ_0, the predicted formaldehyde removal capacity at 100 ppb_v would be 227 μg/g-GAC compared to the 23 μg/g-GAC observed at this lower concentration and higher relative humidity. The lack of similarity between these two removal capacities could be the result of several factors including extrapolation of the QL isotherm to equilibrium concentrations that are two orders of magnitude below the range over which the isotherm was developed or the competition between water vapor and formaldehyde for the surface. The comparison is further complicated by the potential for removal of formaldehyde, a hydrophilic contaminant, via two potential mechanisms: 1) adsorption onto the activated carbon and 2) dissolution into water vapor that has condensed in the micropores of the activated carbon. Further research examining adsorption in low relative humidity systems would be useful for evaluating these removal mechanisms and characterizing the single-solute formaldehyde isotherm at low concentrations; however, such experiments were beyond the scope of this research because the formaldehyde detection system was unstable at relative humidity levels below approximately 40%.

To evaluate formaldehyde removal at an even lower concentration, the low-emitting formaldehyde source was used, as mentioned above in section 3.3, to achieve an

influent concentration of 36 ppb_v more characteristic of mean indoor residential concentrations. In this case, both BPL and Centaur were evaluated for their formaldehyde removal performance. For the duration of experimentation with the two GACs, the emission rate of the formaldehyde permeation tube was monitored and found to be relatively consistent with a rate of 13.6 ng/min as determined from Figure 4.6. Continuous column effluent formaldehyde concentrations were normalized by the influent formaldehyde concentration (36 ppb_v) and are presented in Figure 4.11 with respect to thousands of bed volumes fed to BPL and Centaur columns. Both columns were fed approximately 1 million bed volumes. By this time, BPL had achieved 100% breakthrough. Centaur had not yet achieved complete breakthrough. Instead, after 1 million bed volumes, the effluent formaldehyde concentration was fluctuating between 65-70% of the influent concentration.

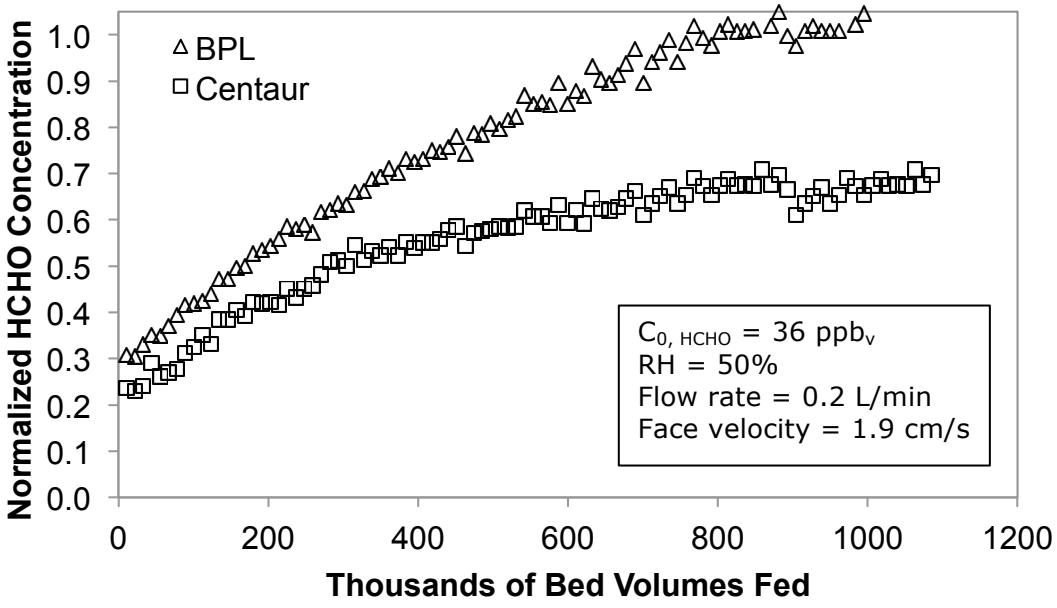

Figure 4.11. Effluent formaldehyde concentrations for BPL (△) and Centaur (□) normalized by the influent formaldehyde concentration (36 ppb_v) and presented with respect to thousands of bed volumes fed.

Because complete breakthrough was not yet achieved for Centaur, it was not possible to make a direct comparison between the maximum formaldehyde removal capacity of BPL and the maximum formaldehyde removal capacity of Centaur, which had not yet been exhausted. Therefore, to compare these two GACs better, apparent surface loading based on the mass of formaldehyde removed was calculated and plotted with respect to thousands of bed volumes fed. The results were normalized by GAC mass packed in the column and are shown in Figure 4.12. The rate of apparent surface loading for BPL began to decrease after approximately 200,000 bed volumes fed and reached a plateau after approximately 600,000 bed volumes fed. The maximum removal capacity achieved by BPL was 19 μg/g-GAC. In contrast, even after 1 million bed volumes fed, Centaur maintained a relatively steady rate apparent surface loading. For the same number of bed volumes fed, Centaur removed 40 μg/g-GAC, or approximately twice the removal of BPL. However, it is not possible to conclude definitively that Centaur reached a steady state formaldehyde removal rate because the experimental data was not collected for a long enough period.

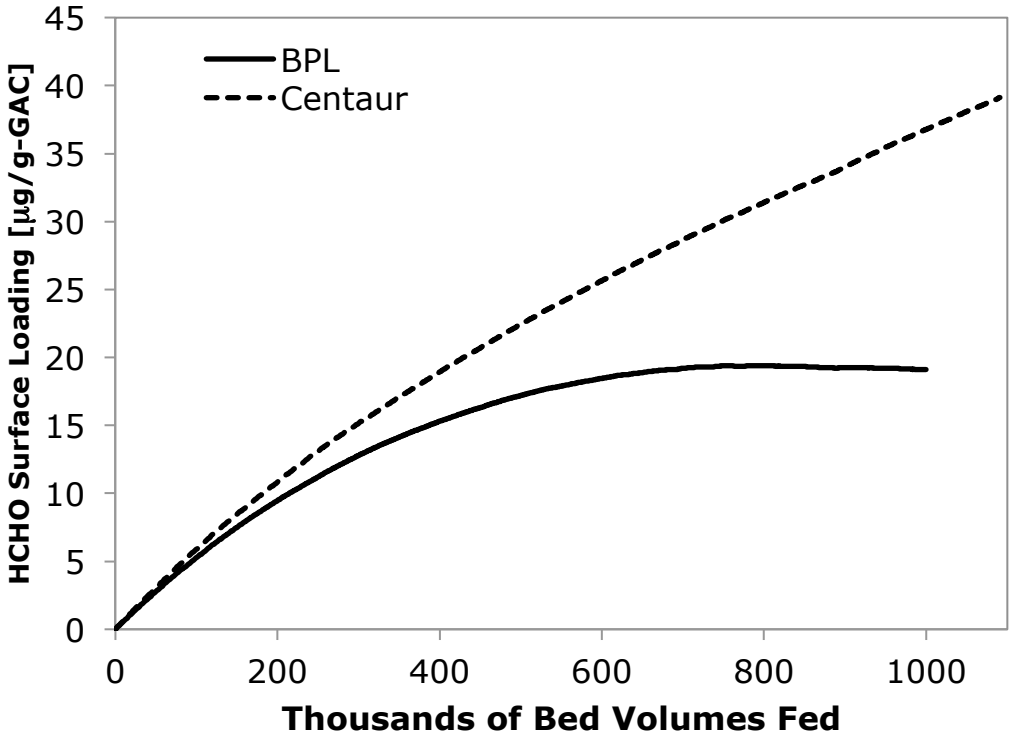

Figure 4.12. Surface loading of formaldehyde for BPL (—) and Centaur (---) normalized by the mass of GAC in the column and presented with respect to thousands of bed volumes fed.

Because the structural characteristics of the two GACs are so similar, it is most valuable to consider differences in surface chemical characteristics to explain the difference observed between the two GACs with respect to formaldehyde removal. For removal of formaldehyde by GAC at low ppm_v concentrations, higher surface density of basic functional groups on GAC are associated with increased formaldehyde removal capacity (Carter et al., 2011), but this relationship was only demonstrated for dry, non-humidified systems. Results from this study indicate that surface basicity continues to play a strong role in formaldehyde removal by GAC at lower, ppb_v-level formaldehyde concentrations and even when water vapor is present. Relative to BPL, Centaur has 1.3

times the surface density of basic functional groups and 1.2 times the surface density of electron-donating potential. At 50% RH, BPL and Centaur both adsorb similar quantities of water vapor, which may limit the available surface area for formaldehyde adsorption, but of the GAC surface area that remains available for formaldehyde removal, Centaur would be expected to perform better because the available surface area is more enriched with basic functional groups and electron-donating potential, which appear to play an important role in gas-phase formaldehyde removal. The observed performance of Centaur relative to BPL supports this hypothesis.

4.4 CONCLUSIONS

The experimental work presented in this chapter examined the performance of two commercially available GACs for their ability to remove formaldehyde in a humidified, gas-phase system at formaldehyde concentrations that are pertinent to indoor environments. Outcomes of these experiments were interpreted in light of thorough structural and chemical characterization of the two GACs tested.

To summarize the results from structural and chemical analyses performed, Centaur and BPL share similar structural characteristics but differ with respect to chemical characteristics. BPL may be considered representative of an unmodified GAC that has not undergone any chemical treatment, while Centaur is a commercially available GAC that has undergone modification through chemical treatment. The purpose of chemical treatment, as stated by the manufacturer, is to modify the GAC to contain nitrogen, which it does in trace amounts. Based on the results presented here, chemical treatment has little impact on structural characteristics because both BPL and Centaur have similar surface area, pore volume, and minimum pore diameter. Although BPL and Centaur also have similar elemental composition with respect to their ratio of oxygen to

carbon, the type of surface functional groups are different. Centaur has 26% less acidic surface functional groups, 33% more basic surface functional groups, and 15% more electron-donating potential relative to BPL. Evaluation of the relative distribution of types of oxygen complexes showed that both Centaur and BPL contain oxygen associated with hydroxyl groups. However, Centaur does not contain oxygen associated with carboxylic acid groups, while BPL does, which could explain the difference between the two GACs with respect to surface acidity. The differences observed between Centaur and BPL with respect to surface basicity are likely explained by the lack of acidic functional groups and the high proportion of carbonyl-type oxygen complexes observed in Centaur. Although Centaur contains only trace amounts of nitrogen (0.36 ± 0.33 atomic %), this small fraction of a percent may still contribute to surface basicity and electron-donating potential. Still, oxygen content is much higher than nitrogen content (O/N = 33) of Centaur, and more of the oxygen complexes of Centaur are basic than acidic. Thus, the type and distribution of oxygen-containing surface functional groups of Centaur, to a greater extent than that of nitrogen-containing surface functional groups, explain why Centaur has higher basicity than BPL. Overall, the surface chemical differences between the two GACs, coupled with the lack of structural differences, make it possible to isolate the influence of surface chemical composition on GAC performance with respect to ppb_v-level formaldehyde removal.

From the analysis of formaldehyde removal by packed bed columns of BPL and Centaur, it was concluded that stable basic surface properties of GAC, which were known to be associated with enhanced formaldehyde adsorption at low ppm_v formaldehyde concentrations, remain an important factor for formaldehyde removal at concentrations that were one to two orders of magnitude lower than those previously tested. Even after 1 million bed volumes fed, Centaur, which exhibited increased basicity relative to BPL,

had not reached complete breakthrough and had achieved twice the removal that BPL was able to achieve at complete breakthrough.

Two important conditions were employed for these experiments to ensure the relevance of the results for indoor environments. First, all packed bed column testing was conducted at 50% RH. Thus, the reported formaldehyde removal achieved by either GAC takes into account competition with water vapor that would be anticipated in typical indoor environments. Second, low face velocities characteristic of passive ventilation rates were used during column testing rather than high face velocities typical in HVAC systems. Low face velocities were used to study GAC performance under passive treatment conditions. Even so, it is also informative to consider how these two GACs might perform under passive treatment conditions. In a residential setting, beds of 1-30 kg of GAC may be placed in existing HVAC systems designed to handle 20-50 m^3_{air}/min. If these systems were running approximately 50% of the time, beds of Centaur or BPL would be exhausted within less than a day to several days, which makes the exclusive use of these GAC an unattractive pollutant control strategy. Results from the work presented in this chapter underscore the need to intentionally tailor indoor surfaces to have specific functionality and explore whether such engineered surfaces would make indoor pollutant control feasible. In light of current trends in building construction and operation to reduce building energy consumption, it is important to consider pollutant control technologies that could be implemented to achieve passive pollutant control. Thus, the results reported here are pertinent to addressing both energy efficiency and indoor air quality goals.

Chapter 5: The Influence of Surface Chemical Properties on Formaldehyde Removal by Chemically Treated GAC

5.1 Overview

Indoor environmental quality and building energy consumption are tightly linked (Fisk, 2002). Improving building energy efficiency is an effective way to address national-level challenges such as energy security and independence and global climate change, as well as household-level issues, such as rising energy bills. However, measures to improve energy efficiency may negatively impact indoor environmental quality (US EPA, 2000). Therefore, it is imperative that efforts to improve building energy performance and indoor environmental quality be directed in a coordinated manner.

Residential and commercial building energy use accounts for nearly 40% of total energy consumption in the United States (US DOE, 2008). In each of these sectors, approximately 35% of the energy consumed is used by heating, ventilation, and air-conditioning (HVAC) systems (US DOE, 2008). Reducing the energy use associated with conditioning outdoor air or re-circulated air for the purpose of ventilation is a frequent target of strategies implemented to increase building energy efficiency (Roberson et al., 1998; Russell et al., 2007), but reducing ventilation without pursuing other means to achieve and maintain acceptable concentrations of indoor air pollutants can result in degraded indoor air quality (ASHRAE, 2003). In this context, pollutant control technologies have the potential to not only improve indoor air quality but also reduce ventilation needs in residential and commercial buildings, thereby reducing building energy consumption.

Although relatively few studies examine both the indoor environmental quality and energy efficiency impacts of a given pollutant control technology, one relevant report recently evaluated the removal efficiency of common indoor volatile organic compounds

(VOCs) by activated carbon fiber filters and the associated energy consumption of several filter regeneration protocols (Sidheswaran et al., 2010). Activated carbon fiber filters were exposed to a mixed gas stream with seven VOCs, including formaldehyde, for either 12 or 24 hours. Following the exposure period, activated carbon fiber filters were regenerated with either room temperature or heated outdoor air for varying lengths of time. With the notable exception of formaldehyde, VOC removal efficiencies ranged from 40% to 60%and 60% to 85% for the unheated regeneration and heated regeneration protocols, respectively. Formaldehyde removal efficiency was 15% and 20% for those same respective conditions. These researchers found that the energy cost to achieve the same VOC removal efficiencies using ventilation would be 7 to 50 times higher than the energy cost associated with fan use and air heating (when employed) necessary for the filter-based pollutant control strategies they tested. This result demonstrates the promising role of pollutant control technology with respect to achieving harmonized indoor environmental quality and energy efficiency goals. However, the poor performance of the activated carbon fiber filters with respect to formaldehyde cannot be overlooked because of the human health significance of this pervasive indoor air pollutant. Especially for indoor environmental applications, pollutant control technologies must be developed that remove formaldehyde with the same or better success as they do traditional indoor air pollutants.

Sustained interest in industrial applications of primarily unmodified granular activated carbon (GAC) for gaseous contaminant removal has lead to extensive understanding of the removal of common, hydrophobic VOCs by GAC at concentrations in the low- to high-ppm_v range (Nelson et al., 1974; Nelson et al., 1976a, 1976b). While this knowledge base has supported successful applications of GAC for industrial pollutant control, the usefulness of these data for prediction of GAC performance at much

lower concentrations encountered in indoor environments is limited to traditional, hydrophobic VOCs (VanOsdell et al., 1996). Because formaldehyde is a polar compound with a low boiling point and high vapor pressure, it has been widely expected that this pollutant cannot achieve significant removals in GAC treatment systems (Stern, 1968; VanOsdell et al., 1996; Yao et al., 2009). However, this conclusion was derived from a limited amount of data with conventional activated carbons that have not been optimized for treatment of polar compounds (Sidheswaran et al, 2010). Very little research has been conducted to explore chemically treated GACs that are more suitable for this class of gaseous, polar, organic compounds. In contrast, a significant number of laboratory and field-based research studies have been conducted to investigate formaldehyde removal by non-carbon adsorbents and catalysts including (but not limited to) potassium permanganate, aluminum oxide, alumina powder impregnated with urea and ammonium sulfate, and manganese oxides (Eriksson et al., 1980; Arthur D Little Inc., 1981; Gesser, 1984; Ghosh et al., 1996; Sekine, 1998). The major shortcomings of these technologies have been cost, reduced removal capacities resulting from interferences by and competition with other air pollutants, and diminished (yet unexplained) effectiveness over short timespans (approximately days to weeks). Another significant barrier to widespread adoption of these technologies in indoor environments could be the additional work required to integrate them into residential and commercial environments either passively or within standard HVAC systems. In contrast, GAC that is designed for enhanced formaldehyde removal should be more readily integrated into residential and commercial pollutant control schemes because it already experiences broad application in commercial and residential settings.

Recently, renewed interest in the use of activated carbon for gas-phase formaldehyde removal has generated some promising new findings (Rong et al., 2001;

Song et al., 2007; Sidheswaran et al., 2010). Two studies of gas-phase formaldehyde removal by GAC suggested that increased nitrogen content is associated with increased formaldehyde adsorption (Song et al., 2007; Matsuo et al., 2008). Other researchers have reported similar promising results. Lee et al. (2010) found that for polyacrylonitrile-based activated carbon nanofibers, which contained more than twice the nitrogen content as conventional activated carbon nanofibers, breakthrough times for formaldehyde exposure at 11 ppm_v were more than twice those of the conventional activated carbon nanofibers. In an aqueous system, Tanada et al. (1999) found that the amount of formaldehyde adsorbed by GACs increased with increasing amination of the GAC surface. Introduction of nitrogen-containing surface functional groups to both GAC and activated carbon fibers has also been associated with superior adsorption, increased breakthrough times, greater selectivity, and possible catalytic oxidation of gas-phase compounds (some of which are, to varying degrees, similar to formaldehyde), including acetaldehyde (El-Sayed and Bandosz, 2002), hydrogen sulfide (Adib et al., 2000; Bagreev et al., 2004; Bashkova et al., 2007), methyl mercaptan (Bashkova et al., 2003), and benzoic acid and nitrogen oxide (Abe et al., 2000).

Based on the literature reviewed above, two hypotheses drive the research presented in Chapter 5. The first hypothesis is that increasing GAC nitrogen content will increase formaldehyde removal. The research presented in Chapter 4 demonstrated the potential for improved formaldehyde removal by activated carbon when surface chemical characteristics are tailored for this purpose. Specifically, increased surface basicity was associated with increased formaldehyde removal at ppb_v-level concentrations. Both oxygen and nitrogen surface functional groups contribute to surface basicity, and although Centaur is chemically treated to contain nitrogen, oxygen surface functional groups made a greater contribution to its surface basicity than did nitrogen surface

functional groups in part because Centaur contained a very minimal atomic percent of nitrogen (less than 0.5 atomic %). Furthermore, the specific types of nitrogen surface functional groups present in Centaur were not determined in the work reported in Chapter 4. The goal of the present chapter is to build on the work of Chapter 4 by focusing on nitrogen functional groups and their influence as components of GAC on gas-phase formaldehyde removal.

The second hypothesis guiding the research presented in Chapter 5 is that specific nitrogen functional groups at the GAC surface facilitate enhanced formaldehyde removal via a catalytic mechanism. When no nitrogen is present, or when nitrogen functional groups that are not electron donors are present, the primary formaldehyde removal mechanism is expected to be adsorption. However, the presence of nitrogen functional groups that increase electron density at the GAC surface could promote removal of formaldehyde by catalytic oxidation. Modification of carbon-based materials and their surfaces through incorporation of nitrogen-containing functional groups has resulted in an emerging class of materials, which continue to advance a broad array of applications including: electrode-based sensing (Maldonado and Stevenson, 2005), proton exchange membrane fuel cells (Shao et al., 2008; Qu et al., 2010), microbial fuel cells (Scott et al., 2007, Feng et al., 2011), metal-air batteries (Kichambare et al., 2011; Li et al., 2011; Li et al., 2012), and air-breathing cathodes (Chen and Yang, 2003). Doping of carbons with nitrogen atoms has developed into a robust field of research because conjugation between the nitrogen lone-pair electrons and graphene π-systems may impart numerous attractive material properties that promote catalytic processes (Maldonado and Stevenson, 2005; Ozaki et al., 2007; Allen et al., 2008). The primary process of interest that is enhanced by incorporation of nitrogen atoms at edge plane sites of carbon materials is the catalytic activity of the carbon with respect to oxygen reduction. Although oxygen reduction

reactions (ORRs) are widely appreciated for the role they play in so many of the aforementioned applications, the mechanistic steps that govern ORRs are still only poorly understood. Several researchers have proposed a sequence of reactions by which oxygen reduction proceeds in an aqueous environment to support aqueous electrocatalysis:

$$O_2 \rightarrow O_{2,\,adsorbed} \quad (2)$$

$$O_{2,\,adsorbed} + e^- \leftrightarrows O_2^{\bullet-}{}_{adsorbed} \quad (3)$$

$$O_2^{\bullet-}{}_{adsorbed} + H_2O \leftrightarrows HO_2^{\bullet-}{}_{adsorbed} + OH^- \quad (4)$$

$$HO_2^{\bullet-}{}_{adsorbed} + e^- \leftrightarrows HO_2^-{}_{aqueous} \quad (5)$$

Reactions (2) and (3) are more likely to occur at the surface of GACs that have been modified to contain nitrogen functional groups with electron-donating capacity. The superoxide radical species produced from these sequential reactions can react with formaldehyde also present at the GAC surface and contribute to its overall gas-phase removal by facilitating a catalytic removal mechanism, oxidation of formaldehyde by superoxide radicals. In the specific context of gas-phase air-cleaning applications, several aforementioned researchers have suggested that nitrogen-containing activated carbon materials exhibit catalytic activity (El-Sayed and Bandosz, 2002; Adib et al., 2000; Bagreev et al., 2004; Bashkova et al., 2007), but none have gone beyond this initial suggestion to propose a reaction mechanism. To examine whether catalysis is occurring, it would be desirable to measure the production of superoxide radical species in the gas-phase at the GAC surface, but the challenges associated with such techniques (Ishibashi et al., 2000) were beyond the scope of this dissertation. Another approach would be to measure potential by-products of proposed catalytic oxidation of formaldehyde, which could be, for example, formic acid or carbon dioxide. In either case, the experimental setup employed for this research is constrained by the use of a solid paraformaldehyde permeation source for formaldehyde gas generation, low flow rates, and ppb_v-level

concentrations at which this work is conducted. Under these constraints, the mass of the by-products produced is too minimal, even when concentrated over lengthened sampling times, to meet minimum detection limits of appropriate analytical techniques. To circumvent similar challenges, other researchers have opted to increase the inlet formaldehyde concentration by several orders of magnitude to consequently increase the outlet by-product (*e. g.* carbon dioxide) concentrations (Sidheswaran et al., 2010). However, by shifting to a much higher formaldehyde concentration range, the experimental work is no longer representative of typical commercial and residential indoor environments, and the conclusions drawn regarding formaldehyde removal mechanisms from such analysis would not be applicable to trace environmental concentrations.

In summary, the research presented in this chapter aims to assess the effect of specific nitrogen functional groups on formaldehyde removal at ppb_v-level concentrations and to gain insight into formaldehyde removal mechanisms by GAC with and without nitrogen present. To overcome the challenges associated with elucidating formaldehyde removal mechanisms, several novel approaches, outlined below in section 5.2, were undertaken.

5.2 Methods and Instrumentation

5.2.1 Surface modification and nitrogen-doping of granular activated carbon

Nitrogen-containing functional groups can be incorporated into carbon matrices in several different ways. When incorporated at edge plane sites, it is expected that nitrogen-containing functional groups impart basicity and electron-donating capacity to the activated carbon surface when these groups are pyrrolic and pyridinic. Gas-phase methods have proven to be among the more successful for amination of edge plane sites,

which results in lactams and imides that subsequently convert to pyrrolic and pyridinic nitrogen-containing functional groups upon heating (Jansen and Bekkum, 1995). The chemical treatment process developed in this research was based on methods outlined by Menendez et al. (1996), Biniak et al. (1997), and Adib et al. (2000), and constitutes a novel chemical treatment method for modification of GAC to contain specific nitrogen functional groups. BPL 4x10 (BPL, Calgon Carbon Corporation, Pittsburgh, PA) was selected as the base material for chemical treatment because of its widespread application in gas-phase pollutant control and because it is representative of a common class of GACs that are physically activated, bituminous coal-based materials that have not undergone any chemical treatment.

In the chemical treatment process specifically employed for this research, BPL was oxidized in an aqueous solution of 14% trace metal grade nitric acid (HNO_3). Batches of 50 g of BPL were stirred continuously in a 250 mL, 14% solution of HNO_3, for 4 hours. The nitric acid served to break open ring structures at the basal sheet edges, and at these edge-plane sites, nitrogen-containing functional groups, such as those shown previously in Figure 2.4, are expected to form following exposure to ammonia gas. Oxidized GAC was drained and then continuously rinsed with de-ionized water for 24 hours. The pH of the rinsing filtrate was monitored to ensure it reached a stable, neutral pH of approximately 7 for a minimum of 4 hours. The oxidized, rinsed GAC was then dried in a 105°C oven for 24 hours and stored in a desiccator until the nitrogen-doping phase was initiated. For nitrogen-doping, the oxidized, rinsed GAC was exposed in small batches (20-30 g), contained in ceramic boats within a tube furnace, to a mixture of argon and ammonia gas at high temperature, 950°C, for one and a half hours. The precise mixture of argon and ammonia gas and the GAC exposure time were determined after multiple combinations of gas mixture ratios and exposure times were tested for their

ability to achieve over 1% nitrogen content and to produce nitrogen-containing functional groups that are primarily pyrrolic and pyridinic. This process stands in contrast to commercially available GACs that are modified in aqueous solution with urea or ammonia gas alone and designed for catalytic air or water pollution control. The commercially modified GAC (Centaur) studied in this research serves as a comparison to the nitrogen-modified GAC (BPL-N) produced for this work.

5.2.2 Structural and chemical characterization of granular activated carbon

Structural characterization. For surface area and pore analysis, nitrogen adsorption isotherms were evaluated at 77 K (ASAP 2020, Micromeritics, Atlanta GA). GAC samples were de-gassed on the instrument at 350°C for 24 hours and then weighed to obtain their dry mass before nitrogen adsorption began. Surface area was calculated applying the Brunauer, Emmett, and Teller (BET) model as described in Equation (1) in section 4.2.1. Micropore volume and micropore surface area were evaluated using t-plot analysis. Density Functional Theory was employed to determine the pore size distribution, total pore volume, and micropore volume, assuming slit-shaped pore geometry and evaluating the data with N_2 as the selected adsorbate.

*Chemical characterization***.** X-ray photoelectron spectroscopy (XPS), Raman spectroscopy, and Boehm and iodometric titrations were used to investigate the carbon surface chemical properties.

Surface elemental composition was determined by X-ray photoelectron spectroscopy (XPS). XPS spectra were taken prior to formaldehyde removal experiments using an AXIS Ultra DLD (AXIS Ultra DLD Kratos Analytical, Spring Valley, NY) dual anode (Mg and Al K α source) with 180° hemispherical analyser. After survey spectra were recorded from 0 to 1200 eV for each activated carbon at a pass energy of 20 eV in 1

eV steps, high-resolution spectra of C 1s, O 1s, and N 1s lines were recorded in 0.1 eV steps at a pass energy of 20 eV. Curve-fitting of elemental regions was performed assuming Gaussian peak shapes after using the Shirley algorithm to subtract background for all elemental spectra. Subsequent analysis of the components of each elemental region was accomplished with the CasaXPS software program for the deconvolution of the XP spectra into a minimum number of peaks, which represent different chemical environments surrounding the element.

Raman analysis was completed using an InVia Renishaw system (Renishaw Inc., Hoffman Estates, IL) with incident radiation at a wavelength of 514.5 nm. A 50x aperature was used, so the cross section of the sampling area was approximately 2 μm. Sample measurement was completed over the Raman shift range of 1000 to 2000 cm^{-1}. This range was selected to focus on the Raman bands associated with graphitic (G) and disordered (D) carbon, which appear at approximately 1350 cm^{-1} and 1588 cm^{-1}, respectively. For each GAC considered, first order spectra were measured for a minimum of 10 replicate samples. First-order spectra were normalized to the intensity of the band at 1588 cm^{-1}, and the ratio of the intensity of the G band to the intensity of the D band was calculated.

The Boehm and iodometric titration techniques were employed to complement XPS analysis and to detect and quantify acidic and basic functional groups. For Boehm titrations, as described in section 4.2.1, total HCl uptake by GAC samples corresponded to total basic surface sites, while total NaOH uptake by GAC samples corresponded to total acidic surface sites comprising carboxylic, lactonic, and phenolic groups. Iodometric titrations were also performed with the selected GACs to evaluate total surface basicity, including the electron-donating capacity of Lewis bases. Both the Boehm and iodometric titration techniques were outlined in greater detail in section 4.2.1.

5.2.3 Experimental setup for packed bed columns

Packed bed columns were employed to evaluate the pollutant control performance of BPL, BPL-N, and Centaur GACs with respect to formaldehyde removal. The first set of packed bed column tests was designed to examine the formaldehyde removal capacity and the time to 50% and 95% breakthrough for each GAC at two influent formaldehyde concentrations, 100 and 36 ppb_v. When possible, the time to 95% breakthrough was evaluated to roughly estimate the equilibrium adsorption capacity of the GACs tested. The time to 50% breakthrough was evaluated because it is a common performance metric used by the American Society of Heating, Refrigeration, and Air-conditioning Engineers (ASHRAE) to compare performance of multiple GACs according to Standard 145.1 entitled Laboratory Test Method for Assessing the Performance of Gas-Phase Air Cleaning Systems: Loose Granular Media (ASHRAE, 2008) and because, for the lower of the two test concentrations, 50% breakthrough would approximately correspond to an effluent concentration that begins to exceed the NIOSH chronic recommended exposure level. For the higher of the two test concentrations, the time to 15% breakthrough was also evaluated, as it would correspond to an effluent concentration equivalent to the NIOSH chronic recommended exposure level.

A humidified gas stream with a formaldehyde influent concentration of either 100 or 36 ppb_v was fed to a column with a packed bed of the given GAC. Column effluent formaldehyde concentrations were monitored continuously until at least 95% breakthrough was reached for BPL. For packed bed column testing at each of the two test concentrations, relative humidity (RH) was held constant at 50% and zero-grade nitrogen gas (99.998% purity) was selected as the carrier gas for GAC column testing. GAC formaldehyde removal performance from these experiments were compared in conjunction with comparisons of the structural and chemical properties of the three GACs

to determine what impacts, if any, the presence and type of nitrogen functional groups may have had on formaldehyde removal.

To investigate whether electron-donating nitrogen functional groups might promote catalytic removal of gas-phase formaldehyde, a second set of packed bed column tests was run with ultra-zero air (hydrocarbon-free, Praxair, Austin, TX) and the formaldehyde concentration at 38 ppb_v. This approach provides the GAC column with an abundant source of oxygen gas just as it would experience during household or commercial application. If catalytic removal of gas-phase formaldehyde proceeds via production of superoxide radical species (according to equations (2) and (3) presented in section 5.1), formaldehyde removal by BPL-N in the presence of ultra-zero air should increase relative to the removal observed by the same GAC in the presence of nitrogen gas to a greater extent than BPL performance increases, if BPL performance increases at all. By comparing the formaldehyde removal performance of BPL and BPL-N with oxygen-rich air and with pure nitrogen gas, it is possible to indirectly investigate the likelihood that formaldehyde removal proceeds via a catalytic mechanism on BPL-N.

Furthermore, the second set of packed bed column tests was designed differently from the first set to shed additional light on whether formaldehyde removal might be dominated by a catalytic mechanism for BPL-N relative to being dominated by an adsorption-based mechanism for BPL. Following an initial phase of exposure to ultra-zero air with an inlet formaldehyde concentration of 38 ppb_v for over 600,000 bed volumes fed (a period of time expected to correspond to approximately 50% breakthrough or greater), a regeneration phase was initiated. During the regeneration phase, the packed bed columns were exposed to zero-grade, formaldehyde-free air at room temperature and 50% RH for a period of time (between 24 and 48 hours) to reach approximately 100,000 bed volumes fed. If adsorption were the primary removal

mechanism during formaldehyde exposure, then the effluent formaldehyde concentration profile during the regeneration period when clean, formaldehyde-free, humidified, zero-grade air was passed through the column should exhibit decaying formaldehyde concentrations characteristic of a typical desorption curve. It is expected that the effluent formaldehyde concentration profile for BPL will depict a desorption curve. If, on the other hand, catalysis is the dominant removal mechanism, the effluent formaldehyde concentration profile should reach a steady state concentration or be below detection. The exposure phase and the regeneration phase constituted one cycle, and the effluent formaldehyde concentration was measured continuously throughout both phases. This cycle was repeated at least three times for each GAC column. DNPH samples were also collected once for each phase (formaldehyde exposure and regeneration) of each cycle. These samples were collected and analyzed for formaldehyde according to the same protocol outlined in section 3.3.2.

A third set of packed bed column tests was conducted to continue to investigate whether catalysis or adsorption were the dominant formaldehyde removal mechanisms for BPL-N and BPL, respectively. The same conditions employed for the second set of packed bed column experiments described above were maintained for this third set of experiments, with the exception that the relative humidity was increased to 70%. If catalysis were occurring with BPL-N to remove formaldehyde, and if that catalytic process were not fouled by the presence of water vapor, then the results for both the second and the third set of packed bed column experiments (50% RH and 70% RH, respectively) should be very similar. Given that the primary applications of nitrogen-doped carbon materials have been in aqueous systems, it is reasonable to assume that water vapor should not hinder any catalytic mechanism that might be taking place on the BPL-N surface. Furthermore, BPL column effluent formaldehyde concentrations are still

expected to reflect adsorption as the primary removal mechanism, characterized by an adsorption curve concave to the x-axis and rising towards 100% breakthrough.

A schematic of the experimental setup for all three sets of packed bed column experiments is provided in Figure 5.1. Glass columns (length: 11 cm; inner diameter: 1.5 cm) with PTFE fittings were assembled in the following order: glass wool, glass beads, GAC of a depth specific to achieve a consistent empty bed contact time across all experiments, glass beads, and glass wool. Two columns were operated in parallel. The humidified formaldehyde-laden influent gas stream was split before being sent individually to each column, and a mass flow controller (Omega Engineering Inc., FMA5514ST, Stamford, CT) was used to maintain constant influent flow rates. Effluent lines from the packed bed columns ran through independent, 10 L, stainless steel sampling chambers (Eagle Stainless, CTH-24, Warminster, PA, USA). Within these sealed chambers, effluent formaldehyde concentrations were measured automatically every thirty minutes using the coupled sensor-spectrophotometric devices (CSSD) described in detail in section 3.3.1. Sampling chambers were opened only to change CSSD batteries periodically (approximately every four weeks) and/or to download and save the data and subsequently clear the data so that the data storage (4000 data points) was not exceeded. With the exception of the PTFE column fittings, all gas lines were stainless steel with Swagelok™ stainless steel fittings. Column effluent flow rates were monitored with flow meters to ensure that the expected, individual column flow rates were achieved.

Formaldehyde gas was generated from a solid permeation source heated to 60°C in a Kin-Tek standard gas generator (Kin-Tek, LaMarque, TX, USA; model 491MB) as described in section 3.3.2. Two permeation sources (Kin-Tek, LaMarque, TX, USA; 33896 and 32684) with different certified emission rates were used separately to achieve

the two concentrations tested. The permeation source with the lower emission rate, #33896, was used to achieve an influent formaldehyde concentration of 36 or 38 ppb_v, while the permeation source with the higher emission rate, #32684, was used to achieve an influent formaldehyde concentration of 100 ppb_v.

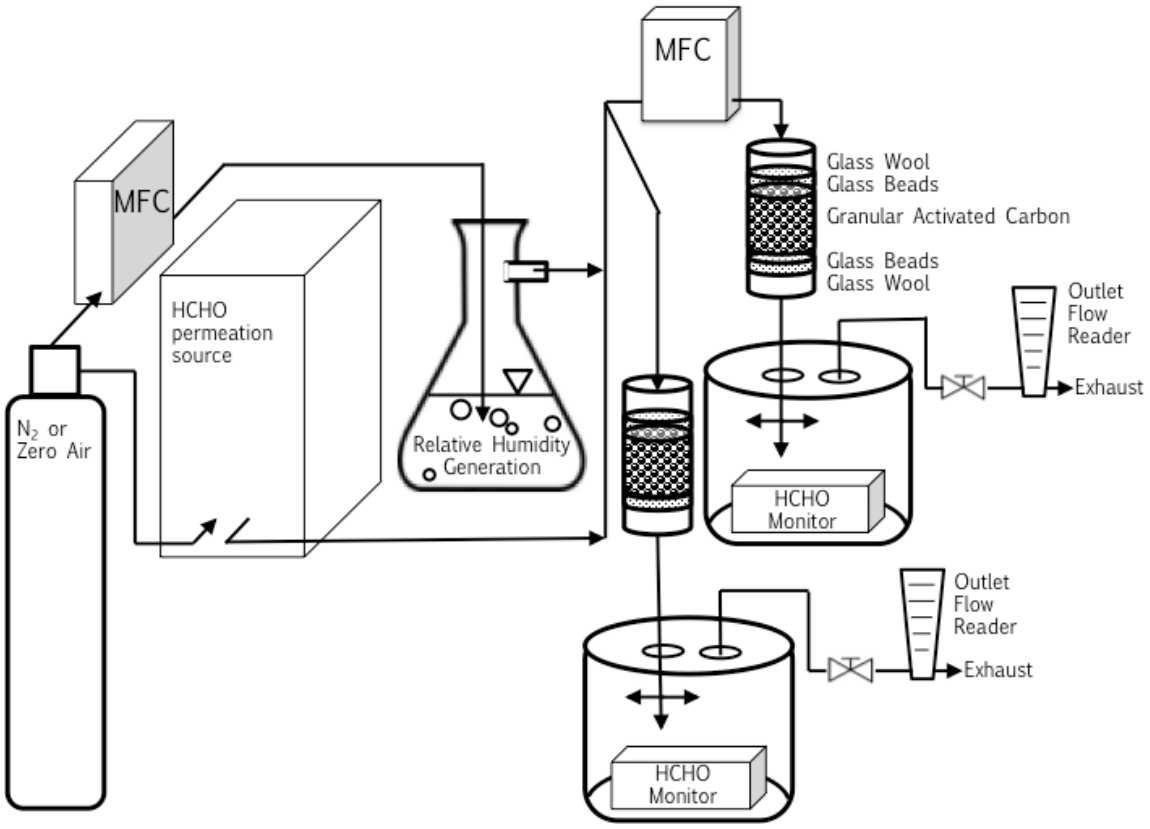

Figure 5.1. Schematic of experimental setup for evaluation of formaldehyde removal through packed GAC columns.

To humidify the influent gas stream to the test column, the gas line coming from the nitrogen or zero air tank that also supplied the Kin-Tek standard gas generator was split, controlled by a mass flow controller (Omega Engineering Inc., FMA5514ST, Stamford, CT), and bubbled through an Erlenmeyer flask filled with de-ionized water to

saturate the gas stream. This humidified gas stream was then rejoined with the formaldehyde-enriched effluent gas stream from the standard gas generator. Summaries of experimental conditions are reported in Tables 5.1 and 5.2.

Table 5.1. Summary of experimental conditions for packed bed column tests of formaldehyde removal at 100 ppb_v by BPL and BPL-N.

Parameter	Units	BPL	BPL-N
Q_K [a]	L/min	0.14	0.14
Q_{RH} [b]	L/min	0.138	0.138
Q_C [c]	L/min	0.138	0.138
Q_{Total} [d]	L/min	0.275	0.275
Emission source, rate	--, ng/min	#32684, 34.6	#32684, 34.6
HCHO concentration	ppb_v	100	100
Column bed depth	cm	5.5	5.5
Empty bed contact time	s	2.1	2.1
Column face velocity	cm/s	2.6	2.6
GAC mass	g	4.343	4.309

[a] Q_K is the flow rate of nitrogen gas passing through the Kin-Tek standard gas generator.

[b] Q_{RH} is the flow rate of nitrogen gas passing through the water-filled flask to humidify the gas stream to the desired relative humidity.

[c] Q_C is the flow rate through the column.

[d] Q_{Total} is the sum of Q_K and Q_{RH}.

Table 5.2. Summary of experimental conditions for packed bed column tests of formaldehyde removal at 36 ppb_v by BPL and BPL-N.

Parameter	Units	BPL	BPL-N
Q_K [a]	L/min	0.15	0.15
Q_{RH} [b]	L/min	0.15	0.15
Q_C [c]	L/min	0.15	0.2
Q_{Total} [d]	L/min	0.3	0.3
Emission source, rate	--, ng/min	#33896, 13.6	#33896, 13.6
HCHO concentration	ppb_v	36.3	36.3
Column bed depth	cm	2.7	3
Empty bed contact time	s	1.9	1.6
Column face velocity	cm/s	1.41	1.8
GAC mass	g	2.633	2.349

[a] Q_K is the flow rate of nitrogen gas passing through the Kin-Tek standard gas generator.

[b] Q_{RH} is the flow rate of nitrogen gas passing through the water-filled flask to humidify the gas stream to the desired relative humidity.

[c] Q_C is the flow rate through the column.

[d] Q_{Total} is the sum of Q_K and Q_{RH}.

5.3 RESULTS AND DISCUSSION

5.3.1 Structural characterization of GAC

All replicate samples of BPL, Centaur, and BPL-N exhibited Type I isotherms for nitrogen adsorption as expected. Refer to Figure 4.6 for a representative example of the nitrogen isotherm with adsorption and desorption branches shown. Nitrogen isotherms with adsorption and desorption branches for each GAC are presented in Appendix A.1 in Figure A-1. The determination of the appropriate range of relative pressures for which the BET plot was constructed considered the coefficient of determination (> 0.999) and the

value of the c parameter ($100 < c < 800$). Given these constraints, the relative pressure range considered for BET evaluation was consistently found to be 0.02 to 0.1 for all samples. The BET specific surface area for BPL and BPL-N are reported in Table 5.3 (values for the parameters reported in Table 5.3 for Centaur are previously reported in Table 4.3). These mean values were determined from two replicate samples for BPL and five replicate samples for BPL-N and were not found to be statistically different based on a two-sided t-test (df: 5, $\alpha = 0.05$, $t_{critical} = 2.571$).

Table 5.3. Summary of structural and chemical characteristics for BPL and BPL-N.

Parameter	**Units**	**BPL**		**BPL-N**	
Structural Characteristics		Mean	**SD**[a]	Mean	**SD**
BET Specific Surface Area	m^2/g-GAC	1089	31	1074	65
t-plot Micropore Surface Area	m^2/g-GAC	792	121	724	62
DFT Total Pore Volume	cm^3/g-GAC	0.42	0	0.41	0.03
DFT Micropore Volume	cm^3/g-GAC	0.36	0.03	0.35	0.02
t-plot Micropore Volume	cm^3/g-GAC	0.32	0.05	0.28	0.02
Chemical Characteristics					
Total Atomic % C		92.1	4.57	95.1	0.77
Total Atomic % O		7.8	4.57	3.33	0.46
Total Atomic % N		nd[b]		1.53	0.34
Surface Density of Acidic Functional Groups	µeq/m^2-GAC	0.317	0.03	0.143	0.06
Surface Density of Basic Functional Groups (Boehm)	µeq/m^2-GAC	0.470	0.05	0.697	0.03
Surface Density of Electron-Donating Potential (iodometric)	µeq/m^2-GAC	6.5	0.35	10.72	0.73

[a] standard deviation

[b] not detected

Table 5.3 also includes mean values and standard deviations for the following additional structural properties: t-plot micropore surface area, t-plot micropore volume,

DFT total pore volume, and DFT micropore volume. For all four of these structural properties, BPL and BPL-N were not found to be statistically different based on two-sided t-tests (df: 5, $\alpha = 0.05$, $t_{critical} = 2.571$) evaluated for each property. Similarly, using the BET surface area, t-plot micropore surface area, t-plot micropore volume, DFT total pore volume, and DFT micropore volume data presented for Centaur in Table 4.3, Centaur and BPL-N were also not found to be statistically different, according to a two-sided t-test (df: 5, $\alpha = 0.05$, $t_{critical} = 2.571$). Based on the pore volume analysis using DFT, micropores account for 86% and 85% of the total pore volume for BPL and BPL-N, respectively. The t-plot micropore surface area accounts for 73% and 67% of the total BET specific surface area for BPL and BPL-N, respectively. The minimum pore diameter measured in this work for BPL and BPL-N was 0.80 and 1.1 nm, respectively. For the same reason discussed in section 4.3.1, size exclusion of formaldehyde should not have a significant negative impact on removal, since the dominant GAC micropores have widths equivalent to between two and five pollutant diameters and the remaining GAC mesopores are even larger. Furthermore, that the BET specific surface area and the available total pore volume and micropore volume are similar among BPL, Centaur, and BPL-N, as illustrated in Figures 5.2 and 5.3, suggests that structural characteristics are not likely to explain observed differences between the two GACs with respect to formaldehyde removal.

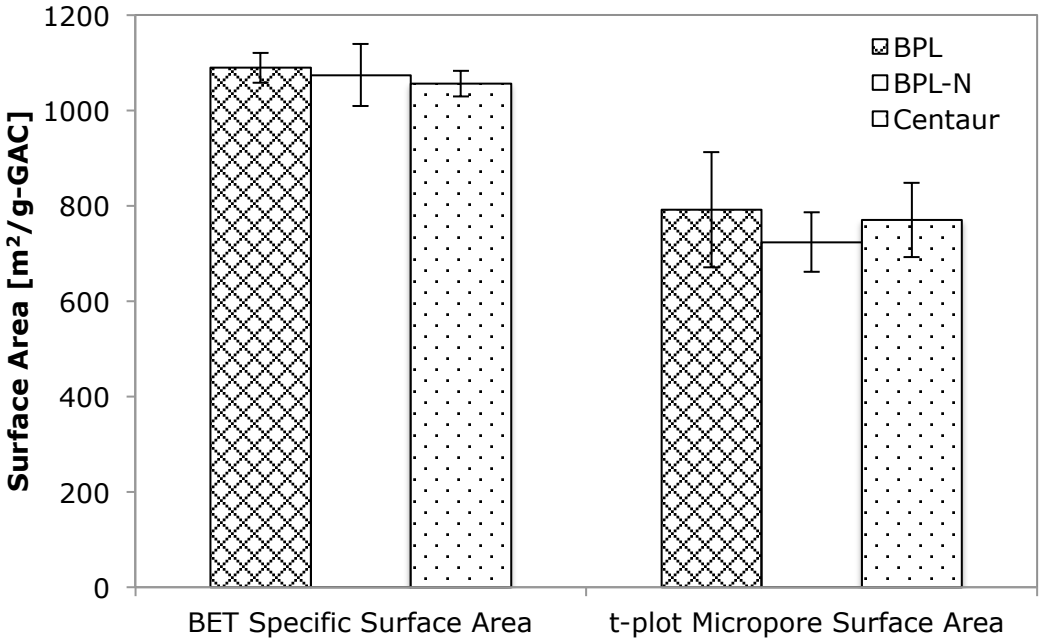

Figure 5.2. Comparison of BPL, BPL-N, and Centaur BET specific surface area and t-plot analysis of micropore surface area.

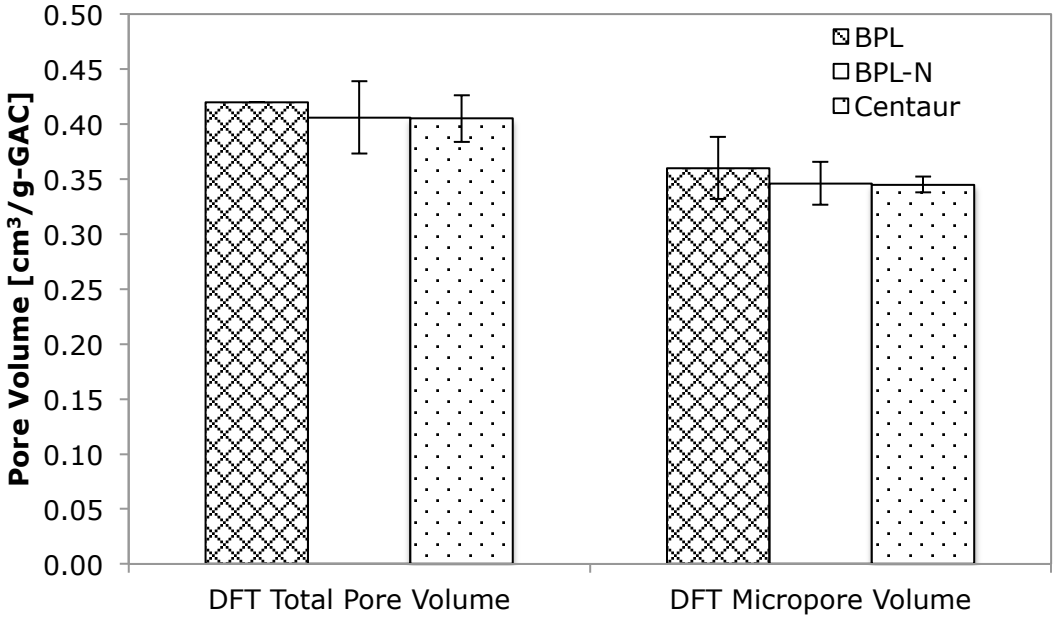

Figure 5.3. Comparison of BPL, BPL-N, and Centaur DFT total pore volume and DFT micropore volume.

In addition to considering how chemical treatment and chemical treatment of BPL GAC impacts bulk properties, such as specific surface area and total and micropore volume, it is important to assess whether the GAC chemical treatment processes alter the pore size distribution. To make this determination, the differential surface area distribution with respect to pore width, shown in Figure 5.4, and the differential pore volume distribution with respect to pore width, shown in Figure 5.5, were generated using DFT analysis. BPL and BPL-N show a similar pattern for differential surface area distribution and differential pore volume distribution. These two GACs also have similar magnitudes through the pore width range from 10 to 13.6 nm, while Centaur differential surface area and differential pore volume distribution is higher than that of BPL and BPL-N over the same range. This observation suggests that a greater proportion of the total surface area and total pore volume is accounted for in this pore width range for Centaur. For pore widths greater than 13.6 nm, all three GACs exhibit the same pattern of differential surface area and differential pore volume distribution. However, BPL-N shows slightly greater peaks in the range from 13.5 to 17.2 nm and in the range from 17.2 to 23.4 nm, indicating that pores within this range make a greater contribution to the total surface area and total pore volume of BPL-N than it does for total surface area and total pore volume of BPL or Centaur. This could be the result of the nitric acid oxidation phase of GAC modification, which breaks bonds within the activated carbon matrix and possibly opens up some of the smallest pores, shifting the distribution of pores towards larger micropores. However, because none of the GACs has pore sizes smaller than the kinetic diameter of formaldehyde or water vapor, it is not expected that this slight variation observed in the BPL-N pore size distribution results in a structurally-based advantage for formaldehyde removal.

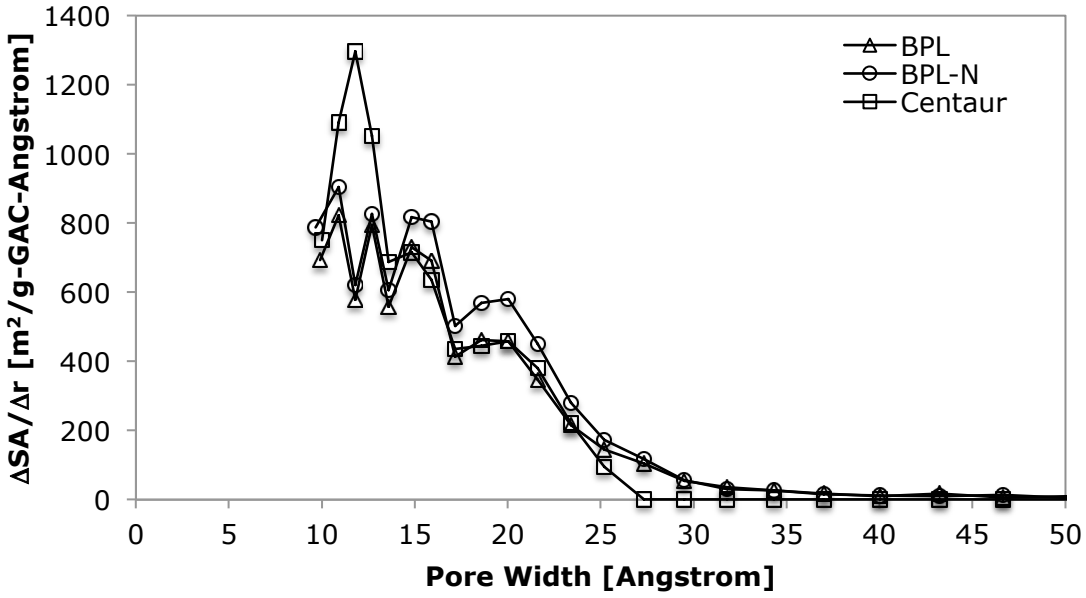

Figure 5.4. Comparison of BPL (△), BPL-N (○), Centaur (□) differential surface area distribution with respect to pore width.

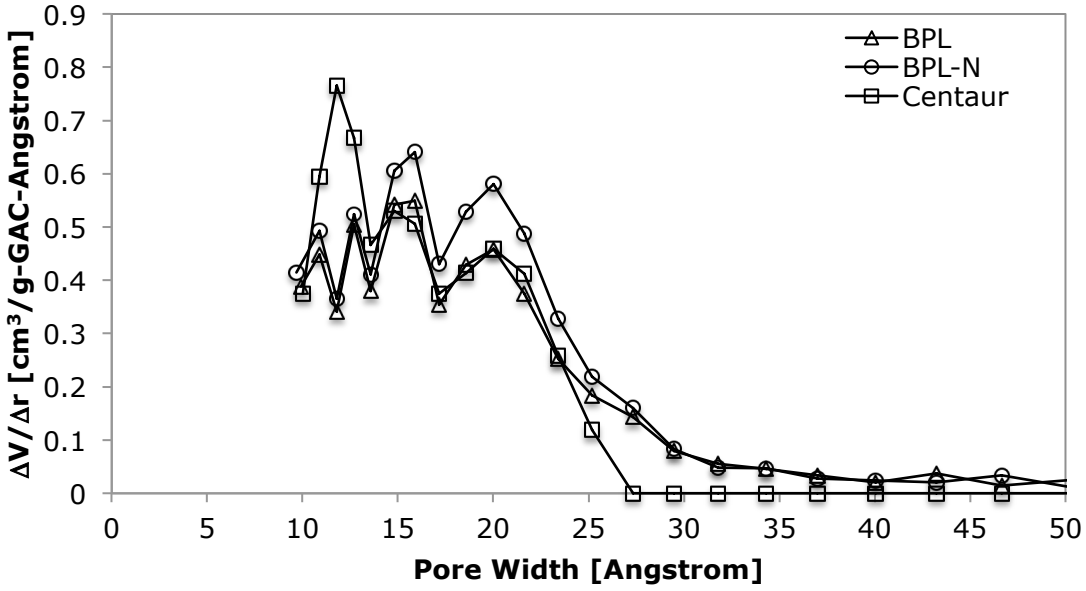

Figure 5.5. Comparison of BPL (△), BPL-N (○), and Centaur (□) differential volume distribution with respect to pore width.

5.3.2 Chemical characterization of GAC

A comparative summary of the quantitative chemical characteristics of BPL and BPL-N, as determined by XPS analysis, Boehm titrations, and iodometric titrations, were reported above in Table 5.3. Focusing first on the XPS results, the elemental compositions of BPL and BPL-N were dominated by carbon and oxygen, with the exception that BPL-N also contains nitrogen, as was expected based on the treatment outlined in section 5.2.1. The oxygen to carbon ratios (O/C) for BPL and BPL-N were 0.087 ± 0.057 and 0.035 ± 0.005, respectively, and were not statistically different (df: 7, $\alpha = 0.05$, $t_{critical} = 2.365$, $t_{calculated} = 2.030$). The major difference between the two GACs is the presence of nitrogen in BPL-N (1.53 atomic % ± 0.34 atomic %) and the absence of nitrogen in BPL. This difference is most clearly observed by comparing the high-resolution N 1s spectra for BPL and BPL-N, shown in Figure 5.6. As was noted in section 4.3.1 and shown in Figure 5.7, Centaur also contains a trace amount of nitrogen (0.36 atomic % ± 0.33 atomic %). Figures 5.6 and 5.7 both confirm that BPL does not contain nitrogen. A comparison of Centaur and BPL-N (Figure 5.8) revealed, however, that the binding energy ranges for the N 1s spectra of the two GACs were different. For BPL-N, the N 1s binding energy range spans from 397.1 eV to 403.2 eV, while for Centaur, the range over which the N 1s peak was integrated was 398.9 eV to 403.3 eV. Centaur shows no evidence of pyridinic nitrogen, which would appear as a peak in the binding energy range from ~397.5 eV to ~399 eV. On the other hand, the most dominant peak in the N 1s spectrum for BPL-N occurs precisely in this range. Deconvolution of the N 1s spectra led to identification of a distribution of chemical environments surrounding the nitrogen measured in both Centaur and BPL-N. The four primary types of chemical environments found for nitrogen in these two activated carbon matrices include: pyridines (397.5-399 eV); lactams, imides, and amides (399.5-400.5 eV); pyrroles

(400.5-401 eV); and alkylammonium, protonated pyridines, and protonated pyrroles (401-403 eV).

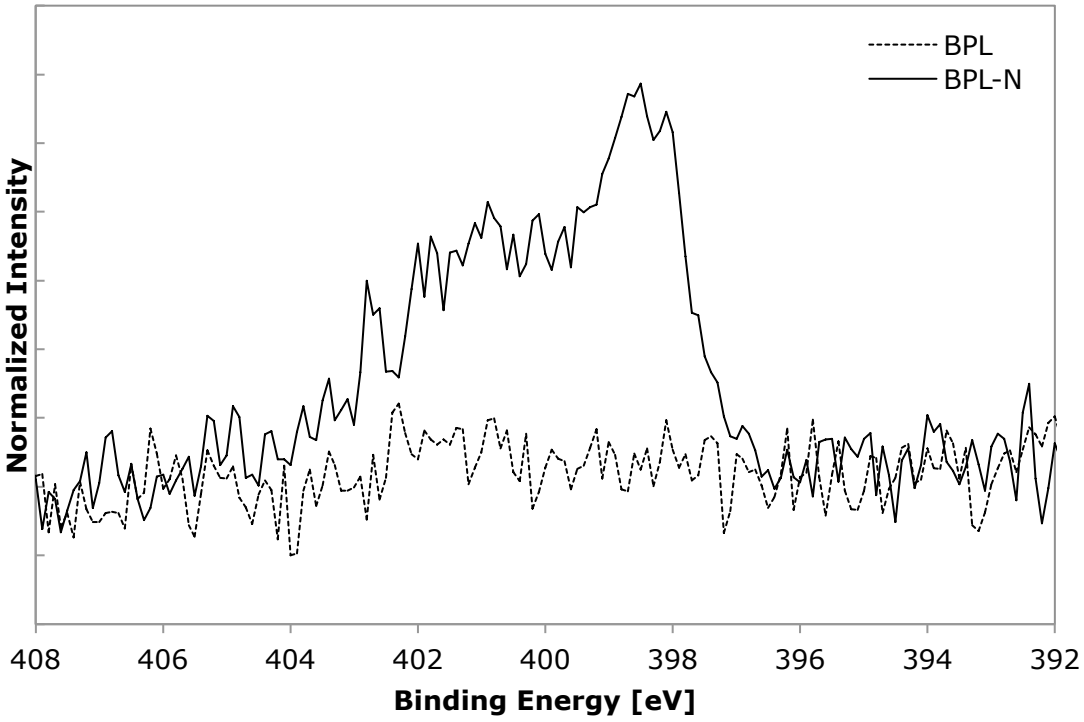

Figure 5.6. Normalized intensity of representative high-resolution XP spectra across binding energy range associated with N 1s electrons for BPL (---) and BPL-N (—).

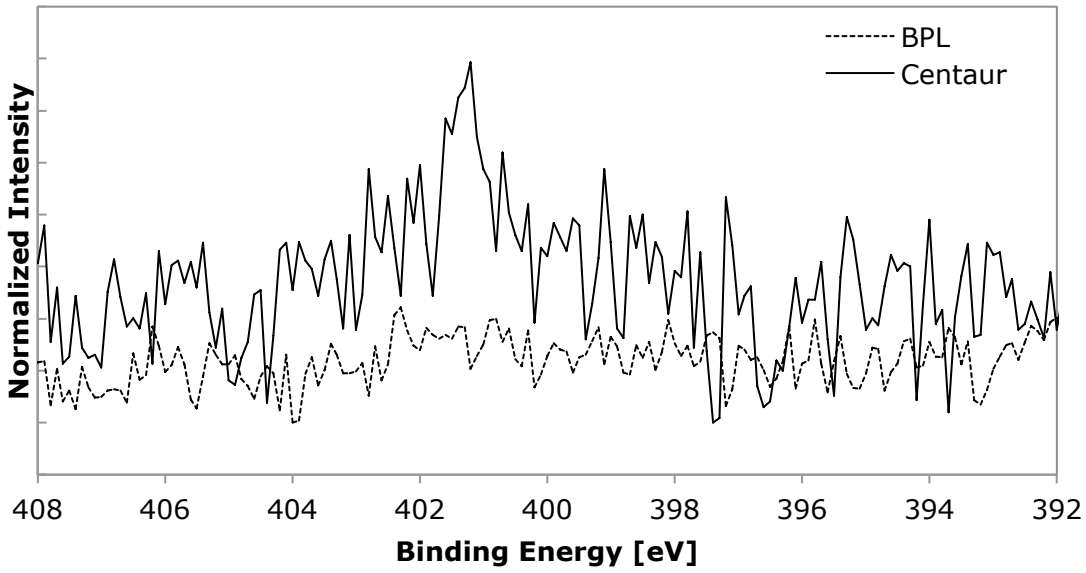

Figure 5.7. Normalized intensity of representative high-resolution XP spectra across binding energy range associated with N 1s electrons for BPL (---) and Centaur (—).

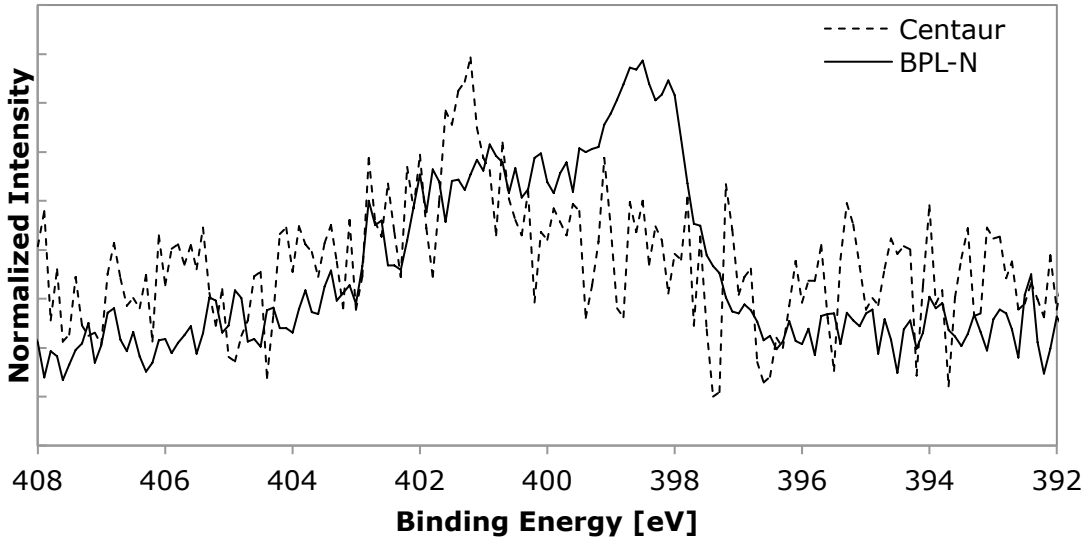

Figure 5.8. Normalized intensity of representative high-resolution XP spectra across binding energy range associated with N 1s electrons for Centaur (---) and BPL-N (—).

The identification and relative distribution among these different nitrogen complexes within each of the two GACs that contain nitrogen is presented in Figure 5.9. The N 1s spectra for two of three replicate samples of Centaur shows that the nitrogen-containing functional groups are entirely protonated. One of the three replicates shows pyrrolic nitrogen being the dominant nitrogen-containing species, with some minor contribution from protonated nitrogen-containing species, as well. In contrast, the N 1s spectra for all four replicate samples of BPL-N reveal that the nitrogen-containing functional groups are split almost equally between pyrrolic and pyridinic types, with the exception of one replicate, which did not exhibit any pyrrolic nitrogen, but did show evidence of lactams, imides, and amides (in addition to the pyridinic nitrogen).

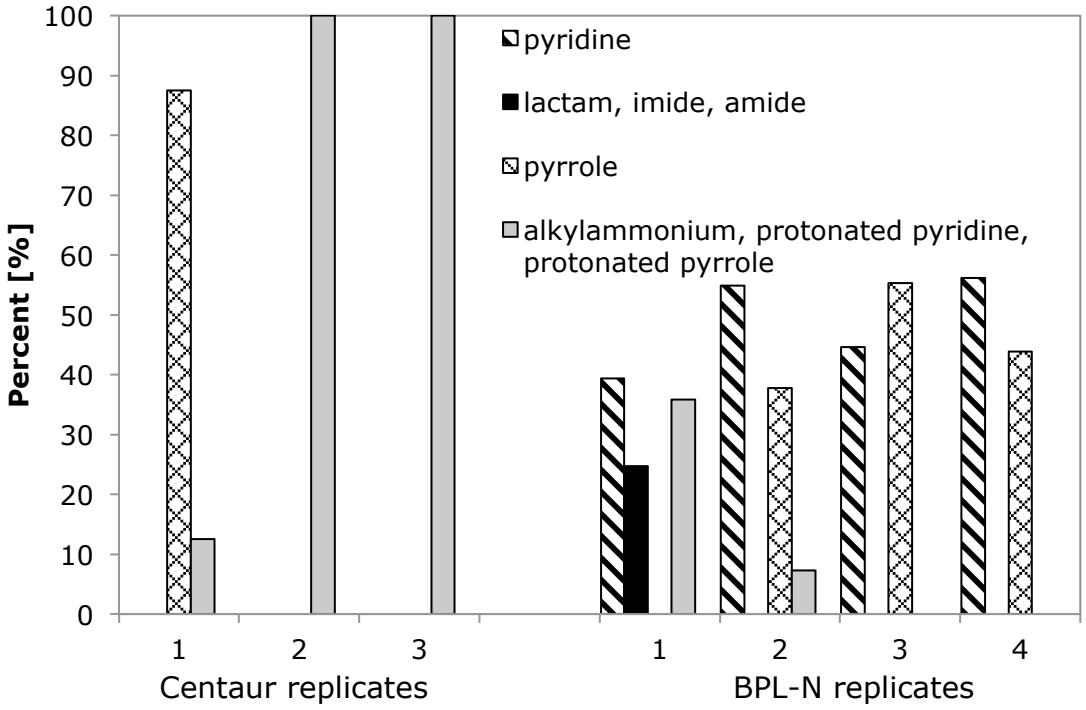

Figure 5.9. Relative distribution of nitrogen-containing functional groups, determined by peak position, for four replicates of BPL-N and three replicates of Centaur.

Nitrogen-containing groups that are pyrrolic and pyridinic have lone pairs of electrons that should contribute additional electron density to the regions within the activated carbon matrix in which they are found. Because this electron density is regionalized and because pyrrolic and pyridinic moieties are directly interspersed within the carbon ring structure, the sp^2-hybridization of the carbon rings should become less continuous and interrupted by sp^3-hybridized bonding. Presented in Figure 5.10, analysis of the C 1s spectra for each of the GACs reveals that the proportion of the carbon that is sp^3-hybridized is greater for BPL-N than for BPL and Centaur. The ratio of sp^2-hybridized carbon to sp^3-hybridized carbon shifts from 2.92 for BPL to 1.49 for BPL-N. Though Centaur contains some nitrogen, it contains only 23% as much nitrogen as was measured in BPL-N, and the ratio of sp^2-hybridized carbon to sp^3-hybridized carbon is more similar to that of BPL, at 4.19. These observed differences further support the conclusion that the types of nitrogen-containing functional groups incorporated into Centaur are different from those incorporated into BPL-N. More specifically, analysis of the N 1s and C 1s spectra demonstrates that the GAC treatment protocol developed for this research resulted in electron-donating nitrogen-containing functional groups in contrast to the protonated nitrogen-containing functional groups present in Centaur.

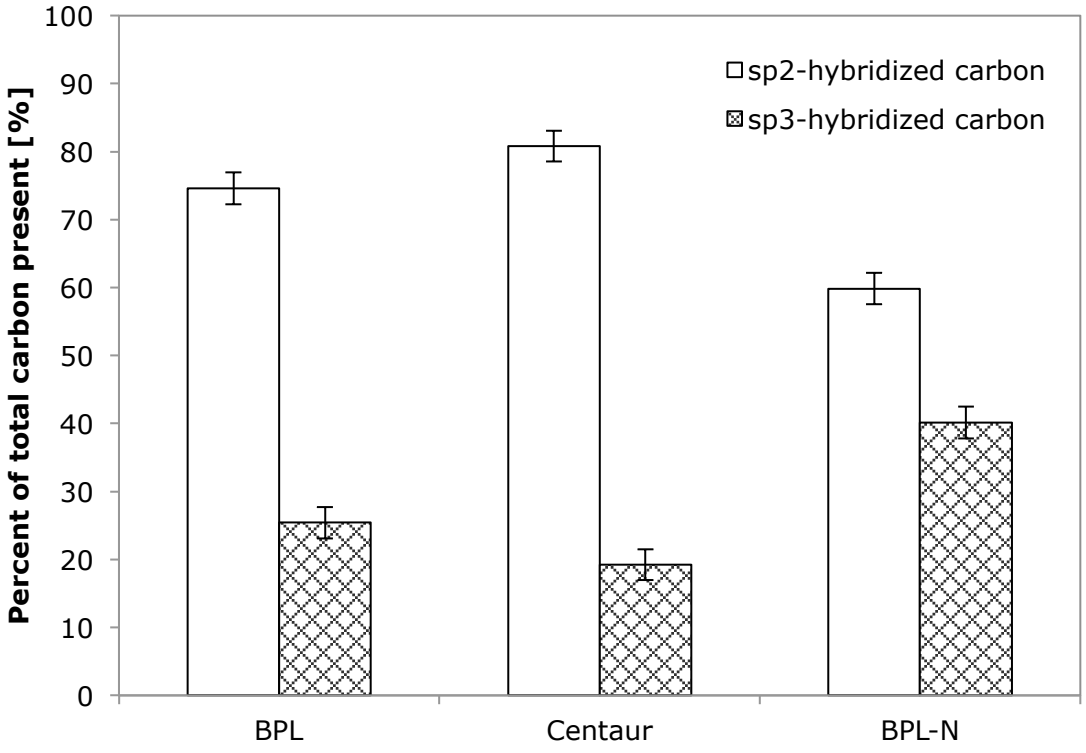

Figure 5.10. Relative distribution of sp^2-hybridized and sp^3-hybridized carbon, determined by peak position, for BPL, Centaur, and BPL-N.

Results from Raman spectroscopic analysis were also used to investigate the extent of disorder in the activated carbon matrix. For all GACs considered, two peaks associated with carbon are evident from Raman analysis. A plot of the normalized intensity of the Raman peak with respect to wavenumber, in Figure 5.11, shows the band (D band) associated with disordered carbon occurs at 1350 cm^{-1} and 1356 cm^{-1} for BPL-N and BPL, respectively. The band (G band) associated with graphitic carbon appears at 1588 cm^{-1} for both BPL and BPL-N. The ratios of the intensities of these two peaks, I_D/I_G, were 0.98 ± 0.02, 0.94 ± 0.04, and 1.04 ± 0.04, for BPL, Centaur, and BPL-N, respectively. For the BPL/BPL-N pair, the difference between their respective I_D/I_G ratios was statistically significant by a two-sided t-test (df: 18, $\alpha = 0.05$, $t_{critical} = 2.101$, $t_{calculated} =$

4.114) indicating that the extent of disorder in BPL-N is greater than that of BPL. This result supports the conclusions drawn from XPS analysis, which showed an increase in sp^3-hybridized carbon at the surface of BPL-N and is best explained by the presence of electron-donating nitrogen-containing functional groups, which disrupt sp^2-hybridization especially near edge plane sites. For the BPL/Centaur pair, the difference between their respective I_D/I_G ratios was statistically significant by a two-sided t-test (df: 18, $\alpha = 0.05$, $t_{critical} = 2.101$, $t_{calculated} = 2.242$). However, in this case, the extent of disorder is greater for BPL than for Centaur. Thus, for the Centaur/BPL-N pair, the I_D/I_G ratio were statistically different (df: 18, $\alpha = 0.05$, $t_{critical} = 2.101$, $t_{calculated} = 5.24$), reflecting a much greater extent of disorder in BPL-N relative to Centaur.

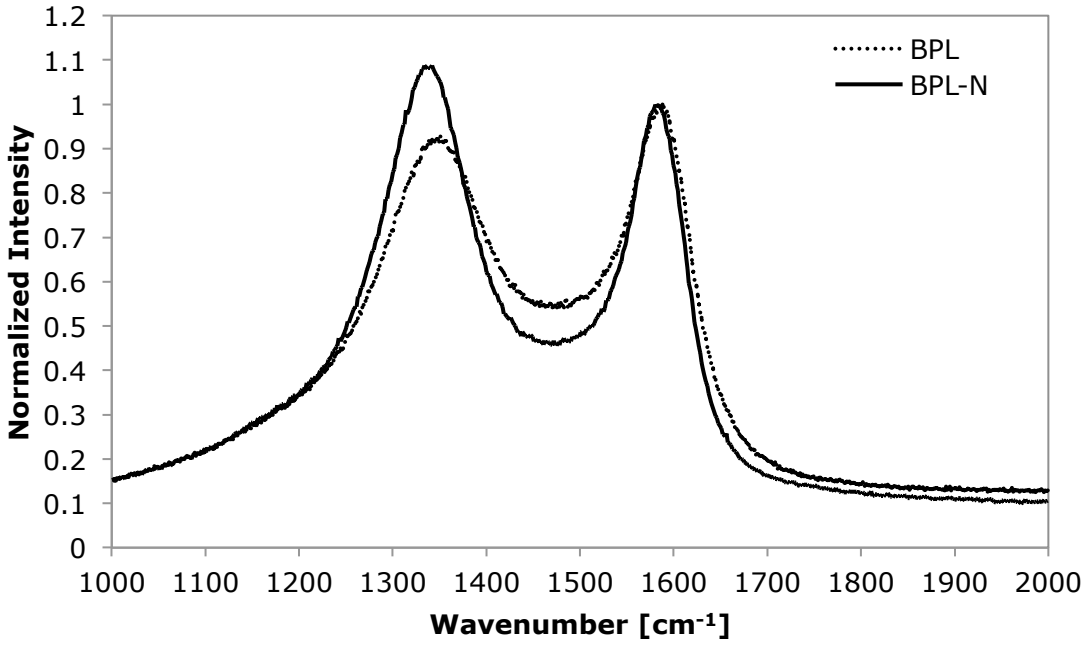

Figure 5.11. Representative first-order Raman spectra of BPL (---) and BPL-N (—) normalized to the intensity of the band at 1588 cm^{-1}.

In addition to spectroscopic analysis, two titration techniques were employed to investigate the presence and density of acidic and basic surface functional groups. Results from Boehm titrations are reported in triplicate in Appendix A.2 in Tables A-1 and A-2. A comparison of BPL and BPL-N yields conclusions similar to those discussed in section 4.3.1. BPL-N has a lower surface density of acidic functional groups, a higher surface density of basic functional groups, and a higher surface density of electron-donating potential relative to BPL. These differences between the mean values of each parameter for BPL and BPL-N were evaluated for their statistical significance using two-sided t-tests (df: 4, $\alpha = 0.05$, $t_{critical} = 2.776$). Based on the results from the titration and statistical analyses, reported in Table 5.4, it can be concluded that the differences between the mean surface densities of acidic functional groups and the mean surface densities of basic functional groups for the two GACs, as determined using the Boehm titration technique, are statistically significant. Similarly, the difference between the mean surface densities of electron-donating potential for the two GACs, as determined using the iodometric titration technique, is also statistically significant.

Table 5.4. Two-sided t-tests for difference between the means for surface densities of acidic and basic functional groups and electron-donating potential for BPL and BPL-N.

	Units	BPL	BPL-N
		Surface Density of Acidic Functional Groups (Boehm)	
mean	μeq/m^2-GAC	0.317	0.143
standard deviation	μeq/m^2-GAC	0.025	0.059
n		3	3
calculated t-value		4.671	
		Surface Density of Basic Functional Groups (Boehm)	
mean	μeq/m^2-GAC	0.470	0.697
standard deviation	μeq/m^2-GAC	0.053	0.027
n		3	3
calculated t-value		6.623	
		Surface Density of Electron-Donating Potential (iodometric)	
mean	μeq/m^2-GAC	6.490	10.715
standard deviation	μeq/m^2-GAC	0.347	0.725
n		3	3
calculated t-value		9.107	

Previously, it has been suggested that enhanced basicity of carbons is a consequence of strong π electron delocalization (Leon y Leon et al., 1992), and Maldonado and Stevenson (2005) have shown that the electron-donating nitrogen sites, produced through nitrogen-doping of carbon nanofibers, increase basicity. It has also been suggested that basicity increases because the activated carbon that contains electron-donating nitrogen sites is less susceptible to oxidation (Mang et al., 1992; Maldonado and Stevenson, 2005), a process that typically corresponds to more acidic surface functional groups. The titration and spectroscopic results presented here support these conclusions that have been reported previously. BPL-N not only has slightly over one and a half times

the surface density of basic functional groups and electron-donating potential, but it also has less than half the surface density of acidic functional groups, relative to BPL.

XPS analysis provides additional information that is complementary to the titration results. Table 5.5 presents a comparison of the O 1s peak positions for BPL and BPL-N and assigns the type of oxygen complexes detected to their corresponding binding energy range.

Table 5.5. Average peak position of component peaks comprising the O 1s region for BPL and BPL-N and associated peak ranges and assignments to specific types of oxygen complexes.

BPL		BPL-N			
O 1s component peak position				Peak Range [eV]	Peak Assignment
Mean	SD[a]	Mean	SD		
530.46	0.18			530-530.9	carbonyl oxygen
531.61	0.23	531.58	0.17	531-531.9	carbonyl oxygen in quinones
532.64	0.24	532.75	nr[b]	532-532.9	carbonyl oxygen in esters, anhydrides, and oxygen atoms in hydroxyl groups
533.63	0.16	533.50	0.41	533-533.9	non-carbonyl oxygen in esters and anhydrides
534.88	0.40	535.47	0.39	534-535.9	oxygen atoms in carboxyl groups
		537.16	nr[b]	> 536	adsorbed water and/or oxygen

[a] standard deviation

[b] not reported (because only one replicate measured)

Figure 5.12 presents the relative distribution (on a percent basis) of the oxygen complexes observed for each replicate of each of the three GACs. Starting with BPL-N,

the majority of the oxygen-containing surface functional groups present were carbonyl oxygen found in quinones and non-carbonyl oxygen in esters and anhydrides. BPL-N also contained a small amount of carboxylic acid groups, which are likely responsible for imparting the minimal surface acidity detected through the Boehm titrations. BPL had the most heterogeneous results of the three GACs. All three carbonyl-type oxygen functional groups were identified and quantified in varying proportions in nearly every BPL replicate. Non-carbonyl oxygen associated with esters and anhydrides were also observed in every BPL replicate. As discussed in section 4.3.1, BPL had oxygen associated with carboxylic acid groups. From Figure 5.12, it is not immediately evident whether this result supports the observation (from Boehm titration results) that BPL has the highest surface acidity of the three GACs because BPL-N also has oxygen associated with carboxylic acid groups in proportions similar to those of BPL. However, taking into account the absolute amount of oxygen contained by BPL and BPL-N (7.8 ± 4.57 atomic % and 3.33 ± 0.46 atomic %, respectively), it becomes clear that because BPL contains almost two and a half times as much total oxygen as BPL-N, BPL would also contain a higher absolute amount of carboxylic acid oxygen. In comparison, Centaur had the highest absolute amount of oxygen (12.0 ± 4.24 atomic %) and the most homogeneous distribution of oxygen complexes (across three replicates) of the three GACs examined. As was noted in section 4.3.1, Centaur did not contain any oxygen associated with carboxylic acid groups. Instead, the three carbonyl-type oxygen groups dominated each replicate, and surface acidity measured by the Boehm titration could be explained by the presence of oxygen associated with hydroxyl groups. A small amount of non-carbonyl oxygen was also detected in each Centaur replicate. Although not as homogeneous as the results for Centaur, BPL-N appears to be more homogeneous than BPL with respect to the type and distribution of surface oxygen complexes. Not only

does this result demonstrate that the chemical treatment process developed in this research to modify BPL and create a GAC enriched in pyridinic and pyrrolic nitrogen functional groups yields reproducible results, but it may also reduce variation in the types of oxygen complexes present in the chemically treated BPL-N.

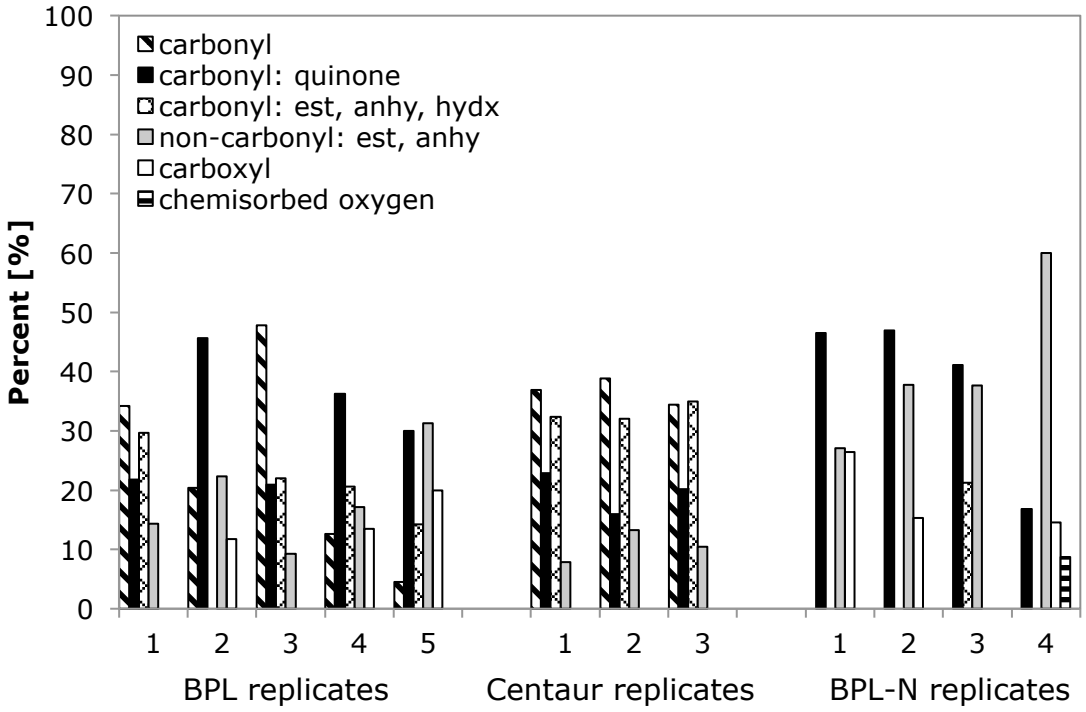

Figure 5.12. Relative distribution of oxygen complexes, determined by peak position, for five replicates of BPL, three replicates of Centaur, and four replicates of BPL-N.

To summarize the impact of modifying the traditional GAC, BPL, through chemical treatment, the results from the structural and chemical characterization of BPL and BPL-N demonstrate that the chemical treatment process successfully incorporates electron-donating, pyridinic and pyrrolic nitrogen-containing functional groups into the activated carbon matrix without compromising the structural properties of the material. The nitrogen-containing functional groups serve to disrupt the regions of sp^2-hybridized

bonding, increasing disorder in the activated carbon matrix. These same groups are electron-rich, contributing a lone pair of electrons to the delocalized, conjugated π electron clouds interspersed between the basal sheets of the activated carbon, in addition to the π electron already donated through bonding. The dual electron contributions increases the basicity and electron-donating potential of BPL-N. By producing a new GAC, BPL-N, that both contains more nitrogen than its precursor and contains nitrogen functional groups that are different from those found in the commercially available, chemically treated GAC, Centaur, it is possible to subsequently evaluate the impact of both nitrogen presence and nitrogen type on the GAC performance with respect to formaldehyde removal.

5.3.3 The influence of surface chemical properties on formaldehyde removal through packed bed GAC columns

The first set of GAC packed bed columns tests was designed to evaluate the relative performance of BPL, Centaur, and BPL-N with respect to formaldehyde removal and investigate the influence of several surface chemical properties including surface basicity, electron-donating potential, and nitrogen presence and type. Formaldehyde removal through packed bed columns of either BPL or BPL-N was first tested at a formaldehyde inlet concentration of 100 ppb_v, 50% relative humidity (RH), and with nitrogen gas as the carrier gas stream. Six-hour, time-weighted averaged effluent formaldehyde concentrations, normalized by the inlet formaldehyde concentration, are shown for the BPL column and the BPL-N column in Figure 5.13. The formaldehyde removal capacity for BPL calculated for 95% breakthrough with respect to the aforementioned experimental conditions was determined to be 23 μg/g-GAC. To reach 95% breakthrough, the number of bed volumes fed was slightly less than 215,000. In contrast, even after approximately twice the number of bed volumes fed (420,000 bed

volumes), BPL-N only reached 70% breakthrough, and the removal capacity at that point was 72 μg/g-GAC, or a little over three times the 95% breakthrough capacity of BPL.

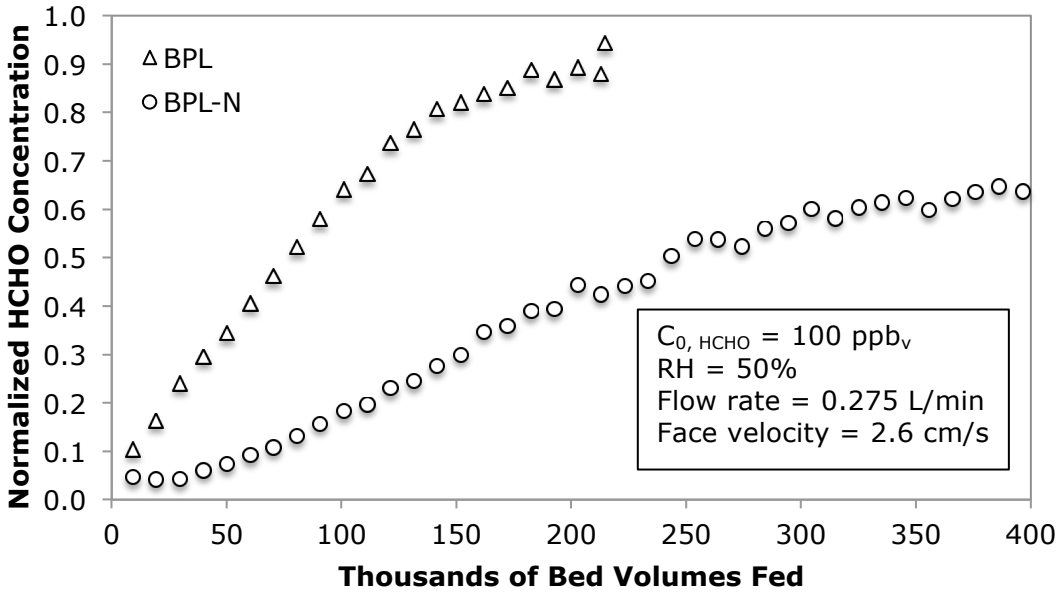

Figure 5.13. Effluent formaldehyde concentrations for BPL (△) and BPL-N (○) normalized by the influent formaldehyde concentration (100 ppb_v) and presented with respect to thousands of bed volumes fed.

Another way to compare performance of BPL and BPL-N is to determine the number of bed volumes fed to a specific breakthrough concentration (referred to as the breakpoint) for each GAC. For the formaldehyde influent test concentration of 100 ppb_v, 15% breakthrough would correspond to an outlet concentration of 15 ppb_v, which is just below the 16 ppb_v NIOSH chronic recommended exposure limit. BPL and BPL-N reached 15% breakthrough after approximately 13,000 and 85,000 bed volumes fed, respectively. BPL-N was operated for seven times as many bed volumes to be fed before 15% breakthrough was reached. Similarly, the formaldehyde removal capacity for BPL-N at 15% breakthrough was 22 μg/g-GAC, which is nearly seven times greater than the

mass of formaldehyde removed by the BPL at the same breakpoint, which was 3.3 μg/g-GAC. Gas-phase pollutant control media are frequently evaluated at 50% breakthrough, as well. For this case, the time to breakthrough was achieved after 70,000 and 240,000 bed volumes fed, and the removal capacities at this point were 14 and 51 μg/g-GAC, for BPL and BPL-N, respectively. BPL-N achieves four times the removal capacity and extends the time to 50% breakthrough by three times that of BPL.

Similar trends emerged from the results of testing formaldehyde removal in packed bed columns of all three selected GACs at a lower influent formaldehyde concentration, 36 ppb_v. In Figure 5.14, six-hour, time-weighted averaged effluent formaldehyde concentrations, normalized by the influent formaldehyde concentration, from packed bed columns of each of the three GACs (two replicates shown for BPL-N) are presented with respect to the number of bed volumes fed. BPL reached 95% breakthrough after slightly more than 675,000 bed volumes, while for BPL-N, breakthrough was not achieved until over five times as many bed volumes (nearly 3.6 million bed volumes) had been fed. Furthermore, at 95% breakthrough, BPL had removed 19 μg/g-GAC, while BPL-N had removed 162 μg/g-GAC at 95% breakthrough, or 8.5 times greater than was removed by BPL. At 50% breakthrough, BPL-N removed more than 12 times the formaldehyde, on a per-mass of GAC basis, as BPL and more than six times that of Centaur.

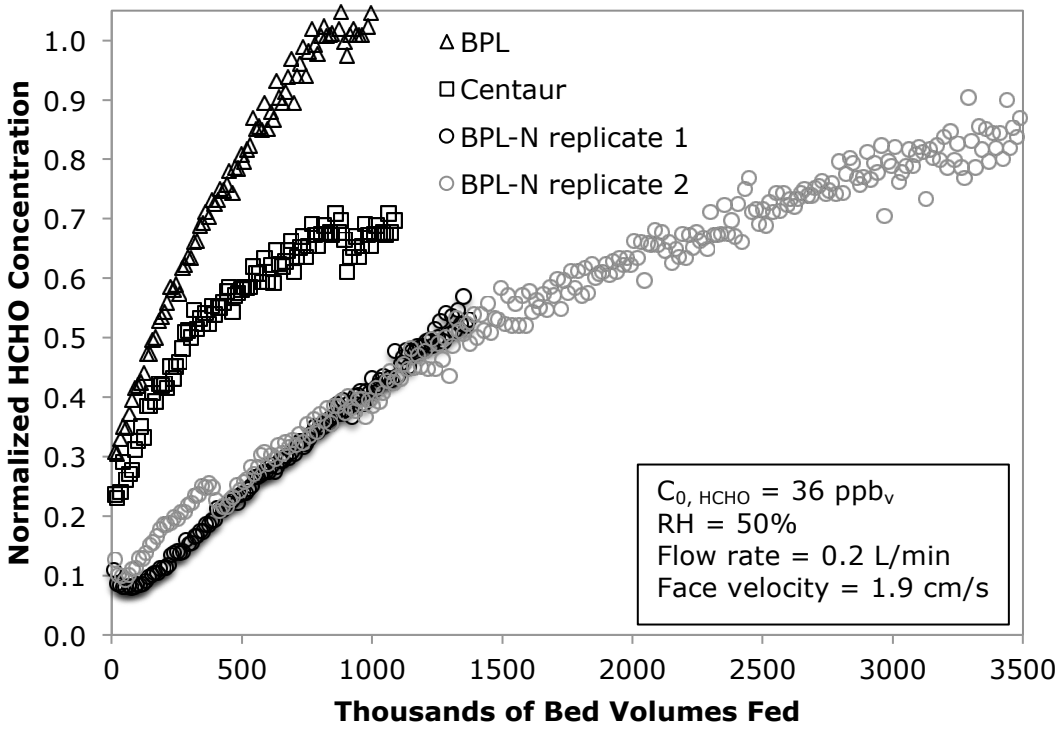

Figure 5.14. Effluent formaldehyde concentrations for BPL (△), Centaur (□), and two replicate columns of BPL-N (○; black and grey) normalized by the influent formaldehyde concentration (36 ppb_v) and presented with respect to thousands of bed volumes fed.

Looking at the apparent mass surface loading of formaldehyde with respect to bed volumes fed (Figure 5.15) illustrates the improved performance of BPL-N over both BPL and Centaur. Not only is BPL-N apparent surface loading of formaldehyde higher than the other two carbons, but the difference increases with increasing bed volumes fed, indicating that BPL-N has the capacity to sustain a given formaldehyde removal efficiency over longer periods of time. While BPL-N apparent surface loading of formaldehyde does not appear to be linear, it does not reach a plateau as rapidly as does BPL. Only after three times as many bed volumes are fed does BPL-N begin to approach an apparent surface loading plateau.

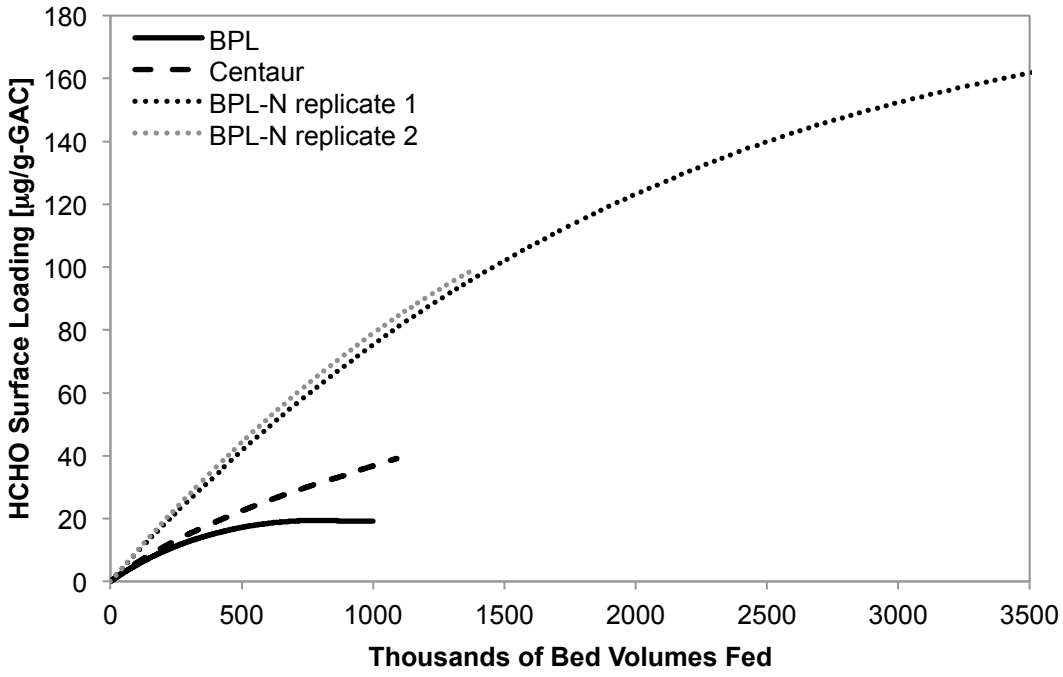

Figure 5.15. Surface loading of formaldehyde for BPL (—), Centaur (---), and BPL-N replicate 1 (•••) and replicate 2 (•••) normalized by the mass of GAC in the column and presented with respect to thousands of bed volumes fed.

For the three GACs considered, apparent formaldehyde surface loading per mass of GAC increased in the following order: BPL < Centaur < BPL-N. Normalizing apparent formaldehyde surface loading with respect to surface area, it is possible to investigate whether there is an association between apparent formaldehyde surface loading and surface basicity, as has been observed previously at higher formaldehyde concentrations (Carter et al., 2011). Apparent formaldehyde surface loading, normalized per meter squared of GAC surface area is plotted with respect to surface density of basic functional groups (Figure 5.16), as determined by the Boehm titration technique, and with respect to electron-donating potential (Figure 5.17), as determined by the iodometric titration technique. Surface density of basic functional groups and electron-donating

potential both have a positive relationship with formaldehyde surface loading at 50% breakthrough. These observations confirm the expectation that GAC surface basicity plays an influential role in formaldehyde removal at ppb_v-level concentrations. Comparing the coefficients of determination reported in Figures 5.16 and 5.17, it also appears that electron-donating potential bore a stronger relationship to apparent formaldehyde surface loading than surface density of basic functional groups does. This outcome suggests that electron-donating potential is a more robust surface parameter than surface density of basic functional groups to use to assess relative GAC performance when multiple GACs of unknown elemental composition are being considered for formaldehyde pollutant control.

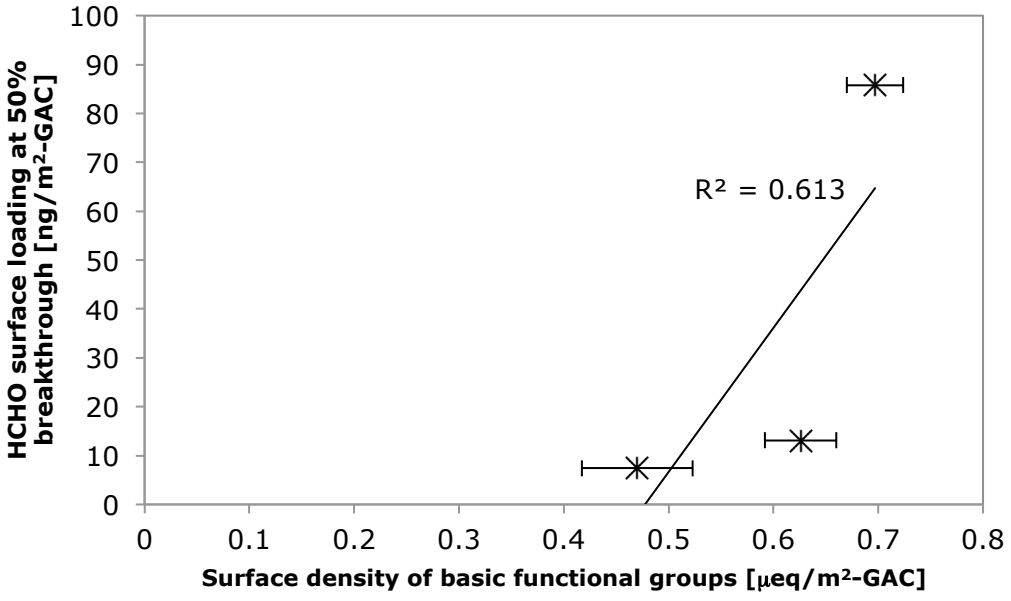

Figure 5.16. Evaluation of relationship between apparent formaldehyde surface loading at 50% breakthrough at 36 ppb_v for BPL, Centaur, and BPL-N and surface density of basic functional groups, as determined by the Boehm titration technique. Coefficient of determination is reported beside the trend line.

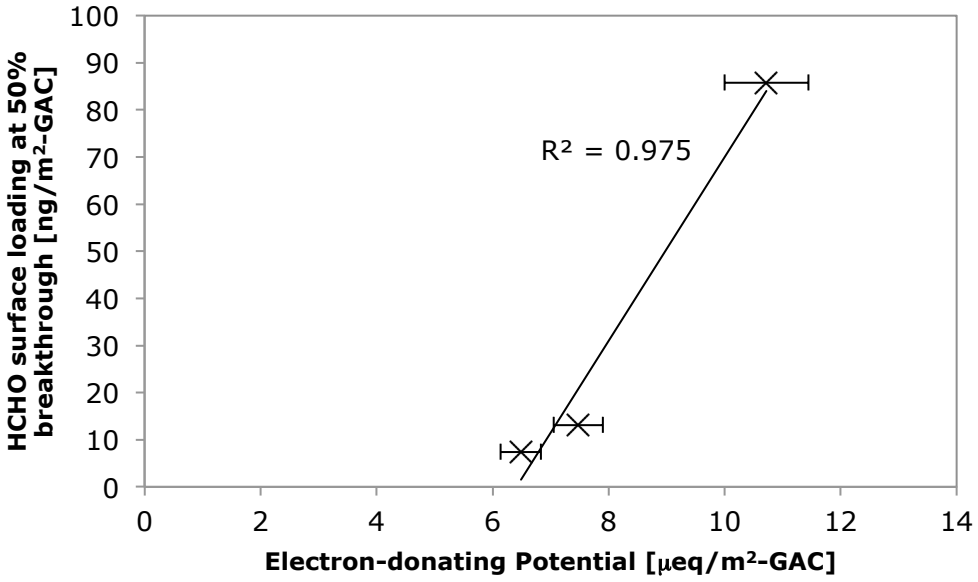

Figure 5.17. Evaluation of relationship between apparent formaldehyde surface loading at 50% breakthrough at 36 ppb_v for BPL, Centaur, and BPL-N and electron-donating potential, as determined by the iodometric titration technique. Coefficient of determination is reported beside the trend line.

One of the primary goals of this chapter was to investigate the role of nitrogen incorporated at the GAC surface with respect to formaldehyde removal. Given the positive association between the two measures of surface basicity evaluated in this research, it is valuable to also consider the relationships between GAC nitrogen content and these same two measures of surface basicity. Plotting both electron-donating potential and surface density of basic functional groups for each of the three GACs with respect to nitrogen content, electron-donating potential appears to have a stronger relationship with GAC nitrogen content than does surface density of basic functional groups (Figure 5.18). BPL-N has the highest nitrogen content, the greatest electron-donating potential, and the highest apparent surface loading of formaldehyde at 50% breakthrough of the three GACs tested. These results support the hypothesis that

enriching GAC with nitrogen enhances gas-phase formaldehyde removal through an associated increase in the electron-donating potential of the GAC. Moreover, nitrogen functional groups can only contribute to GAC electron-donating potential when they have electrons to donate. Pyridinic and pyrrolic nitrogen functional groups donate lone pairs of electrons to the GAC surface, while protonated nitrogen functional groups do not. Not only does BPL-N contain the most nitrogen, but it also contains mainly pyridinic and pyrrolic nitrogen functional groups, making a measurable impact on BPL-N electron-donating potential.

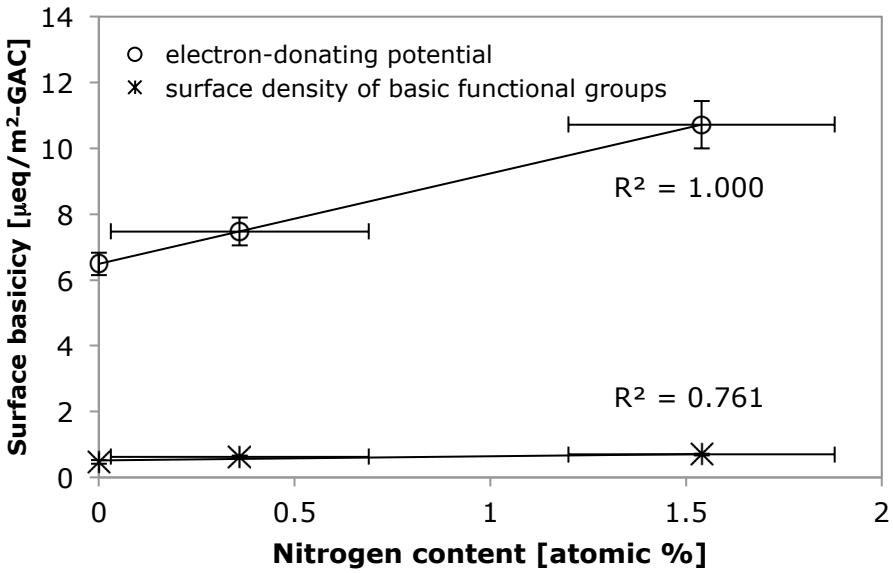

Figure 5.18. Evaluation of relationship electron-donating potential and surface density of basic functional groups for BPL, Centaur, and BPL-N and electron-donating potential with respect to GAC nitrogen content. Coefficients of determination are reported beside the trend line.

5.3.4 Evidence for catalysis of formaldehyde through packed bed GAC columns

The second and third sets of packed bed column experiments were designed to investigate the removal mechanisms driving formaldehyde removal for BPL and BPL-N. Although BPL-N performed much better than BPL with respect to formaldehyde removal

at both 100 and 36 ppb_v in the packed bed tests just discussed, the results did not indicate directly whether catalysis may be occurring. The results presented in section 5.3.3 could reflect enhanced removal by BPL-N (relative to BPL) via a combination of removal mechanisms including adsorption and/or catalysis. The packed bed column tests discussed in section 5.3.3 were all carried out with zero-grade nitrogen gas as the carrier gas. To study whether the oxygen reduction mechanism hypothesized to initiate catalytic removal of formaldehyde was potentially occurring, the second set of packed bed column tests were set up according to the same conditions outlined in Table 5.2, but ultra-zero air was used as the carrier gas instead of nitrogen and the inlet formaldehyde concentration was slightly increased to 38 ppb_v. Effluent formaldehyde concentrations were measured from columns of BPL and BPL-N during three cycles of formaldehyde exposure and regeneration phases, as described in greater detail in section 5.2.3. Under these conditions, it would be expected that the performance of BPL with respect to formaldehyde removal would remain similar to the performance observed when nitrogen gas was the carrier gas. On the other hand, the formaldehyde removal by BPL-N would be expected to improve more dramatically than would be observed with BPL. If catalysis were occurring, the effluent formaldehyde concentration should reach steady state during the formaldehyde exposure phase. During the regeneration phase, the effluent formaldehyde concentration should not decrease as would be expected if the formaldehyde were reversibly adsorbed to the surface. On the other hand, during the exposure phases of multiple, sequential cycles of exposure and regeneration, effluent formaldehyde concentrations from the BPL-N column should not increase as would be expected if irreversible (in contrast to reversible) adsorption were occurring.

Over the course of the first cycle of exposure and regeneration phases of the experiment, in excess of 650,000 bed volumes of formaldehyde-containing gas were fed

to the activated carbon. The BPL GAC showed progression towards complete breakthrough, as would be expected if adsorption were the dominant removal mechanism (Figure 5.19). On the other hand, BPL-N maintained 80-87% removal of formaldehyde throughout the entire time the column was exposed to an influent gas stream contaminated with formaldehyde. Once the influent gas stream was changed to be only ultra-zero air without formaldehyde (regeneration phase), the effluent formaldehyde concentration exiting the column with BPL showed the beginning of a decay profile (closed triangles in Figure 5.19), but for BPL-N, effluent formaldehyde concentrations (closed circles, Figure 5.19) were the same as during the phase of formaldehyde exposure. This result would suggest that the formaldehyde is not being removed via reversible adsorption because, during regeneration, no desorption was observed.

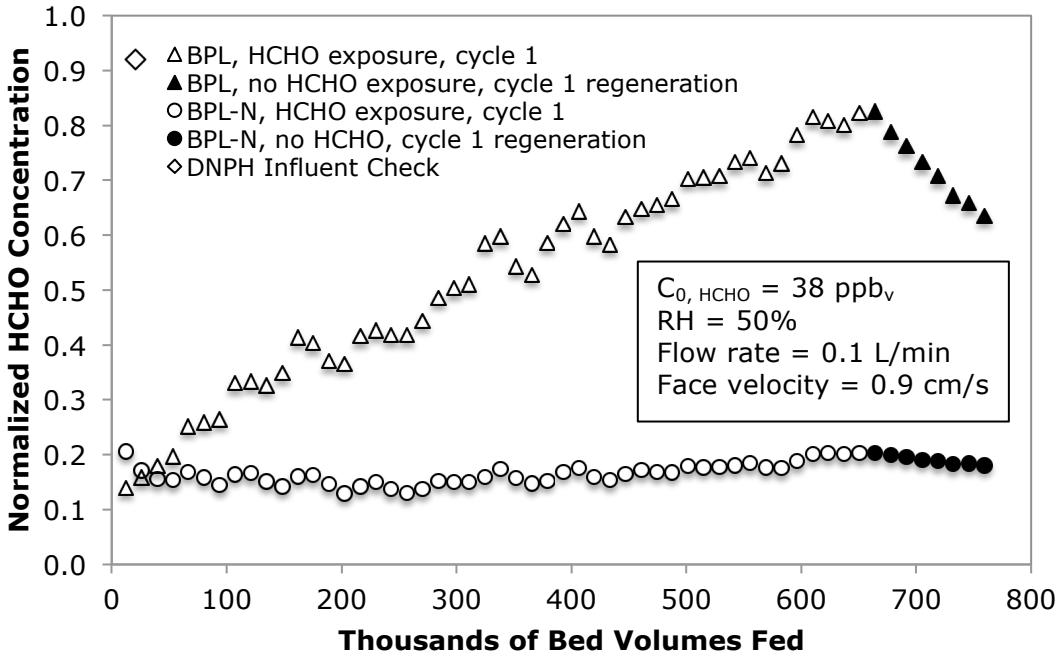

Figure 5.19. Cycle 1. Effluent formaldehyde concentrations for BPL and BPL-N during formaldehyde exposure (△,○) and regeneration (▲,●) normalized by the influent formaldehyde concentration (38 ppb_v) and presented with respect to thousands of bed volumes fed. The influent formaldehyde concentration, as measured with DNPH, is also shown (◇).

The markedly different column responses to formaldehyde exposure and regeneration continued for two more cycles. During cycles 2 and 3, the formaldehyde exposure phase lasted in excess of 100,000 bed volumes fed, while the column regeneration phase also lasted in excess of 100,000 bed volumes fed. During the formaldehyde exposure phase of the second (Figure 5.20) and third (Figure 5.21) cycles, BPL removed almost none of the influent formaldehyde, showing that the formaldehyde removal capacity had been exhausted. Formaldehyde breakthrough characteristic of adsorption had occurred, and the column with BPL was not capable of regenerating over the length of time allotted for regeneration. In cycle 2 (Figure 5.20), BPL-N consistently

removed approximately 76% of the influent formaldehyde during the entire formaldehyde exposure phase, and no change in effluent formaldehyde concentrations was detected during the regeneration phase of cycle 2. Throughout the formaldehyde exposure phase of cycle 3, formaldehyde removal by the column containing BPL-N returned to approximately 85%. Again, no change in effluent formaldehyde concentrations from the column containing BPL-N was detected during the third regeneration phase. The percent removal during the formaldehyde exposure phase of cycle 2 was slightly less (5-10%) than what was observed during the first and third cycles (Figure 5.19, Figure 5.21).

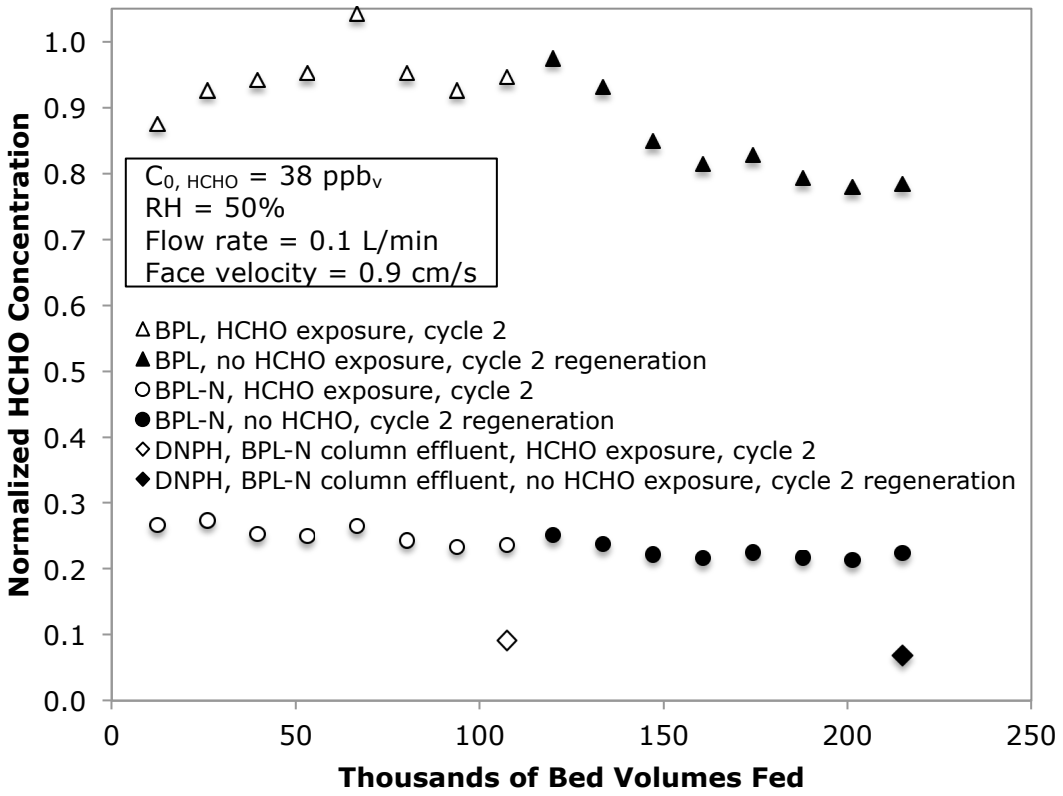

Figure 5.20. Cycle 2. Effluent formaldehyde concentrations for BPL and BPL-N during formaldehyde exposure (△,○) and regeneration (▲,●) normalized by the influent formaldehyde concentration (38 ppb_v) and presented with respect to thousands of bed volumes fed. BPL-N column effluent formaldehyde concentrations, as measured with DNPH, are also shown for the HCHO exposure phase (◇) and the regeneration (no HCHO) phase (◆).

DNPH measurements were taken simultaneously with the CSSD monitoring as a check against the CSSD formaldehyde concentrations. DNPH measurements during the formaldehyde exposure phase and the column regeneration phase of cycle 2 of the effluent concentrations of formaldehyde were 3.5 and 2.6 ppb_v, respectively. During the same phases of cycle 3, the effluent formaldehyde concentrations, as determined using DNPH, were 4.0 and 3.9 ppb_v, respectively. For cycles 2 and 3, DNPH measurements were slightly below CSSD formaldehyde measurements. It is possible that the CSSDs

were becoming slightly less sensitive to formaldehyde over time. Also, the effluent formaldehyde concentrations from the column containing BPL-N taken during these three cycles were nearing expected detection limits of the experimental system.

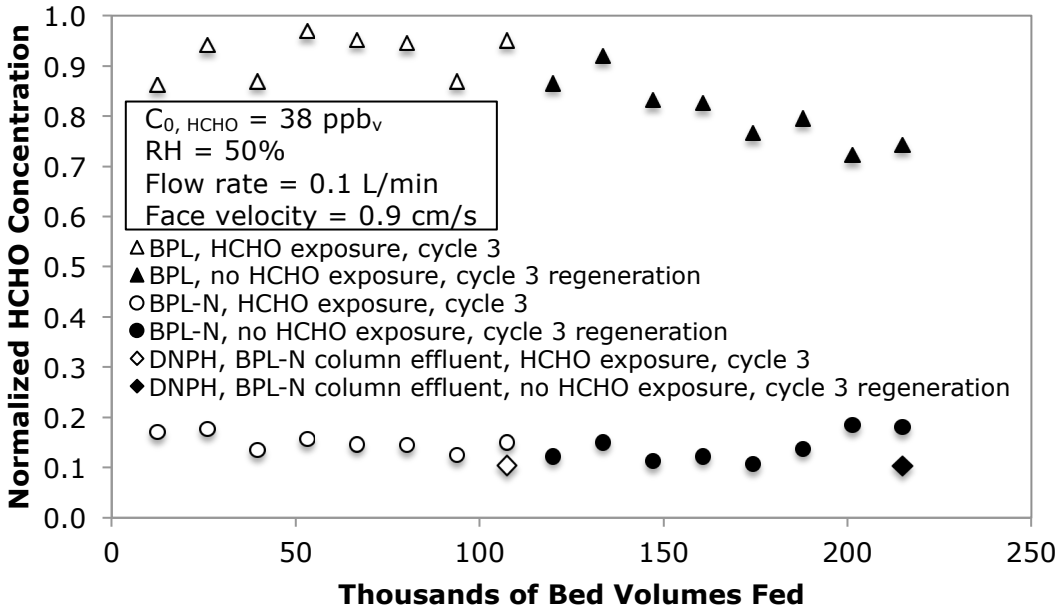

Figure 5.21. Cycle 3. Effluent formaldehyde concentrations for BPL and BPL-N during formaldehyde exposure (△,○) and regeneration (▲,●) normalized by the influent formaldehyde concentration (38 ppb_v) and presented with respect to thousands of bed volumes fed. BPL-N column effluent formaldehyde concentrations, as measured with DNPH, are also shown for the HCHO exposure phase (◇) and the regeneration (no HCHO) phase (◆).

As outlined in section 5.2.3, BPL and BPL-N packed bed columns were also monitored for their effluent formaldehyde concentrations under the same conditions of the aforementioned second set of packed bed experimental conditions (Table 5.2), using ultra-zero air as the carrier gas and increasing the relative humidity to 70% RH. BPL and BPL-N packed bed columns were exposed to formaldehyde in excess of 2 million bed volumes fed, followed by a regeneration phase (formaldehyde-free air) of approximately 100,000 bed volumes fed. As with the second set of packed bed column tests run at 50%

RH, the effluent formaldehyde concentrations from the column containing BPL rose steadily towards 100% breakthrough during the formaldehyde exposure phase (Figure 5.22). After approximately 2.15 million bed volumes fed, the effluent formaldehyde concentration had reached 87% breakthrough. Effluent formaldehyde concentrations from the column containing BPL-N remained relatively steady during the entire formaldehyde exposure phase, maintaining 82-90% formaldehyde removal according to the CSSD formaldehyde concentrations reported (Figure 5.22).

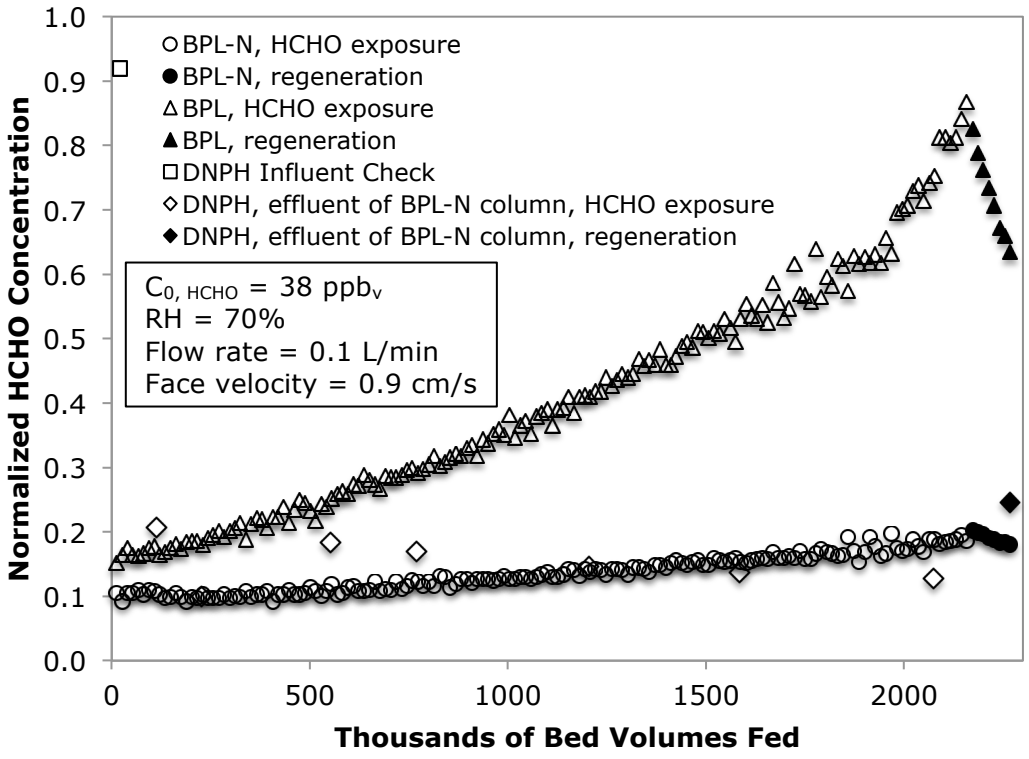

Figure 5.22. Effluent formaldehyde concentrations for BPL and BPL-N during formaldehyde exposure (△,○) and regeneration (▲,●) normalized by the influent formaldehyde concentration (38 ppb_v) and presented with respect to thousands of bed volumes fed. BPL-N column effluent formaldehyde concentrations, as measured with DNPH, are also shown for the HCHO exposure phase (◇) and the regeneration (no HCHO) phase (◆).

During the regeneration phase of the BPL and BPL-N packed bed columns tests conducted at 70% RH, effluent formaldehyde concentrations followed trends similar to those observed for each respective column when tested at 50% RH (Figure 5.20). Effluent formaldehyde concentrations from the BPL column began to decay according to a desorption profile, while effluent formaldehyde concentrations from the BPL-N column remained similar to the effluent concentrations observed during the formaldehyde exposure phase.

Effluent formaldehyde concentrations from the BPL-N column reported by the CSSD appeared to increase slowly over the course of the formaldehyde exposure phase and decrease slightly over the course of the column regeneration phase; however, DNPH formaldehyde concentrations measured simultaneously from the BPL-N column did not reproduce either of these trends. In fact, DNPH formaldehyde concentrations appeared to drop slightly over the course of the formaldehyde exposure phase, and the single DNPH measurement taken during the regeneration phase was higher than all of the DNPH formaldehyde concentrations reported for the formaldehyde exposure phase. For this reason, formaldehyde concentrations in the experimental chambers were monitored for several days with no column apparatus present and ultra-zero, formaldehyde-free air running through the chambers to determine the background formaldehyde concentration of the experimental system. Using both the CSSDs and DNPH measurements, chamber background formaldehyde concentrations were found to be approximately 10 to 12 ppb_v, which corresponded to normalized formaldehyde concentrations of 0.25-0.3 (Figure 5.23). The CSSD and DNPH measurements of effluent formaldehyde concentrations from the BPL-N columns presented in Figure 5.19-22 are below the background formaldehyde levels of the experimental chambers. Thus, it would be reasonable to interpret from these results that formaldehyde concentrations from the BPL-N column are

steadily below the detection limit of the experimental system during both the formaldehyde exposure phase and the formaldehyde-free regeneration phase.

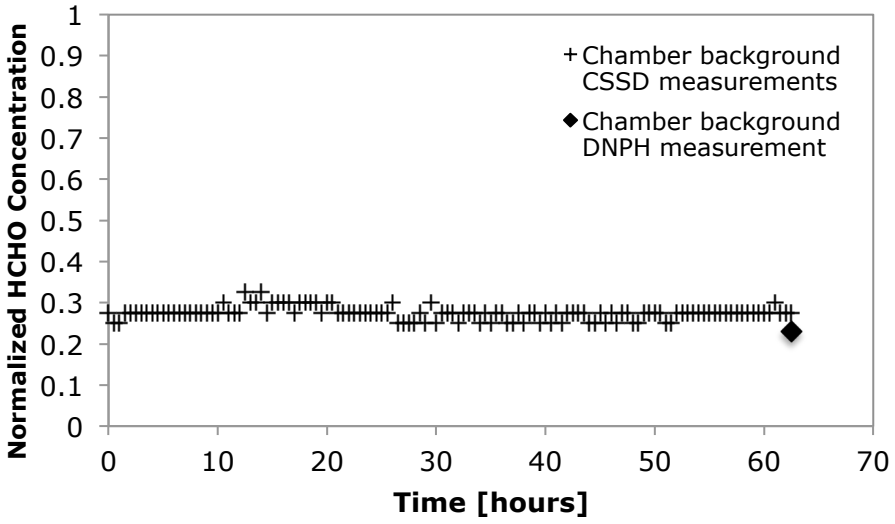

Figure 5.23. CSSD (+) and DNPH (◆) measurements of formaldehyde concentrations in experimental chambers when no columns are present and only ultra-zero, formaldehyde-free air passes through experimental system. Formaldehyde concentrations are normalized by hypothetical influent formaldehyde concentration, 38 ppb_v.

The results from the two sets of packed bed column experiments discussed in this section strongly support the hypothesis that formaldehyde removal by BPL-N occurs via a catalytic mechanism. Comparing results from the BPL-N columns when they are tested with formaldehyde-containing pure nitrogen gas (oxygen-poor case) and with formaldehyde-containing ultra-zero air (oxygen-rich case), Figure 5.24 shows that normalized effluent formaldehyde concentrations for the oxygen-rich case achieve a steady state, whereas they steadily increase for the oxygen-poor case. This result suggests that the dominant mechanism for formaldehyde removal by BPL-N is not the same for the two cases. For BPL, the shape of the normalized effluent formaldehyde concentration curves does not change whether pure nitrogen gas or ultra-zero air is used as the carrier

gas. However, even when BPL is exposed to oxygen-rich air, the effluent formaldehyde concentrations decrease slightly, suggesting that catalytic removal of formaldehyde may also be occurring in addition to adsorption, although to a much more minimal extent relative to BPL-N. This explanation of the data is consistent with the expectation that surface electron-donating potential promotes oxygen reduction at the GAC surface, which could lead to catalytic oxidation of pollutants. Since BPL has some electron-donating potential, it should also be capable of promoting some catalytic removal of formaldehyde in an oxygen-rich environment. BPL-N has more electron-donating potential, and therefore the difference between the oxygen-rich and the oxygen-poor case is greater.

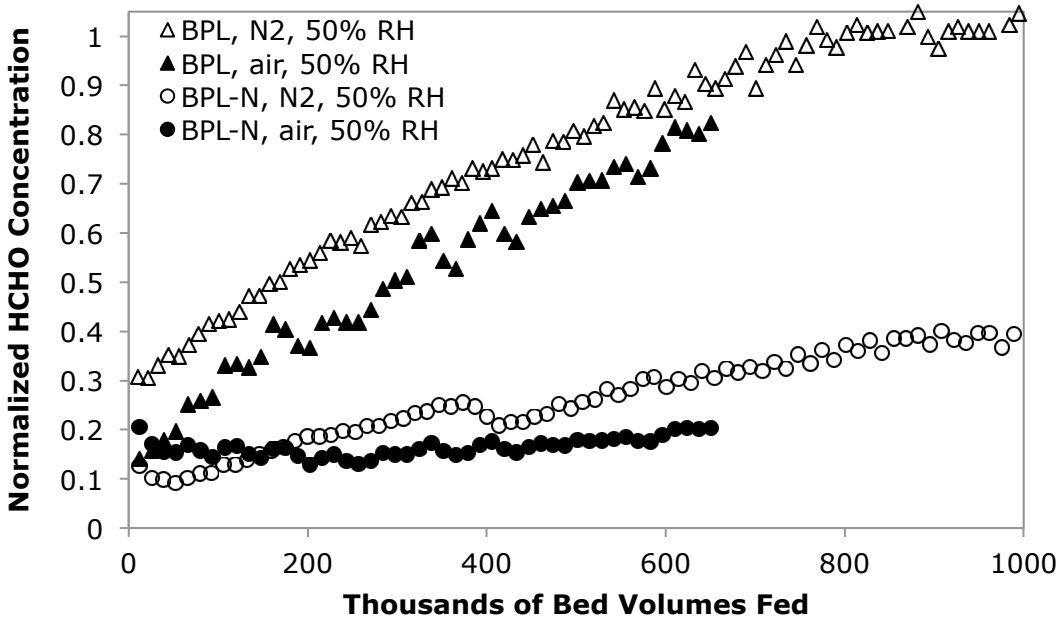

Figure 5.24. Effluent formaldehyde concentrations for BPL and BPL-N columns run with pure nitrogen carrier gas (△,○) and ultra-zero air (▲,●) normalized by the influent formaldehyde concentration (38 ppb_v) and presented with respect to thousands of bed volumes fed.

Considering only the oxygen-rich case, BPL and BPL-N performance differ considerably. Effluent formaldehyde concentrations from columns containing BPL steadily increase toward 100% breakthrough, which is characteristic of adsorption-based removal. In contrast, effluent formaldehyde concentrations from columns containing BPL-N fluctuate between 10 and 25% of the inlet concentration over the course of all three cycles of formaldehyde exposure and column regeneration (with formaldehyde-free ultra-zero air). This steady state behavior from the columns containing BPL-N is suggestive of catalysis rather than adsorption. Furthermore, during the regeneration cycles, formaldehyde effluent concentrations from BPL columns exhibit a decay curve characteristic of desorption following reversible adsorption, while formaldehyde effluent concentrations from BPL-N during the regeneration phase do not change relative to the exposure phase. Irreversible adsorption is also an unlikely removal mechanism to explain the results observed from the BPL-N columns because formaldehyde removal capacity does not diminish over the course of the three cycles. Although the CSSD formaldehyde monitors do show a slight reduction in formaldehyde removal capacity during the exposure phase of the second cycle, the DNPH results show consistent 85% removal of formaldehyde across all three cycles, and for the third cycle, CSSD report effluent formaldehyde concentrations that correspond to approximately 85% removal again.

Finally, the impact of increasing relative humidity on BPL performance and the lack of impact on BPL-N performance provide additional support that BPL-N formaldehyde removal proceeds via a catalytic mechanism. Figure 5.25 provides a comparison of normalized effluent formaldehyde concentrations from BPL and BPL-N columns for 50% and 70% relative humidity. The difference between the 50% RH and the 70% RH case for BPL supports the conclusion drawn in Chapter 4 that multiple mechanisms may be driving formaldehyde removal by this GAC. In particular,

dissolution of formaldehyde, a hydrophilic compound, into water vapor that has condensed into the GAC micropores may play a larger role in formaldehyde removal at the higher relative humidity level. Increasing relative humidity did not demonstrate a strong impact on effluent formaldehyde concentrations from the column containing BPL-N. While BPL-N results for the 50% RH case and the 70% RH case vary slightly in magnitude, the steady state behavior is unchanged, strengthening the over-arching conclusion that a catalytic mechanism provides the best explanation of BPL-N formaldehyde removal.

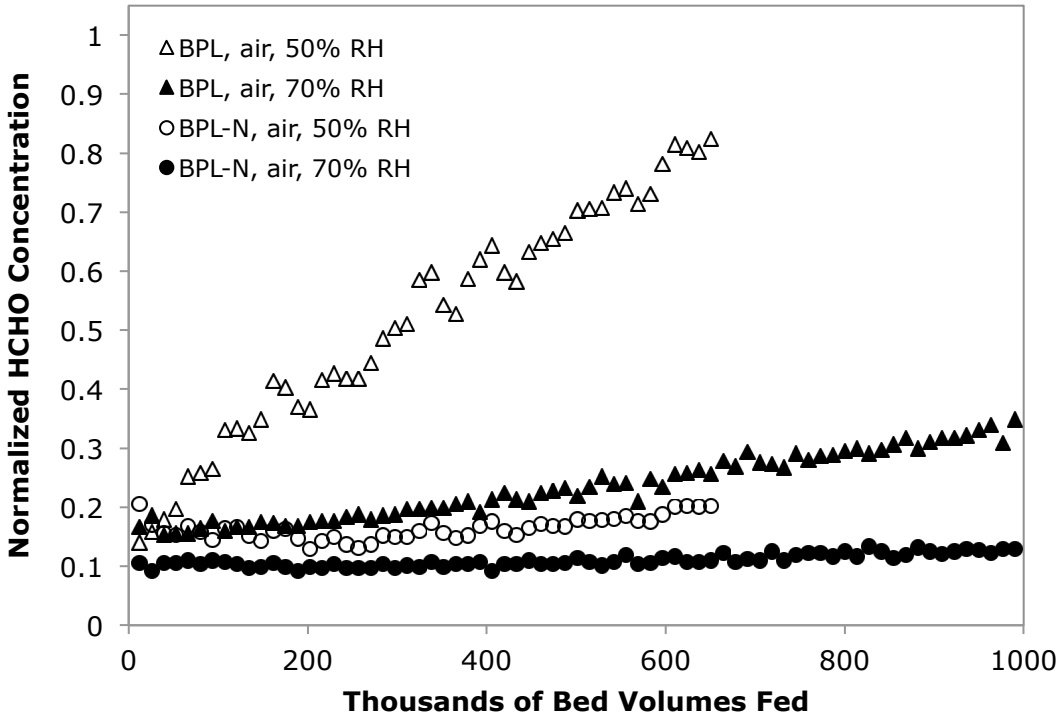

Figure 5.25. Effluent formaldehyde concentrations for BPL and BPL-N columns run at 50% RH (△,○) and 70% RH (▲,●) normalized by the influent formaldehyde concentration (38 ppb_v) and presented with respect to thousands of bed volumes fed.

5.4 CONCLUSIONS

The GAC chemical treatment process employed in this research produced the desired nitrogen-doping, and the types of nitrogen complexes formed at the BPL-N surface were electron-donating, pyridinic and pyrrolic nitrogen functional groups. Increasing nitrogen content with these specific nitrogen functional groups was also associated with an increase in overall electron-donating potential and basicity of the BPL-N GAC surface.

Increasing electron-donating nitrogen content in GAC through chemical treatment greatly improves GAC performance with respect to formaldehyde removal. BPL-N removed substantially more formaldehyde than BPL was capable of removing at both a high and moderate indoor formaldehyde concentration (100 ppb_v and 36 ppb_v). BPL-N also removed more formaldehyde on a per-GAC mass basis than did Centaur, a commercially available GAC that is chemically treated by the manufacturer to contain nitrogen. Centaur contained primarily protonated nitrogen functional groups, in contrast to the pyridinic and pyrrolic nitrogen functional groups developed in BPL-N. As a result, BPL-N had greater electron-donating potential than Centaur, which could explain the increased formaldehyde removal by BPL-N relative to Centaur.

Another major conclusion that emerges from the results presented in this chapter is that the removal mechanism by which BPL-N most successfully removes formaldehyde is very likely to be catalytic oxidation. Relative to its own performance in an oxygen-poor environment, formaldehyde removal by BPL-N improved in an oxygen-rich environment. The difference between the effluent formaldehyde concentration profiles developed for BPL-N with and without oxygen present suggested that different removal mechanisms were controlling formaldehyde removal in each case. When oxygen was not present, the effluent formaldehyde concentration profile from the BPL-N column

was characteristic of adsorption. With abundant oxygen present during the second set of packed bed column tests, the concentration profile from the BPL-N column was more characteristic of catalysis because it maintained steady state removal efficiency between 75 to 85% of the influent formaldehyde. In contrast, BPL reached 100% breakthrough after approximately 700,000 bed volumes fed. However, BPL removal of formaldehyde also improved, although to a limited degree, suggesting that the oxygen-rich conditions, in the presence of the minimal electron-donating potential present at the BPL surface, supported some minimal catalytic oxidation of formaldehyde. Thus, a catalytic removal mechanism could explain the enhanced removal of formaldehyde by both BPL and BPL-N in an oxygen-rich environment, with BPL-N performance still being far superior to BPL. This conclusion is consistent with the findings of other researchers who observed that nitrogen-doped carbon nanofibers had a more reducing nature (Maldonado and Stevenson, 2005). Furthermore, previous research revealed that oxygen is more likely to be reductively adsorbed as O•- on nitrogen-doped carbons that exhibit strong Lewis basicity (or electron-donating potential) rather than forming chemisorbed, acidic oxygen functionalities (Stoehr et al., 1991; Strelko et al., 2004). The adsorbed O•- on nitrogen-doped carbons exhibited enhanced catalytic activity for oxidative decomposition of NO_2 and SO_2 (Stoehr et al., 1991) and hydrogen peroxide (Maldonado and Stevenson, 2005). In light of this previous research, it is reasonable to conclude that a catalytic oxidation mechanism is responsible for the enhanced formaldehyde removal exhibited by BPL-N and, to a lesser extent, BPL.

Chapter 6: Conclusions

6.1 Overview

While gas-phase formaldehyde removal is a top priority for achieving healthy indoor environmental quality, traditional approaches including source removal and ventilation have been inadequate and pollutant control technology development has been undervalued. Prior to this research, the influence of GAC surface properties on gas-phase removal of hydrophilic pollutants, and formaldehyde specifically, had not been reported in the literature. Also, the role of nitrogen at the GAC surface, especially as it relates to promoting a catalytic removal mechanism for formaldehyde, had not been adequately studied. To review, the goals stated at the outset of the research presented in this dissertation were to:

1. advance formaldehyde measurement techniques and detection methods by evaluating emerging technology for continuous formaldehyde measurement at lower concentrations than have been tested previously;
2. assess the ability of commercially available activated carbon to control gas-phase formaldehyde concentrations under conditions relevant to indoor environments;
3. elucidate the influence of structural and chemical properties of activated carbon on gas-phase removal of formaldehyde; and
4. design, prepare, and characterize physicochemical properties and performance of activated carbon media that is modified to enhance gas-phase removal of formaldehyde.

6.2 Results and Significance

With respect to continuous formaldehyde measurement, CSSDs were found to perform comparably to internationally standardized DNPH measurements of gas-phase

formaldehyde concentrations. These devices demonstrated the ability to measure formaldehyde concentrations below 10 ppb_v, and method detection limits, evaluated at 5 and 10 ppb_v, were 1.9 and 2.0 ppb_v, respectively. This result provided the evidence needed to justify using this new sensor technology for the work subsequently carried out for this dissertation. During evaluation of the CSSDs, it was observed that formaldehyde measurements were unreliable when relative humidity (RH) was less than approximately 40%. However, formaldehyde measurements were robust above 40% RH, which is a level typically encountered or exceeded in indoor environments to provide occupant comfort. CSSDs were also used to measure formaldehyde concentrations for the first time on a continuous basis in a field setting, which made it possible to observe temporal variations in formaldehyde concentrations. Evaluating this emerging formaldehyde sensor technology on a continuous basis and at formaldehyde concentrations below 10 ppb_v provided proof of robust performance needed to extend the use of the CSSDs for laboratory-based research. In addition, the results presented for continuous monitoring of formaldehyde concentrations in a field setting demonstrated the potential for these devices to support the work of a wide range of professions that address indoor environmental quality including industrial hygienists, environmental engineers and regulators, and occupational safety and health professionals.

Results from the second task showed that coal-based BPL and Centaur GACs are capable of formaldehyde removal at ppb_v-level concentrations. At the lower of the two test concentrations, 36 ppb_v, Centaur removed twice the amount of formaldehyde (40 μg/g-GAC) as BPL (19 μg/g-GAC) over the same number of bed volumes fed (1 million). Based on the water vapor isotherms also developed for BPL and Centaur, the onset of capillary condensation of water vapor in the micropores of the two GACs occurs between 40 and 50% RH, suggesting that water vapor and formaldehyde may be in

competition for access to GAC surface sites and that there is potential for dissolution of formaldehyde into pores that undergo capillary condensation. The surface characterization undertaken complemented these findings by providing valuable information about the structural and chemical properties of BPL and Centaur. Structurally, BPL and Centaur surface areas, pore volumes, and pore size distributions were very similar. The oxygen-to-carbon ratios in the two GACs were also very similar, but the types of oxygen functional groups were different with the most salient difference being the presence of carboxylic acid groups in BPL and their absence in Centaur. Thus, the two GACs were found to differ most with respect to surface density of acidic and basic functional groups and electron-donating potential. Centaur had lower surface acidity, higher surface basicity, and higher electron-donating potential than BPL. In light of previous work by Carter et al. (2011) that demonstrated a positive association between higher surface densities of basic functional groups and increased formaldehyde removal at ppm_v-level concentrations, the results from packed bed column studies presented in Chapter 4 extended evidence of this relationship to ppb_v-level concentrations.

Previous work by other researchers had indicated that increased nitrogen content in GAC was associated with increased formaldehyde removal in both aqueous (Tanada et al., 1999) and gas-phase systems (Song et al., 2007). While Centaur was found to contain trace amounts of nitrogen (0.36 ± 0.33 atomic %), this work focused on creating a GAC with higher nitrogen content to more reliably examine the influence of surface-based nitrogen on gas-phase formaldehyde removal. Thus, a major outcome of research undertaken in Chapter 5 was the design and preparation of nitrogen-doped GAC, BPL-N, developed using BPL as the base material. BPL-N contained 1.54 ± 0.34 atomic % N. In addition to total nitrogen content, XPS analysis revealed that BPL-N was dominated by pyridinic and pyrrolic nitrogen functional groups, while the majority of nitrogen

functional groups in Centaur were protonated. Because of the lone pair of electrons associated with pyridinic and pyrrolic nitrogen groups, BPL-N had higher electron-donating potential than either Centaur or BPL. Electron-donating potential was also found to have a stronger positive association with formaldehyde removal than surface density of basic functional groups. Evaluating formaldehyde removal at 36 ppb_v, by the time 50% breakthrough was achieved in the packed bed GAC columns, BPL-N removed 12 times as much formaldehyde as BPL and six times as much formaldehyde as Centaur on a mass of formaldehyde per mass of GAC basis. This finding underscores the value of molecular-level understanding of GAC surface chemical properties for design of GACs that effectively remediate indoor environments with low pollutant concentrations.

Another critical outcome of this work was the evidence presented to support the hypothesis that a catalytic mechanism, rather than an adsorption-based mechanism, drives formaldehyde removal at the GAC surface, when that surface contains electron-donating nitrogen functional groups. Three key results presented in Chapter 5 support this argument. First, when the carrier gas was changed from oxygen-poor (zero-grade nitrogen gas) to oxygen-rich (ultra-zero air), the profile of normalized effluent formaldehyde concentrations from packed beds containing BPL-N maintained 75-85% removal of formaldehyde, while for BPL the effluent concentration profile still increased to 100% breakthrough as would be characteristic of adsorption. Second, when BPL and BPL-N GAC columns were regenerated with formaldehyde-free air, effluent formaldehyde concentrations from BPL columns exhibited a decaying concentration profile characteristic of desorption that follows reversible adsorption. In contrast, effluent formaldehyde concentrations from BPL-N columns were already so low during the formaldehyde exposure phases that, during regeneration phases, effluent concentrations remained the same (15-25% of the influent concentration, or 6-10 ppb_v) as when the

columns were exposed to formaldehyde. During both the formaldehyde exposure phases and the regeneration phases, effluent formaldehyde concentrations from the BPL-N columns approached the detection limit of the experimental system. Finally, when the relative humidity was increased from 50% to 70%, no change in effluent formaldehyde concentrations was observed from BPL-N columns, suggesting that the dominant formaldehyde removal mechanism in these columns was unaffected by the increased presence of water vapor. On the other hand, the BPL column continued to produce effluent formaldehyde concentration profiles during the formaldehyde exposure and regeneration phases that were characteristic of adsorption and desorption for both 50% and 70% RH. At 70% RH, formaldehyde removal capacity by BPL increased and the time to 50% breakthrough was extended relative to the packed bed column studies of BPL conducted at only 50% RH. This result suggested that multiple mechanisms, including possible dissolution of formaldehyde in water vapor condensed in the micropores of BPL, may facilitate formaldehyde removal and that different removal mechanisms may dominate at different relative humidity levels for GACs that have not been chemically treated. Significantly, the results from this research strongly suggest that catalytic removal of formaldehyde is a dominant removal mechanism on BPL-N and at least a contributing mechanism on BPL.

One final outcome of the research undertaken in Chapter 5 that should not go overlooked is that BPL-N was capable of maintaining effluent formaldehyde concentrations below the NIOSH chronic recommended exposure limit over the entire duration of testing. Tailoring GAC surfaces to contain electron-donating nitrogen functional groups shows promise for achieving one of the most critical indoor air quality goals: reducing human exposure to formaldehyde.

6.3 FUTURE WORK

This research advanced formaldehyde detection methods for indoor environments and laboratory settings and shed new light on the influence of surface chemical properties of GAC on gas-phase formaldehyde removal. The findings from this research also brought to light several promising lines of future work.

First, there would be great value in characterizing formaldehyde isotherms on GAC that has not been chemically treated over the concentration range from 10 to 10,000 ppb_v at several relative humidity levels corresponding to no capillary condensation, onset of capillary condensation, and complete pore-filling by water vapor condensed in the micropores of the GAC. These studies would help to distinguish at what relative humidity levels competition between formaldehyde and water vapor is dominant and at what relative humidity levels dissolution of formaldehyde into water vapor condensed in GAC micropores becomes a stronger driving force for formaldehyde removal by GAC.

Findings from the fourth research task highlighted the positive influence of electron-donating nitrogen functional groups on formaldehyde removal by GAC. To apply this result to development of pollutant control technology, it would be advantageous to investigate chemical treatment techniques that could impart varying amounts of nitrogen to the GAC surface, while maintaining the pyridinic and pyrrolic nature of the nitrogen functional groups. In this way, optimal levels of nitrogen for formaldehyde removal could be determined through evaluation of a series of nitrogen-doped GACs with increasing pyridinic and pyrrolic nitrogen content.

Most importantly, research that could further confirm whether catalysis is driving formaldehyde removal at the surface of GACs that contain electron-donating nitrogen functional groups would be very valuable. Measurement of oxygen reduction in aqueous systems at the surface of nitrogen-doped carbon-based materials is regularly used to

verify and quantify production of superoxide radicals at the carbon surface. Such techniques should be adapted so their results may apply to gas-phase systems, as well.

Finally, formaldehyde removal performance of BPL-N and similarly developed GACs should be evaluated at larger, possibly residential, scales to evaluate the ability of these materials to effectively and efficiently deliver air that has formaldehyde levels below health guideline values. To achieve both indoor environmental quality goals with respect to formaldehyde and maintain or improve building energy efficiency, chemically treated GAC materials could be evaluated in traditional HVAC systems, as well as in arrangements designed for passive pollutant control.

Appendices

A.1. Nitrogen Adsorption Isotherms

Nitrogen gas adsorption isotherms at 77 K for BPL, Centaur, and BPL-N are shown in Figure A-1.

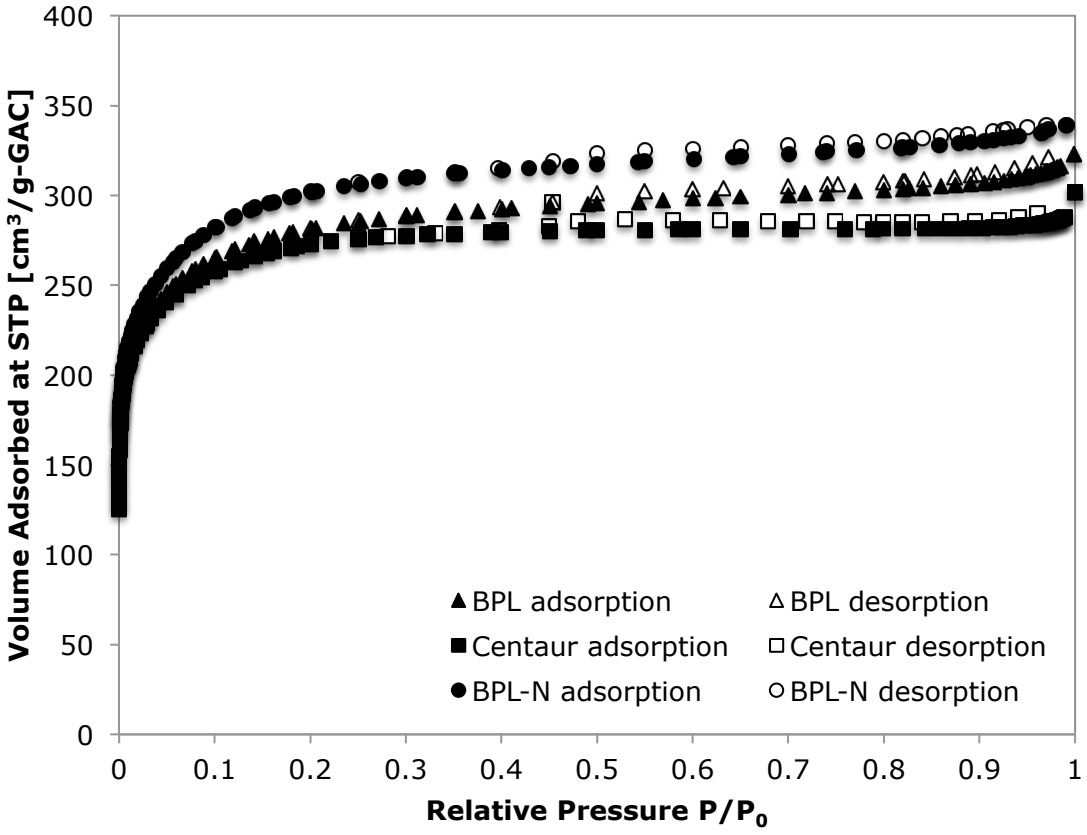

Figure A-1. Adsorption (closed symbols) and desorption (open symbols) branches of nitrogen sorption isotherms on BPL (△, ▲), Centaur (□, ■), and BPL-N (○,●).

A.2. Boehm Titrations

Boehm titration results for surface density of acidic sites for BPL, Centaur, and BPL-N are shown in Table A-1.

Table A-1. Triplicate measurements of NaOH uptake by BPL, Centaur, and BPL-N to determine surface density of acidic functional groups.

	Mass	NaOH Conc.	NaOH Uptake	NaOH Uptake
	[mg]	[N]	[N]	[meq]
BPL replicate 1	158.8	0.048	0.003	0.058
BPL replicate 2	152.9	0.049	0.002	0.048
BPL replicate 3	141.5	0.049	0.002	0.049
Centaur replicate 1	144.2	0.050	0.001	0.027
Centaur replicate 2	124.5	0.049	0.002	0.036
Centaur replicate 3	140.3	0.049	0.002	0.036
BPL-N replicate 1	168.5	0.050	0.001	0.014
BPL-N replicate 2	171.9	0.049	0.002	0.035
BPL-N replicate 3	138.6	0.050	0.001	0.025

Table A-2. Triplicate measurements of HCl uptake by BPL, Centaur, and BPL-N to determine surface density of acidic functional groups.

	HCl Conc.	HCl Uptake	HCl Uptake	HCl Conc.
	[N]	[N]	[meq]	[N]
BPL replicate 1	0.044	0.004	0.082	0.044
BPL replicate 2	0.045	0.004	0.073	0.045
BPL replicate 3	0.044	0.004	0.074	0.044
Centaur replicate 1	0.043	0.005	0.106	0.043
Centaur replicate 2	0.043	0.005	0.103	0.043
Centaur replicate 3	0.043	0.005	0.105	0.043
BPL-N replicate 1	0.043	0.005	0.108	0.043
BPL-N replicate 2	0.043	0.005	0.107	0.043
BPL-N replicate 3	0.043	0.005	0.108	0.043

References

Abe, M., Kawashima, K., Kozawa, K., Sakai, H., & Kaneko, K. (2000). Amination of activated carbon and adsorption characteristics of its aminated surface. *Langmuir*, *16*(11), 5059-5063.

Adib, F., Bagreev, A., & Bandosz, T. J. (2000). Adsorption/oxidation of hydrogen sulfide on nitrogen-containing activated carbons. *Langmuir*, *16*(4), 1980-1986.

Allen, B. L., Kichambare, P. D., & Star, A. (2008). Synthesis, characterization, and manipulation of nitrogen-doped carbon nanotube cups. *ACS nano*, *2*(9), 1914-1920.

Arthur D. Little Inc., (1981). Formaldehyde concentration level control in mobile homes. *A Report to the HCHO Institute by Arthur D. Little, Inc*., Cambridge, MA.

ASTM D 5197. (2003). American Society for Testing and Materials: West Conshohocken, PA.

ASHRAE. (2003). Ventilation for acceptable indoor air quality. American Society of Heating, Refrigerating and Air-Conditioning Engineers. ASHRAE 62-2001.

ASHRAE. (2008). Laboratory test method for assessing the performance of gas-phase air-cleaning systems: loose granular media. American Society of Heating, Refrigerating and Air-Conditioning Engineers. ASHRAE 145.1-2008.

Ataka, Y., Kato, S., Murakami, S., Zhu, Q., Ito, K., Yokota, T. (2004). Study of effect of adsorption building material on formaldehyde concentrations: development of measuring methods and modeling of adsorption phenomena. *Indoor Air,* Supplement 8: 51-64.

Bagreev, A., Angel Menendez, J., Dukhno, I., Tarasenko, Y., Bandosz, T. J. (2004). Bituminous coal-based activated carbons modified with nitrogen as adsorbents of hydrogen sulfide. *Carbon*, *42*(3), 469-476.

Barker, L. E., Luman, E. T., McCauley, M. M., Chu, S. Y. (2002). Assessing equivalence: an alternative to the use of difference tests for measuring disparities in vaccination coverage. *American Journal of Epidemiology*; *156* (11): 1056-1061.

Barro, R., Regueiro, J., Llompart, M., & Garcia-Jares, C. (2009). Analysis of industrial contaminants in indoor air: Part 1. Volatile organic compounds, carbonyl compounds, polycyclic aromatic hydrocarbons and polychlorinated biphenyls. *Journal of Chromatography A*, *1216*(3), 540-566.

Barton, S. S., Evans, M. J. B., Halliop, E., MacDonald, J. A. F. (1997). Acidic and basic sites on the surface of porous carbon. *Carbon*, *35*(9): 1361-1366.

Bashkova, S., Bagreev, A., & Bandosz, T. J. (2003). Adsorption/oxidation of CH3SH on activated carbons containing nitrogen. *Langmuir*, *19*(15), 6115-6121.

Bashkova, S., Baker, F. S., Wu, X., Armstrong, T. R., & Schwartz, V. (2007). Activated carbon catalyst for selective oxidation of hydrogen sulphide: On the influence of pore structure, surface characteristics, and catalytically-active nitrogen. *Carbon*, *45*(6), 1354-1363.

Bell, R. P. (1966). The reversible hydration of carbonyl compounds. In Gold, V. eds. *Advances in Physical Organic Chemistry*, Academic Press Inc. (London) Ltd. London, 1-27.

Billings, J. S. (1893). Ventilation and Heating, New York, The Engineering Record.

Bimer, J., Satbut, P. D., Bertoiecki, S., Boudou, J., Broniek, E., Siemieniewska, T. (1997). Modified active carbons from precursors enriched with nitrogen functions: sulfur removal capabilities. *Fuel*, *77*(6): 519-525.

Biniak, S., Szymanski, G., Siedlewski, J., Swiatkowski, A. (1997). The characterization of activated carbons with oxygen and nitrogen surface groups. *Carbon*, *35*(12): 1799-1810.

Boehm, H. P. (1994). Some aspects of the surface chemistry of carbon blacks and other carbons. *Carbon*, *32*(5), 759-769.

Boehm, H. P. (2002). Surface oxides on carbon and their analysis: a critical assessment. *Carbon*, *40*: 145-149.

Brown, S. K., Sim, M. R., Abramson, M. J., Gray, C. N. (1994). Concentrations of Volatile Organic Compounds in Indoor Air—a Review. *Indoor Air*, 4: 123-134.

Cal, M.P.; Rood, M.J.; Larson, S.M. (1997). Gas phase adsorption of volatile organic compounds and water vapor on activated carbon cloth. *Energy Fuels*, *11*: 311-315.

CARB. (2007). Airborne toxic control measure to reduce formaldehyde emissions from composite wood products. *California Code of Regulations*, 93120-93120, 12, title 17: 1-59.

CA OEHHA (2008). Air toxics hot spots program risk assessment guidelines. Technical support document for the derivation of noncancer reference exposure levels, OEHHA, California Environmental Protection Agency. http://oehha.ca.gov/air/allrels.html [Accessed 31 Jan, 2011].

CA OEHHA. (2008). Acute, 8-hour, and chronic recommended exposure limits (RELs). *Technical Support Document for Noncancer RELs, Appendix D1* 2008; California Environmental Protection Agency, Office of Environmental Health Hazard Assessment, Air Toxicology and Epidemiology Branch, Sacramento, CA: 128-169.

CA OEHHA. (2009). Methodologies for derivation, listing of available values, and adjustments to allow for early life stage exposures. *Technical Support Document for Cancer Potency Factors. Appendix A: Hot Spots Unit Risk and Cancer Potency Values* 2009; California Environmental Protection Agency, Office of Environmental Health Hazard Assessment, Air Toxicology and Epidemiology Branch, Sacramento, CA.

Carmody, O., Frost, R., Xi, Y., & Kokot, S. (2007). Surface characterisation of selected sorbent materials for common hydrocarbon fuels. *Surface Science*, *601*(9), 2066-2076.

Chen, C. Y., Yang, P. (2003). Performance of an air-breathing direct methanol fuel cell. *Journal of Power Sources*, *123*(1), 37-42.

Colombo, A., Bortoli, M., Knoppel, H., Pecchio, E., Vissers, H. (1993). Adsorption of selected volatile organic compounds on a carpet, a wall coating, and a gypsum board in a test chamber. *Indoor Air*, *3*(4): 276-282.

de Gouw, J., Warneke, C. (2006). Measurements of volatile organic compounds in the earth's atmosphere using proton-transfer-reaction mass spectrometry. *Mass Spectrometry Reviews, 26*(2): 223-257.

Daisey, J. M.; Angell, W. J. (2003). Indoor Air Quality, Ventilation and Health Symptoms in Schools: an Analysis of Existing Information. *Indoor Air*, *13*: 53-64.

Destaillats, H.; Lunden, M. M.; Singer, B. C.; Coleman, B. K.; Hodgson, A. T.; Weschler, C. J.; Nazaroff, W. W. (2006). Indoor secondary pollutants from household product emissions in the presence of ozone: a bench-scale chamber study. *Environmental Science and Technology*, *40* (14): 4421-4428.

Dimitrova, Y., Peyerimboff, S. D. (1993). Theoretical study of hydrogen-bonded formaldehyde water complexes. *Journal of Physical Chemistry*, *97*: 12731-12736.

Dimotakis, E. D., Cal, M. P., Economy, J., Rood, M. J., Larson, S. M. (1995). Chemically treated activated carbon cloths for removal of volatile organic compounds from gas streams: evidence for enhanced physical adsorption. *Environmental Science and Technology*, *29*(7): 1876-1880.

Doornkamp, C., Ponec, V. (2000). The universal character of the Mars and Van Krevelen mechanism. *Journal of Molecular Catalysis A: Chemical*, *162*: 19-32.

Dresselhaus, M. S., Dresselhaus, G., Sugihara, K., Spain, I. L., Goldberg, H. A. (1988). Graphite Fibers and Filaments, *Springer Series in Materials Science*, 5, Springer-Verlag, Berlin.

Dresselhaus, M. S., Dresselhaus, G., Saito, R., Jorio, A. (2005). Physics Reports, *409*: 47–99.

El-Sayed, Y., Bandosz, T. J. (2002). Acetaldehyde adsorption on nitrogen-containing activated carbons. *Langmuir*, *18*(8), 3213-3218.

Eriksson, B., Johanssin, L., Svedung, I., (1980). Filtration of formaldehyde contaminated indoor air. *The Nordest Symposium on Air Pollution Abatement by Filtration and Respiratory Protection*, Copenhagen, Denmark.

FEMA. (2008). FEMA response to formaldehyde in trailers (redacted). Department of Homeland Security, Office of Inspector General, Washington, DC.

Ferus, M., Cihelka, J., Civis, S. (2008). Formaldehyde in the environment-Determination of formaldehyde by laser and photoacoustic detection. *Chemicke Listy, 102*(6): 417.

Feng, L., Yan, Y., Chen, Y., Wang, L. (2011). Nitrogen-doped carbon nanotubes as efficient and durable metal-free cathodic catalysts for oxygen reduction in microbial fuel cells. *Energy & Environmental Science*, *4*(5), 1892-1899.

Figueiredo, J. L., Pereira, M. F. R. (2010). The role of surface chemistry in catalysis with carbons. *Catalysis Today*. 150:2.

Fisk, W. J., Brager, G., Brook, M., Burge, H., Cole, J., Cumming, J., Levin, H., Loftness, V., Logee, T., Mendell, M. J., Persily, A., Taylor, S., Zhang, J. (2002). A priority agenda for energy-related indoor environmental quality research. *Proceedings of the 9th International Conference on Indoor Air Quality and Climate, Indoor Air 2002*, Monterey, CA: 984-989.

Franz, M., Arafat, H. A., Pinto, N. G. (2000). Effect of chemical surface heterogeneity on the adsorption mechanism of dissolved aromatics on activated carbon. *Carbon*. *38*(13): 1807-1809.

Furmaniak, S., Gauden, P. A., Terzyk, A. P., & Rychlicki, G. (2008). Water adsorption on carbons—Critical review of the most popular analytical approaches. *Advances in Colloid and Interface Science*, *137*(2), 82-143.

Gesser, H. D. (1984). The reduction of indoor formaldehyde gas and that emanating from urea formaldehyde foam insulation (UFFI). *Environment International*, 10: 305-308.

Ghosh, T. K., Lee, S. Y., Hines, A. L. (1996). Removal of formaldehyde rom indoor environments during desiccant-dehumidification of air. *Indoor Air* 2: 205-210.

Gilbert, N. L., Guay, M., Gauvin, D., Dietz, R. N., Chan, C. C., Levesque, B. (2008). Air change rate and concentration of formaldehyde in residential indoor air. *Atmospheric Environment*, *42*: 2424-2428.

Gong, K., Du, F., Xia, Z., Durstock, M., & Dai, L. (2009). Nitrogen-doped carbon nanotube arrays with high electrocatalytic activity for oxygen reduction.*Science*, *323*(5915), 760-764.

Gordon, S., Callahan, P., Nishioka, M., Brinkman, M., OÕRourke, M., Lebowitz, M., Moschandreas, D. (1999). Residential environmental measurements in the National Human Exposure Assessment Survey (NHEXAS) pilot study in Arizona: preliminary results for pesticides and VOCs. *Journal of Exposure Analysis and Environmental Epidemiology*; *9*: 456–470.

Gregg,S. J., Sing, K.S.W. (1982). Adsorption, surface area, and porosity, 2nd ed.; Academic Press: London, NY.

Hak, C., Pundt, I., Trick, S., Kern, C., Platt, U,, Dommen, J., Ordóñez, C., Prévôt, A. S. H., Junkermann, W., Astorga-Lloréns, C., Larsen, B. R., Mellqvist, J., Strandberg, A, Yu, Y., Galle, B., Kleffmann, J., Lörzer, J. C., Braathen, G. O., Volkamer, R. (2005). Intercomparison of four different in-situ techniques for ambient formaldehyde measurements in urban air. *Atmospheric Chemistry and Physics, 5*: 2881-2900.

Health Canada. (2006). Residential indoor air quality guideline: formaldehyde. *Health Canada*; 4120, ISBN: 0-662-42661-4.

Henschel, D. B. (1998). Cost analysis of activated carbon versus photocatalytic oxidation for removing organic compounds from indoor air. *Journal of the Air & Waste Management Association*, *48*: 985-994.

HK IAQ MG. (2003). A guide on indoor air quality certification scheme for office and public places. Government of Hong Kong Special Administrative Region, Indoor Air Quality Management Group.

Ho, S. S. H., Yu, J. Z., Chu, K. W., & Yeung, L. L. (2006). Carbonyl emissions from commercial cooking sources in Hong Kong. *Journal of the Air & Waste Management Association*, *56*(8), 1091-1098.

Hodgson, A. T., Rudd, A. F., Beal, D., Chandra, S. (2000). Volatile organic compound concentrations and emission rates in new manufactured and site-built houses, *Indoor Air*, *10*, 178–192.

Hodgson, A. T., Levin, H. (2003). Volatile organic compounds in indoor air: a review of concentrations measured in North America since 1990. *Report No. LBNL-51715*, Lawrence Berkeley National Laboratory: Berkeley, CA

Huh, M. H. (1994). Equivalence testing as an alternative to significance testing. *Journal of Korean Statistical Society*; *23*: 199–206.

Hun, D. E., Siegel, J. A., Morandi, M. T., Stock, T. H. and Corsi, R. L. (2009). Cancer risk disparities between Hispanic and non-Hispanic White populations: the role of exposure to indoor air pollution, *Environmental Health Perspectives*, *117*: 1925–1931.

International Standard Organization (ISO) 16000-3. (2001). ISO: Geneva, Switzerland.

Ishibashi, K. I., Fujishima, A., Watanabe, T., & Hashimoto, K. (2000). Generation and deactivation processes of superoxide formed on TiO2 film illuminated by very weak UV light in air or water. *The Journal of Physical Chemistry B*, *104*(20), 4934-4938.

Jansen, R. J. J., Van Bekkum, H. (1995). XPS of nitrogen-containing functional groups on activated carbon. *Carbon*, *33*(8), 1021-1027.

Junkermann W, Burger J.M. (2006). A new portable instrument for continuous measurement of formaldehyde in ambient air. *Journal of Atmospheric & Oceanic Technology*; *23*: 38-45.

Karanfil, T., Kilduff, J. E. (1999). Role of granular activated carbon surface chemistry on adsorption of organic compounds. 1. Priority pollutants. *Environmental Science and Technology*, *33*(18): 3217-3224.

Kichambare, P., Kumar, J., Rodrigues, S., & Kumar, B. (2011). Electrochemical performance of highly mesoporous nitrogen doped carbon cathode in lithium–oxygen batteries. *Journal of Power Sources*, *196*(6), 3310-3316.

Klauss, A. K., Tull, R. H., Roots, L. M., Pfafflin, J. R. (1970). History of changing concepts in ventilation requirements, ASHRAE Journal,12, 51–55.

Lázló, K. (2001). Analysis of active sites on synthetic carbon surfaces by various methods. *Analytical Sciences Supplement*, *17*: 1741-1745.

László, K. (2005). Characterization and adsorption properties of polymer-based microporous carbons with different surface chemistry. *Microporous and Mesoporous Materials*, *80*(1), 205-211.

Lee, K. J., Shiratori, N., Lee, G. H., Miyawaki, J., Mochida, I., Yoon, S. H., Jang, J. (2010). Activated carbon nanofiber produced from electrospun polyacrylonitrile nanofiber as a highly efficient formaldehyde adsorbent. *Carbon*, *48*(15), 4248-4255.

Leon y Leon, C. A., Solar, J. M., Calemma, V., Radovic, L. R. (1992). Evidence for the protonation of basal plane sites on carbon. *Carbon*, *30*(5), 797-811.

Li, Y., Wang, J., Li, X., Liu, J., Geng, D., Yang, J., Sun, X. (2011). Nitrogen-doped carbon nanotubes as cathode for lithium–air batteries. *Electrochemistry Communications*, *13*(7), 668-672.

Li, Y., Wang, J., Li, X., Geng, D., Banis, M. N., Li, R., Sun, X. (2012). Nitrogen-doped graphene nanosheets as cathode materials with excellent electrocatalytic activity for high capacity lithium-oxygen batteries. *Electrochemistry Communications*, *18*, 12-15.

Lillo-Rodenas, M. A., Carratala-Abril, J., Cazorla-Amoros, D., Linares-Solano, A. (2002). Usefulness of chemically activated anthracite for the abatement of VOC at low concentrations. *Fuel Processing Technology*, *77-78*: 331-336.

Lindinger, W., Jordan, A. (1998). Proton-transfer-reaction mass spectrometry (PTR–MS): on-line monitoring of volatile organic compounds at pptv levels. *Chemical Society Reviews, 27*(5): 347-375.

Lisovskii, A. E., Aharoni, C. (1994). Carbonaceous deposits as catalysts for oxydehydrogenation of alkylbenzenes. *Catalysis Reviews in Science and Engineering*, *36*: 25-29.

Li, L., Quinlivan, P. A., Knappe, D. R. U. (2002). Effects of activated carbon surface chemistry and pore structure on the adsorption of organic contaminants from aqueous solution. *Carbon*, *40*: 2085-2100.

Liu, W., Zhang, J., Zhang, L., Turpin, B. J., Weisel, C. P., Morandi, M. T., Stock, T. H., Colome, S., Korn, L. R. (2006). Estimating contributions of indoor and outdoor sources to indoor carbonyl concentrations in three urban areas of the United States. *Atmospheric Environment*, *40*: 2202-2214.

Maldonado, S., Morin, S., Stevenson, K. J. (2005). Electrochemical oxidation of catecholamines and catechols at carbon nanotube electrodes.*Analyst*, *131*(2), 262-267.

Malkin-Weber, M., Coulter, J., Dixon, T., Hannas, B., Hassel, S., Kingston, J. (2009). Measured formaldehyde in high performance homes with outdoor air intakes. *Indoor Air Quality Association 12th Annual Meeting*, Fort Worth, Texas, USA.

Mandin C, Bonvallot N, Kirchner S, Keirsbulck M, Alary R, Cabanes P, Dor F, LeMoullec Y, Mullot J, Peel A, Rousselle C. (2009). Development of French indoor air quality guidelines. *Clean*; *37*(6): 494-499.

Mang, D., Boehm, H. P., Stanczyk, K., Marsh, H. (1992). Inhibiting effect of incorporated nitrogen on the oxidation of microcrystalline carbons. *Carbon*, *30*(3), 391-398.

Martos, P. A., Pawliszyn J. (1998). Sampling and determination of formaldehyde using solid-phase microextraction with on-fiber derivatization. *Anayltical Chemistry* 1998; *70*: 2311-2320.

Maruo, Y. Y., Nakamura, J., Uchiyama, M. (2008). Development of formaldehyde sensing element using porous glass impregnated with b-diketone. *Talanta*; *74*: 1141-1147.

Maruo, Y. Y., Yamada, T., Nakamura, J., Izumi, K., Uchiyama, M. (2010). Formaldehyde measurements in residential indoor air using a developed sensor element in the Kanto area of Japan, *Indoor Air*; *20*: 486-493.

Matsuo, Y., Nishino, Y., Fukutsuka, T., Sugie, Y. (2008). Removal of formaldehyde from gas phase by silylated graphite oxide containing amino groups. *Carbon*, *46*(8), 1162-1163.

Matthews, T. J., Fung, K. W., Tromberg, B. J., Hawthorne, A. R. (1986). Impact of indoor environmental parameters on formaldehyde concentrations in unoccupied research houses, *JAPCA, 3*; 1244–1249.

McGwin Jr., G.; Lienert, J.; Kennedy Jr., J. L. (2010). Formaldehyde exposure and asthma in children: a systemic review. *Environmental Health Perspectives, 113*(3): 313–317.

Menendez, J. A., Phillips, J., Xia, B., Radovic, L. R. (1996). On the modification and characterization of chemical surface properties of activated carbon: in the search of carbons with stable basic properties. *Langmuir*, *12*: 4404-4410.

Mikhalovsky, S. V., Zaitsev, Y. P. (1997). Catalytic properties of activated carbons i. Gas-phase oxidation of hydrogen sulphide. *Carbon*, *35*(9): 1367-1374.

Mochida, X., Hirayama, T., Kisamori, S., Kawano, S., Fujitau, H. (1992). Marked increase of SO_2 removal ability of poly(acrylonitrile)-based active carbon fiber by heat treatment at elevated temperatures. *Langmuir*, *8*: 2290-2294.

Montes-Moran, M.A.; Suarez, D.; Menedez, J.A; Fuente, E. (2004). On the nature of basic sites on carbon surfaces: an overview. *Carbon*, *42*: 1219-1225.

Morrison, G. C.; Nazaroff, W. W. (2002). Ozone interactions with carpet: secondary emissions of aldehydes. *Environmental Science and Technology*, *36*(10): 2185-2192.

Morrison, G. (2008). Interfacial chemistry in indoor environments. *Environmental Science and Technology*, *42*(10): 3495-3499.

Nash, T. (1953). The colorimetric estimation of formaldehyde by means of the Hantzsch reaction. *Biochemical Journal, 55*(3): 416.

National Research Council. (2011). Review of the Environmental Protection Agency's draft IRIS assessment of formaldehyde, Board on Environmental Studies and Toxicology. *The National Academies Press*; Washington, DC.

Nelson, G. O., Harder, C. A. (1974). Respirator cartridge efficiency studies: V. Effect of solvent vapor. *American Industrial Hygiene Association Journal* 35:391-410.

Nelson, G. O., Harder, C. A. (1976). Respirator cartridge efficiency studies: VI. Effect of concentration. *American Industrial Hygiene Association Journal* 37(5): 205-216.

Nelson, G. O., Harder, C. A. (1976). Respirator cartridge efficiency studies: VI. Effect of relative humidity and concentration. *American Industrial Hygiene Association Journal* 37(5): 280-288.

New York State Commission on Ventilation. (1931). School Ventilation Principles and Practices, New York, Bureau of Publications, Teachers College, Columbia University.

NIOSH. (2009). Pocket Guide to Chemical Hazards; United States Department of Health and Human Services, Public Health Service, Centers for Disease Control and Prevention: Cincinnati, OH.

Nowicki, P., Pietrzak, R., Wachowska, H. (2008). Comparison of physicochemical properties of nitrogen-enriched activated carbon prepared by physical and chemical activation of brown coal. *Energy and Fuels*, *22*(6): 4133-4138.

O'Brien, P. J., Siraki, A. G., Shangari, N. (2005). Aldehyde sources, metabolism, molecular toxicity mechanisms, and possible effects on human health. *Critical Reviews in Toxicology*, *35*: 609-662.

CA OEHHA (2008). Air toxics hot spots program risk assessment guidelines. Technical support document for the derivation of noncancer reference exposure levels, OEHHA, California Environmental Protection Agency. http://oehha.ca.gov/air/allrels.html [Accessed 31 Jan, 2011].

Offermann, F. J. (2009). Ventilation and indoor air quality in new homes. California Air Resources Board and California Energy Commission, PIER Energy-Related Environmental Research Program. Collaborative Report. *CEC-500-2009-085*.

Oliveira, L. C., Silva, C. N., Yoshida, M. I., Lago, R. M. (2004). The effect of H_2 treatment on the activity of activated carbon for the oxidation of organic contaminants in water and the H_2O_2 decomposition. *Carbon*, *42*(11), 2279-2284.

Olivier, J.P., Conklin, W.B., Szombathely, M., (1995). DFT A program for the calculation of total surface area and the distribution of pore area and volume from a density functional theory of adsorption and condensation within porous solids. 200- 42814-01, Norcross, GA.

Qu, L., Liu, Y., Baek, J. B., Dai, L. (2010). Nitrogen-doped graphene as efficient metal-free electrocatalyst for oxygen reduction in fuel cells. *ACS nano*, *4*(3), 1321-1326.

Radovic, L. R., Rodriguez-Reinoso, F. (1997). Carbon materials in catalysis. *Chemistry and Physics of Carbon*. 25, ed. P. A. Thrower. Marcel Dekker, New York, 243.

Rappaport, S. M., Kupper, L. L. (2004). Variability of Environmental Exposures to Volatile Organic Compounds. *Journal of Exposure Analysis and Environmental Epidemiology*, *14*: 92-107.

Roberson, J. A., Brown, R. E., Koomey, J. G., Greenberg, S. E. (1998). Recommended ventilations strategies for energy-efficient production homes. *LBNL-40378*: 1-43.

Rodriguez-Reinoso, F. (1998). The role of carbon materials in heterogeneous catalysis. *Carbon*, *36*(3), 159-175.

Rodriguez-Reinoso, R., Molina-Sabio, M. (1998). Textural and chemical characterization of microporous carbons. *Advances in Colloid and Interface Science, 76-77*: 271-294.

Rong, H. Q., Ryu, Z. Y., Zheng, J. T. (2001). Study on the properties of different activated carbon fibers and their adsorption characteristics for formaldehyde. *Acta Metallurgica Sinica*, *14*(6): 467-472.

Russell, M., Sherman, M., Rudd, A. (2007). Review of residential ventilation technologies. *HVAC&R Research*, *13*(2), 325-348.

Salthammer, T.,, Mentese, S. (2008). Comparison of analytical techniques for the determination of aldehydes in test chambers. *Chemosphere, 73*(8): 1351-1356.

Salthammer, R., Mentese, S., Marutzky, R. (2010). Formaldehyde in the indoor environment. *Chemical Reviews*, *110*(4): 2536-2572.

Sandner, F., Dott, W., Hollander, J. (2001). Sensitive indoor air monitoring of formaldehyde and other carbonyl compounds using the 2, 4-dinitrophenylhydrazine method. *International Journal of Hygiene and Environmental Health, 203*(3): 275-279.

Schauer, J. J., Kleeman, M. J., Cass, G. R., & Simoneit, B. R. (2002). Measurement of emissions from air pollution sources. 4. C1-C27 organic compounds from cooking with seed oils. *Environmental Science and Technology*, *36*(4), 567-575.

Scott, K., Rimbu, G. A., Katuri, K. P., Prasad, K. K., Head, I. M. (2007). Application of modified carbon anodes in microbial fuel cells. *Process Safety and Environmental Protection*, *85*(B5), 481-488.

Sekine, Y. (1998). Application of recycled materials to purifying environment. *Chemical Engineering of Japan*, 62(6): 308-310.

Shah, D., Kissick, K., Ghorpade, A., Hannah, R., Bhattacharyya, D. (2000). Pervaporation of alcohol–water and dimethylformamide–water mixtures using hydrophilic zeolite NaA membranes: mechanisms and experimental results. *Journal of Membrane Science*, *179*(1), 185-205.

Shao, Y., Sui, J., Yin, G., Gao, Y. (2008). Nitrogen-doped carbon nanostructures and their composites as catalytic materials for proton exchange membrane fuel cell. *Applied Catalysis B: Environmental*, *79*(1), 89-99.

Sidheswaran, M., Destaillats, H., Sullivan, D. P., Fisk, W. J. (2010). New air cleaning strategies for reduced commercial building ventilation energy. *LBNL-4026E*: 1-82.

Silberstein, S., Grot, R. A., Ishiguro, K. and Mulligan, J. L. (1988). Validation of models for predicting formaldehyde concentrations in residences due to press-wood products, *JAPCA, 38*; 1403–1411.

Singh, K. P., Mohan, D., Tandon, G. S., Gupta, G. S. D. (2002). Vapor-phase adsorption of hexane and benzene on activated carbon fabric cloth: equilibria and rate studies. *Industrial Engineering and Chemistry Research*, *41*: 2480-2486.

Sherman, M. H., Hodgson, A. T. (2004). Formaldehyde as a basis for residential ventilation rates. *Indoor Air, 14*(1): 2-8.

Shimodaira, N., Masui, A. (2002). Raman spectroscopic investigations of activated carbon materials. *Journal of Applied Physics*, *92*(2): 902-909.

Song, Y., Qiao, W., Yoon, S. H., Mochida, I., Guo, Q., Liu, L. (2007). Removal of formaldehyde at low concentration using various activated carbon fibers. *Journal of Applied Polymer Science*, *106*(4), 2151-2157.

Standard, A. S. H. R. A. E. (1989). Standard 62-1999, Ventilation for Acceptable Indoor Air Quality. *American Society of Heating, Refrigerating, and Air-Conditioning Engineers, Inc.,* Atlanta, Ga.

Stern, A.C. (1968). Air pollution: Sources of air pollution and their control, 2nd Edition, *Academic Press*, New York, New York.

Stoehr, B., Boehm, H.P., Schloegl, R., (1991). Enhancement of the catalytic activity of activated carbons in oxidation reactions by thermal treatment with ammonia or hydrogen cyanide and observation of a superoxide species as a possible intermediate. *Carbon*, *29*(6): 707-720.

Strelko, V. V., Kartel, N. T., Dukhno, I. N., Kuts, V. S., Clarkson, R. B., Odintsov, B. M. (2004). Mechanism of reductive oxygen adsorption on active carbons with various surface chemistry. *Surface Science*, *548*(1), 281-290.

Suarez, D., Menéndez, J. A., Fuente, En. Montes-Morán, M. A. (1999). Contribution of pyrone-type structures to carbon basicity: an ab initio study. *Langmuir*, *15*:3897.

Sullivan, P. D., Stone, B. R., Hashisho, Z., Rood, M. J. (2007). Water adsorption with hysteresis effect onto microporous activated carbon fabrics.*Adsorption*, *13*(3-4), 173-189.

Sun, G., Wang C., Zhan, L, Qiao W., Liang X., Ling L. (2008). Influence of high temperature treatment of activated carbon on performance of supercapacitors. *Journal of Materials Science and Engineering*, *2*(12): 41-48.

Sundell, J., Levin, H., Nazaroff, W. W., Cain, W. S., Fisk, W. J., Grimsrud, D. T., Weschler, C. J. (2011). Ventilation rates and health: multidisciplinary review of the scientific literature. *Indoor air*, *21*(3), 191-204.

Tanada, S., Kawasaki, N., Nakamura, T., Araki, M., Isomura, M. (1999). Removal of formaldehyde by activated carbons containing amino groups.*Journal of colloid and interface science*, *214*(1), 106-108.

Thompson, C. M.; Subramaniam, R. P.; Grafström, R. C. (2008). Mechanistic and dose considerations for supporting adverse pulmonary physiology in response to formaldehyde. *Toxicology and Applied Pharmacology*. *233*: 355–359.

Tichenor, B. A., Guo, Z., Dunn, J. E., Sparks, L. E., Mason, M. A. (1991). The interaction of vapour phase organic compounds with indoor sinks. *Indoor Air*, *1*(1): 23-25.

Tokumitsu, S., Izumi, K., Utiyama, M., & Maruo, Y. Y. (2008, October). Interferences of various gases on porous glass-based formaldehyde sensors. In *Control, Automation and Systems, 2008. ICCAS 2008. International Conference on* (pp. 974-977). IEEE.

Tomita, A., Tamai, Y. (1971). Catalytic effect of surface groups on carbon in the hydrolysis of hexanitrocobaltate (III). *Journal of Colloid and Interface Science*, *36*(1): 153-154.

Tredgold, T. (1836). Principles of Warming and Ventilation — Ventilating Public Buildings, 3rd edition, London, M. Taylor.

U. S. Congress. House of Representatives. Committee on Energy and Commerce. 2010. Formaldehyde standards for composite materials. 111th Congress 2nd Session, H.R. 4805, 111-509:1-9.

U.S. Department of Energy (DOE). (2008). *Buildings Energy Data Book, Section* 1.1.1.

U.S. EPA. (1991). Office of Research and Development, Washington, DC.

U.S. EPA. (1996). Proposed guidelines for carcinogen risk assessment. *Federal Register*; *61*(79): 17960-18011.

U.S. EPA Method TO-11A. (1999). U.S. EPA: Cincinnati, OH.

U.S. EPA. (2000). Energy cost and IAQ performance of ventilation systems and controls. *U.S. Office of Air and Radiation, Indoor Environments Division*, EPA-4-2-S-01-001.

U.S. EPA. (2010). Toxicological review of formaldehyde inhalation assessment. Office of Research and Development, Washington, DC.

Vairavamurthy, A., Roberts, J. M., Newman, L. (1992). Methods for determination of low molecular weight carbonyl compounds in the atmosphere: A review. *Atmospheric Environment. Part A. General Topics, 26*(11): 1965-1993.

VanOsdell, D. W., Owen, M. K., Jaffe, L. B. Sparks, L. E. (1996). VOC removal at low contaminant concentrations using granular activated carbon. *Journal of the Air and Waste Management Association*, 46(9): 883-890.

Wallace, L.A. (1991). Personal Exposure to 25 Volatile Organic Compounds: EPA's 1987 TEAM Study in Los Angeles, California. *Toxicological and Industrial Health*, *7*: 203-208.

Wallace, L. A. (2001). Human Exposure to Volatile Organic Pollutants: Implications for Indoor Air Studies. *Annual Review of Energy and the Environment*, *26*: 269-301.

Wang, H.; Morrison, G. C. (2006). Ozone-initiated secondary emissions rates of aldehydes from indoor surfaces in four homes. *Environmental Science and Technology*, *40*(17): 5263-5268.

Ward, P. M., Peters, P. A. (2007). Self-help housing and informal homesteading in peri-urban America: settlement identification using digital imagery and GIS. *Habitat International*; *31*: 205-218.

Weisel, C. P., Zhang, J., Turpin, B. J., Morandi, M. T., Colome, S., Stock, T. H., Spektor, D. M., Korn, L., Winer, A. M., Kwon, J., Meng, Q. Y., Zhang, L., Harrington, R., Liu, W., Reff, A., Lee, J. H., Alimokhtari, S., Mohan, K., Shendell, D., Jones, J., Farrar, L., Maberti, S., Fan, T. (2005). Relationship of Indoor, Outdoor, and Personal Air (RIOPA): Part I. collection methods and descriptive analyses. *HEI Report No. 130 (Pt. 1) NUATRC Report No. 7*; Health Effects Institute, Boston, MA; National Urban Air Toxics Research Center, Houston, TX.

Weschler, C. J. (2000). Ozone in indoor environments: concentration and chemistry. *Indoor Air*, *10*(4): 269-288.

Weschler, C. J. (2006). Ozone's impact on public health: contributions from indoor exposures to ozone and products of ozone-initiated chemistry. *Environmental Health Perspectives*, *114*: 1489-1496.

Weschler, C. J. (2009). Changes in indoor pollutants since the 1950s. *Atmospheric Environment*, *43*(1): 153-169.

WHO. (1987). Air quality guidelines for Europe, Copenhagen, World Health Organization Regional Office for Europe. *WHO Regional Publications, European Series* 1987; 23.

WHO, International Agency for Research on Cancer. (2006). Monographs on the evaluation of carcinogenic risks to humans: formaldehyde, 88.

WHO. (2010). WHO guidelines for indoor air quality: selected pollutants. The WHO Centre for Environment and Health, Bonn Office.

Wieslander, G., Norba¨ck, D., Bjo¨rnsson, E., Janson, C., Boman, G. (1997). Asthma and the indoor environmental: the significance of emission of formaldehyde and volatile organic compounds from newly painted indoor surfaces. *International Archives of Occupational and Environmental Health*, *69*: 115-124.

Wisthaler, A., Apel, E. C., Bossmeyer, J., Hansel, A., Junkermann, W., Koppmann, R., Brauers, T. (2008). Technical Note: Intercomparison of formaldehyde measurements at the atmosphere simulation chamber SAPHIR. *Atmospheric Chemistry and Physics*, *8*(8), 2189-2200.

Won, D., Nong, G., Yang, W,. Scheibinger, H. (2011). Characterizing commercially available formaldehyde sensors. In: *Proceedings of Indoor Air 2011*; a126.

Wu, P. C., Li, Y. Y., Lee, C. C., Chiang, C. M., Su, H. J. (2003). Risk assessment of formaldehyde in typical office buildings in Taiwan. *Indoor air*, *13*(4), 359-363.

Xiao, G. G., Zhang, Z., Weber, J., Ding, H., McIntosh, H., Desrosiers, D., Norg, G., Won, D. Y., Dunford, J., Tunney, J., Darcovich, K., Diaz-Quijada, G. (2011). Trace amount formaldehyde gas detection for indoor air quality monitors. *NRCC-54484*.

Yao, M., Zhang, Q., Hand, D. W., Perram, D. L., Taylor, R. (2009). Investigation of the treatability of the primary indoor volatile organic compounds on activated carbon fiber cloths at typical indoor concentrations. *Journal of the Air & Waste Management Association*, *59*(7), 882-890.

Yonge, D. R., Kelnath, T. M., Poznanska, K., Jiang, Z. P. (1985). Single-solute irreversible adsorption on granular activated carbon. *Environmental Science and Technology*, *79*: 690-694.

Zawadzki, J. (1988). in: P.A. Thrower (Ed.), Chemistry and Physics of Carbon, Marcel Dekker, New York, 147.

Zhang, J., Smith, K. R. (1996). Hydrocarbon emissions and health risks from cookstoves in developing countries**.** *Journal of Exposure Analysis and Environmental Epidemiology, 6*(2): 147-61.

Zhou, J., Sui, Z., Zhu, J., Li, P., Chen, D., Dai, Y., Yuan, W. (2007). Characterization of surface oxygen complexes on carbon nanofibers by TPD, XPS and FT-IR. *Carbon*, *45*: 785-796.

Vita

Ellison Milne Carter was born and raised in Valparaiso, Indiana. Ellison's secondary education was a combination of home-schooling and attendance at Morgan Township School, a gymnastics school, and finally Valparaiso High School. She went on to graduate from Indiana University at Bloomington with a B. S. in Biology and a B. A. in Spanish. After working at several biological stations in Costa Rica, Ellison returned to the U. S. and entered the graduate program in Environmental and Water Resources Engineering in the Department of Civil, Architectural, and Environmental Engineering at the University of Texas at Austin (UT). She received her M. S. in Civil Engineering at UT and continued her research at UT in pursuit of a doctorate degree in Civil Engineering.

Permanent address (or email): ellison.carter@gmail.com

This dissertation was typed by Ellison Milne Carter.